AN APPLICATION OF THE CODA METHODOLOGY FOR MOMENT-RATE SPECTRA USING THREE BROADBAND STATIONS IN TURKEY

by

TUNA EKEN
B.S., Geophysics, Istanbul University

Submitted to
Boğaziçi University
Kandilli Observatory and Earthquake Research Institute
in partial fulfillment of
the requirements for the degree of
Master of Science
in
Geophysics

Boğaziçi University
2003

ACKNOWLEDGEMENTS

My thesis advisor Prof. Niyazi Türkelli has been considerably helpful and encouraging since the beginning of this study. I would like to thank him for his numerous advices and thoughtful discussions which provided much-needed guidance throughout this work.

An important part of my thesis was completed during my stay at Lawrence Livermore National Laboratory (LLNL), USA. I would like to thank Dr. Kevin Mayeda for his personality, guidance and hospitality. His physical insights, great deal of guidance and numerous advices remarkably helped me for understanding the methodology. Dr. Rengin Gök, Jennifer O' Boyle, Dr. Michael Pasyanos, Dr. Steve Myers and Dr. William R. Walter from LLNL, Dr. Rami Hofstetter, from Geophysical Institute of Israel (GII) and Assoc. Prof. Douglas Dreger, PhD. Student Wu-Cheng CHI from UC Berkeley Seismological Laboratory are also acknowledged for providing me with assistance at various stages of this work.

The waveform data used in this study were obtained from the Seismological Laboratory of BU-Kandilli Observatory and Earthquake Research Institute and GEOFON Data Center. I would like to thank all members of these institutions for providing researchers with available data.

I would like to thank to all members of the Geophysical Department, especially Prof. Mustafa Aktar, Prof. Cemil Gürbüz, Prof. Balamir Üçer, and Assoc. Prof. Hayrullah Karabulut for their important comments and discussions. I am grateful to Dr. Gonca Örgülü for providing me with parametric data and for her useful comments and advices with regard to the methodology. Special thanks are to Dr. Tolga Bekler, Dr. Ekrem Zor, Tolga Komut, Rıza Pektas, Dean Childs, Fatih Bulut and my fellow graduate students for their assistance from many respects.

Most importantly, I would like to thank my family for their understanding, support, and never-ending patience during my education.

This work was performed under the auspices of the U.S. Department of Energy by Boğazici University Kandilli Observatory and Earthquake Research Institute under contract No. DE-FC03-01SF22416/A000.

ABSTRACT

In this study, an empirical magnitude calibration method developed by Mayeda et al., (2003) was tested by using both local and regional distance earthquakes that occurred along the North Anatolian Fault Zone as well as throughout the broader region of Turkey. The method is based on source spectra that are derived from time-domain amplitude measurements of coda envelopes for 14 consecutive narrow frequency bands ranging between 0.02-8.0 Hz. Previous application of the methodology to earthquakes in the western United States and Dead Sea Rift regions (Mayeda and Walter, 1996; Mayeda et al., 2003) show that the moment magnitudes, M_W(coda), based on coda envelopes are significantly more stable and unbiased than conventional narrowband regional magnitudes which are obtained from direct phase measurements. Coda envelopes have a number of properties that make it a desirable choice for sparse station monitoring: 1) the coda envelopes are nearly insensitive to the radiation pattern and directivity of the earthquake source, 2) the coda is not as sensitive to lateral crustal heterogeneity because of the crustal averaging due to scattering, 3) clipped data can be used for fitting the envelopes after the clipped portion of the seismogram.

During the calibration study, the empirical magnitude calibration method was applied in order to calibrate the three broadband stations, ISP, ISK and MALT in Turkey. Therefore, 182 common events, which mostly occurred along the North Anatolian Fault zone near the Marmara region and recorded at both stations ISP and ISK, 137 common earthquakes, which are distributed over the broader region of Turkey recorded by stations ISP and MALT, were used. After applying the method to both pairs of datasets, consistent source spectra that were validated by equivalent seismic moment estimations from long period waveform modeling and derived moment magnitudes (M_W) were obtained. This study resulted in amplitude measurements that are a factor of 3 to 4 less variable than distance-corrected direct wave measurements (i.e., P_g, L_g, and surface waves). Upon comparing our coda-derived moment magnitude, M_W(coda)'s with those from long-period waveform modeling, M_W(waveform), a standard deviation of 0.17 for ISP-ISK and 0.14 for ISP-MALT station pair was observed comparable to the results of previous studies (Mayeda and Walter, 1996; Mayeda *et al.*, 2003). After calibrating the stations ISP, ISK and MALT, for some recent earthquakes such as the Pülümür earthquake of January 27, 2003, M_W = 6.1, the Urla earthquake of the April 10, 2003, M_W = 5.7 and the Bingöl earthquake of the May 1, 2003, M_W = 6.4, M_W(coda) values were estimated. The successful application of the method is remarkably important considering

we are studying a much larger region with significant lateral complexities. With these calibrations we can extend the measurement of stable Mw to significantly smaller events, which could otherwise not be waveform, modeled due to poor signal-to-noise ratio.

ÖZET

Bu çalışmada Mayeda ve diğ. (2003) tarafından geliştirilen, ampirik bir manyitüd kalibrasyon yöntemi Türkiye' nin geniş bir bölümü ve Kuzey Anadolu Fay Zonu boyunca meydana gelen lokal ve bölgesel uzaklıkta ki depremler kullanılarak test edildi. Method, 0.02-8.0 Hz arasında düzenli bir şekilde birbirini izleyen 14 adet kısa frekans bandı için koda zarflarının zaman ortamında ki genlik ölçümlerinden türetilen kaynak spektralarına dayanmaktadır. Methodun, Amerika Birleşik Devletleri' nin batısı ve Ölü Deniz Rift Bölgesi' nde meydana gelen depremler kullanılarak yapılan önceki uygulamarı (Mayeda ve Walter, 1996; Mayeda ve diğ., 2003) koda zarflarından elde edilen moment manyitüdlerinin [M_W(coda)] direk dalga ölçümlerinden elde edilen geleneksel kısa band genişlikli bölgesel manyitüdlerden önemli ölçüde daha istikrarlı ve güvenilir olduğunu göstermektedir. Koda zarfları, seyrek istasyonlardan oluşan sismik ağların yerine getirdiği izleme calışmaları için, kendi kullanımını cazip hale getiren bir çok özelliğe sahiptir: 1) Koda zarfları deprem kaynağının doğrultusu ve yayınım şekline karşı neredeyse duyarsızdır, 2) Saçılmış dalga alanının ortalaması özelliğine sahip olan koda dalgaları, kabuğun yanal süreksizliklerine karşı duyarlı değildir, 3) Zarfların karşılaştırılması sırasında kesilmis veri (clipped data), sismogramın kesilen kısmından sonrası için kullanılabilir.

Kalibrasyon çalışması süresince, ampirik manyitüd kalibrasyon methodu, Türkiye' de üç adet broadband istastonunu (ISP, ISK ve MALT) kalibre etmek için uygulandı. Bu nedenle, çoğunlukla Kuzey Anadolu Fay Zonu' nun Marmara Bölgesi'ne yakın yerlerinde meydana gelmiş olan ve hem ISK ve hem de ISP broadband istasyonları tarafından kaydedilmiş 182 adet ortak deprem ile Türkiye'nin geniş bir bölümü üzerinde dağılım gösteren ve ISP and MALT broad band istasyonları tarafından kaydedilen 137 adet ortak deprem verisi kullanıldı. Yöntemin heriki veri-setine uygulanmasından sonra, uzun periyod dalga modellemelerinden elde edilmiş eşdeğer sismik moment ve bu moment değerlerinden türetilmiş moment manyitüdleri tarafından doğrulanan tutarlı kaynak spektraları elde edildi. Bu çalışma, uzaklık-düzeltilmesi yapılmış direk dalga ölçümlerinden (direk gelen P, S ya da Lg veya yüzey dalgaları gibi) 3 veya 4 kez daha az değişkenlik gösteren genlik ölçümleri verdi. Koda genliklerinde türetilen moment manyitüd [M_W(coda)] değerlerinin, uzun-periyod dalga modellemesi ile elde edilen moment manyitüd [M_W(waveform)] değerleri ile kıyaslanması ile, ISP-ISK istasyon çifti için 0.17 ve ISP-MALT istasyon çifti için 0.14 gibi önceki calışmaların (Mayeda ve Walter, 1996; Mayeda ve diğ., 2003) sonuçları ile mukayese edilebilecek standart

sapma değerleri gözlendi. ISP, ISK and MALT istasyonlarının kalibrasyonundan sonra, 27 Ocak, 2003 Pülümür (M_W=6.1), 10 Nisan, 2003 Urla (M_W=5.7) ve de 1 Mayıs, 2003 Bingöl (M_W=6.4) depremleri gibi yakın zamanlarda meydana gelmiş olan bazı depremlerin M_W(coda) değerleri hesaplandı. Yöntemin başarı ile uygulanması, belirgin yanal karmaşıklıklara sahip daha geniş bir bölge üzerinde çalışıyor olduğumuz düşünüldüğünde fevkalade önemlidir. Bu kalibrasyon sonuçlarıyla, biz istikrarlı M_W ölçümlerini, zayıf sinyal-gürültü oranından dolayı dalga modellemesi yapılamayacak kadar önemli ölçüde küçük depremlere kadar genişletebiliriz.

TABLE OF CONTENTS

LIST OF FIGURES

Figure B.8 The gamma, γ values plotted versus distance at some frequency bands, a) gamma, γ values obtained at 0.7-1.0 Hz for the events recorded at ISP and MALT stations, b) gamma, γ values obtained at 1.0-1.5 Hz for the events recorded at ISP and MALT stations.

LIST OF TABLES

LIST OF SYMBOLS

a_1, a_2 and a_3	Station, attenuation and distance dependent constants
τ	Signal duration in seconds
Δ	Epicentral distance (km)
$Q(\Delta,h)$	Distant and depth dependent factor
μ	Rigidity or shear wave resistance
u	Average fault displacement
A	Rupture area
A_{max}	Maximum ground amplitude
$\Omega(\omega)$	Source displacement amplitude
k	Proportionality constant
ω	Angular frequency
ω_0	Corner frequency
ρ	Rock density
υ_S	Shear-wave velocity
Ω_0	Spectral level of low frequency shear waves
Q	Quality factor
Qc	Coda attenuation factor
Qa	Intrinsic Q
Qs	Scattering Q
v	Velocity
r	Epicentral distance
r_0	Reference distance
r_n	Distance from the station to the nth scatterer
t	Time
f	Center frequency
N(r)	Number of the scatterers
$P(\omega \backslash t)$	Power spectral density
$\varnothing(\omega \backslash r)$	Fourier transform of displacement
$A(\omega \backslash r)$	Coda amplitude

σ	Density of scatterers
S	Source term
a and m	Constants related to the geometrical spreading
b	A parameter regarding quality factor Q
c	Source factor
v(t)	Band pass filtered seismogram
h(t)	Hilbert transform of v(t)
N	Noise
e(t\f)	Narrowband coda envelope at center frequency f
E(t\f)	Noise-corrected narrowband coda envelope
v_0, v_1 and v_2	Velocity parameters.
$W_0(f)$	S wave source amplitude
S(f)	Site response
T(f)	S-to-coda transfer function
D(r, f)	Effect of geometrical spreading and attenuation
H	Heaviside step function
v(r)	Distance dependent peak velocity of direct arrival (S wave)
$\gamma(r)$ and b(r)	Distance dependent coda shape factors
b_0, b_1 and b2	Coda shape parameters that control the late coda decay
γ_0, γ_1 and γ_2	Coda shape parameters that control the early coda decay
$P(f,r)$	Source normalized coda amplitude
p_1 and p_2	Path parameters
M_L	Local magnitude
M_S	Surface waves magnitude
M_W	Moment magnitude
m_b	Body waves magnitude
M_d	Duration magnitude
M_W(coda)	Coda-derived moment magnitude
M_W(waveform)	Waveform modeled moment magnitude
M_0	Seismic moment

1. INTRODUCTION

The magnitude concept, which is related to the energy released after an earthquake, constitutes one of the major part of the seismology. Since, it is used to establish accurate and reliable regional earthquake catalogs and determine the seismic hazard potential of a region while it gives important information about the source size and its characteristics, a stable and reliable magnitude estimations is crucial for sparse local and regional seismic networks at regional distances. Moreover, in the context of underground nuclear explosion monitoring, accurate magnitude estimations is important to be able to increase the efficiency of seismic discriminants (*e.g.*, M_s:m_b, m_b:M_o) and determine nuclear explosion yield since seismic discriminants are usually obtained by using some techniques based on the ratio of amplitudes of long-period surface waves to short-period body waves (M_s:m_b) or the ratio of amplitudes of P waves to S waves.

Today, in seismology, there are a lots of efforts to get a better way to estimate a stable regional magnitude. We will mention about main basic approaches being used in magnitude determinations in chapter two. Especially at regional distances, the variability of direct arrivals causes an amplitude scattering. Thus, the multi-station averaging is necessary to reduce the amplitude scatters. Because of the limited number of stations at regional distances, it becomes difficult to measure a reliable and stable magnitude for small to moderate sized events when the distance between stations is large enough (~ 1500 km). The time-domain measurements, which contain a large portion of a seismogram allow us to average the scattered wavefield. This results in the stability of coda analysis.

Contrary to the traditional regional magnitudes (e.g., $m_b(P_n)$, $m_b(P_g)$, $m_b(L_g)$, M_s, M_d), the method based on coda-derived moment-rate spectra which is used in this study gives us reliable and stable results because it is not affected by undesirable effects of source radiation pattern, 3-D path heterogeneity. They are also insensitive to the phase blockage and destructive and constructive interferences near the recording site.Although direct arrivals on seismograms seems to be clipped in some cases, coda can be used for estimating source spectra .

First, in 1969, Keiiti Aki observed the later portion of a seismogram and he called this wavefield "coda waves". According to Aki, coda waves are described as scattered waves caused by random heterogeneity in the Earth's litosphere. He also emphasized coda waves could be used to estimate the source excitation characteristics. In the following years, Aki and Chouet (1975) proposed the single back scattering model which explains the coda excitation and the coda envelopes of local earthquakes phenomenologically. In 1993, Mayeda applied coda method to Nevada Test Site explosions (NTS) data recorded by four regional broadband stations of Lawrence Livermore National Laboratory (LLNL). Finally, he found that an m_b obtained by ~1 Hz. regional coda envelopes were considerably more stable (factor of 4 to 5) than those based on P_n and L_g. Hartse *et al.* (1995) analyzed 27 NTS explosions and 15 southern Great Basin earthquakes by applying the coda method. They formed 'type curves' which reflects the average shape of all individual coda decay curves for a special frequency band and defined a relative source size of an event as the amplitude difference between and individual event coda decay curve and the type curve. In another study, Mayeda and Walter (1996) obtained the coda-based source spectra of the earthquakes throughout the western United States by using observed narrowband coda envelopes. Their study was different than Hartse's and Mayeda's studies in two ways. First, they observed earthquakes at regional distances. Second, they used 2-D distance dependent multiple scattering model were in order to form a synthetic narrowband coda envelopes.

Mayeda *et al.* (2003) developed an emprical methodology based on the amplitude measurements of narrowband S-coda envelopes for finding moment-rate spectra (Figure 1.1). They tested their approach on local and near-regional events located along the Dead Sea rift without using complicated scattering models. Their basic approach was to use only the single back scattering model of Aki to define the coda wave excitation. The emprical formulation comprised the distance-derived changes in coda envelope shape both for local and regional distances and the S-to-coda transfer function effects. In addition to finding coda shape factors which control the coda decay, the other innovation in this approach was that they did not need any therotical assumption explaining coda excitation and scattering in the correction of the measurements for path effects. They demonstrated also the larger scatter associated with coda duration magnitudes (M_d), direct wave magnitudes or amplitudes and attributed this large scatter to firstly the duration which is the function of the predominant frequency of the event, which may strongly carry the effects of the station site response and secondly to the coda attenuation properties which may vary laterally.

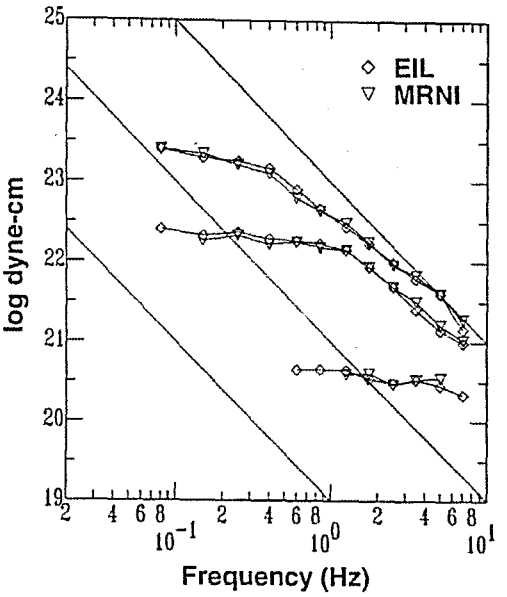

Figure 1.1 Some source spectra examples obtained from S-coda amplitude measurements. Triangles represent the coda amplitudes measured at station MRNI while diamonds show those measured at station EIL for the same events. From the figure, a strong consistency between two stations is easily seen (Mayeda *et al.*, 2003).

In the following chapter, summary information about some basic approaches that are still in use for quantifying the size of earthquakes (i.e., local magnitude, M_L, surface waves magnitude, M_s, body waves magnitude, m_b and moment magnitude, M_W) is given. In chapter 3, the concept of coda is examined and some major studies based on coda waves in various research fields of seismology are compiled. In chapter 4, the basis of the single backscattering model that plays an important role in the development of the method used in this study as well as the evolution of other theories and approaches with regard to coda waves are presented. In chapter five, coda derived magnitude calibration method is applied to the earthquakes in and around Turkey by making use of the observations from three broad band stations namely ISP, ISK, MALT. The main goal of this study is to show that the stable coda-derived magnitude methodology is transportable from a region to another region. During the application of the method, dimensionless coda envelope amplitudes of each earthquake in our data-set are measured and then coda amplitude measurements are corrected for distance and frequency dependent effects to be able to tie coda-based moment rate spectra to an absolute scale, seismic moment-rate spectra, and to make moment magnitude estimations based on coda

amplitude measurements. Coda-based moment magnitude estimation results are validated by those obtained by the waveform modeled moment magnitudes and consistent moment magnitudes estimations based on coda magnitude methodology are presented in this chapter. Finally in chapter 6, results are discussed and compared with those obtained from the previous studies using the same approach. Also, some advantages of the coda-based magnitude methodology are listed.

2. BASIC APPROACHES IN SIZING UP EARTHQUAKES

Today, sizing up an earthquake is related to the determining of seismic moment which characterizes a mechanical process that takes place over the opposite sides of a fault due to the interaction between the blocks of the crust. Seismic moment is obtained from spectral analysis of seismic waves in frequency domain as well as from the field observations of rupture area and average slip. However, seismologists started to study on estimating the size of earthquakes in the earlier times. For this purpose, they benefited from the amplitudes of direct phases such as P or S wave and developed several some magnitude scales that are determined from the amplitudes or duration measurements of seismic waves. Today there are 4 basic magnitude scale based on the amplitude measurements. These are local magnitude, M_L, surface waves magnitude, M_s, body waves magnitude, m_b and moment magnitude, M_W respectively. The use of another approach based on the total duration of the signal on a seismogram is also quite widespread in sizing up local earthquakes (Duration magnitude, M_d).

2.1. Local Magnitude, M_L

In the early 1930s, Charles Richter first introduced a magnitude scale, M_L to classify the relative size of local earthquakes in California. The local magnitude, M_L, developed by Richter (1935) is given by:

$$M_L = \log A_{max} - \log A_0 \text{ (km)} \qquad (2.1)$$

where A_{max} is the maximum amplitude in mm on the Wood-Anderson seismogram and A_0 is the displacement of a reference event with M_L=0 that corresponds to $A_0 = 1x10^{-3}$ m at an epicentral distance of 100 km. Local magnitude scale, M_L devised by Richter is basically obtained by taking the logarithm of the largest deflection on a certain point of a seismogram and then correcting it for the epicentral distance. Since the M_L values show a variability for the same earthquake due to the stations and source radiation pattern, they are averaged in a least square sense in order to obtain an M_L value. However it does not represent a measure of physical quantity such as energy, velocity, etc.

2.2. Surface Waves Magnitude, M_s

At large distances, the long-period seismograms are composed of of surface waves and the amplitudes of surface waves change strongly with increasing source depth. In 1940s, Gutenberg and Richter used surface waves in magnitude estimations for shallow earthquakes with an epicentral distance greater than 600 km. They introduced the following equation to calculate a magnitude scale based on surface waves :

$$M_s = \log A_{max} - \log A_0 (\Delta^0) \qquad (2.2)$$

where A_{max} indicates maximum ground amplitude in microns for surface waves observed on a long-period seismogram with a period of 20 seconds and A_0 represents the amplitude of a reference event with $M_s = 0$. A_0 is a distant-dependent parameter.

2.3. Body Waves Magnitude, m_b

Although surface waves magnitude, M_s is designed for distant earthquakes, the use of surface waves brings some disadvantages along in determining magnitude since surface waves are sensitive to the focal depth. This results in that deep earthquakes do not yield efficient and observable surface waves on long-period seismograms. For intermediate and deep earthquakes, Gutenberg used short-period body wave amplitudes (P, PP, and S) and developed the general form of body wave magnitude scale, m_b:

$$m_b = \log(A_{max}/T) - Q(\Delta,h) \qquad (2.3)$$

where A_{max} is the maximum ground amplitude in micron, T is the period (second) and $Q(\Delta,h)$ is a distant and depth dependent factor. General expectation was that these three magnitude scales must give rougly the same magnitude value for a common earthquake. But Richter (1958) observed that M_L, M_s, and m_b could be the same only at around magnitude 6.75. Gutenberg and Richter suggested an emprical relationship between M_s, and m_b expressed by:

$$mb = (1-a).M_s + b = 0.63.M_s + 2.5 = M_s - 0.37.(M_s - 6.76) \qquad (2.4)$$

Although the use of direct phase amplitudes is regarded as an alternative way for determining earthquake magnitude, it has also some disadvantages. Since many observatories use low-dynamic range instruments in their local and regional networks, recording of even moderate-sized earthquake often suffer from an extensive signal clipping of the direct phase arrivals. Moreover, today it is obvious that the energy distribution as a function of frequency vary with the size of earthquakes. Aki (1967) showed that the low frequency waves contained a larger part of radiated seismic energy than higher frequencies as the size of earthquakes increased. For larger earthquakes, below the corner frequency, amplitude spectrum yields rougly flat shape and much higher level compared with smaller events. Such a freqeuncy-dependent behavior in spectral content results in the saturation of magnitude measured from the peak amplitudes with a major frequency higher than the corner frequency.

2.4. Duration Magnitude, M_d

Bisztricsany (1958) was the first person who treated signal duration instead of using maximum amplitudes of seismic wave types in magnitude determinations. He correlated the magnitudes changing between 5.0 and 8.0 with duration of surface waves at epicentral distances between 4^0 and 160^0. Later on, Soloviev (1965) utilized only total duration for magnitude estimations in a similar way. Tsumura (1967) made a study on magnitude estiminatios from total duration measurements for local earthquakes recorded by the Wakayama microearthquake network in Japan. Finally he developed an emprical relationship between total duration and magnitude calculated by Japan Meteorological Agency. General form of the relationship between signal duration and magnitude is defined by :

$$M_d = a_1 + a_2.\log(\tau) + a_3.\Delta \qquad (2.5)$$

where τ is signal duration in seconds, Δ is epicentral distance (km) and a_1, a_2 and a_3 are constants depending on the station, attenuation and distance, respectively. Another emprical formula between signal duration and local magnitude of 351 earthquakes in central California was introduced by Lee et al., (1972). They measured the signal duration starting from P waves and found the following relation :

$$M_d = -0.87 + 2.0.\log\tau + 0.0035.\Delta \qquad (2.6)$$

where τ indicates signal duration (seconds) and Δ is distance in km.

Signal duration-based approach has become a prevalent technique in magnitude estimations of local earthquakes since 1972. However the use of duration has brought some difficulties and drawbacks along due to the fact that it was sensitive local structure, noise and instrument type. Mayeda (2003) pointed out that there was a large interstation scatter between the coda duration magnitudes measured from two short-period stations separated by roughly 50 km (Figure 2.1). He ascribed this large scatter to the predominant frequency that affected on coda duration and to the geographic biases.

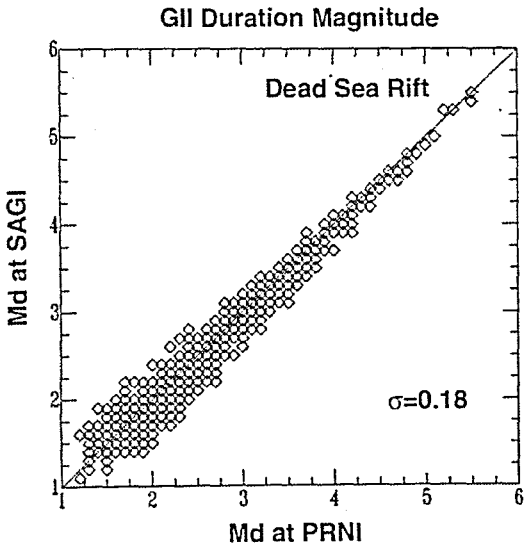

Figure 2.1 The relation between Md determined for the same events from the data of two stations, PRNI and SAGI rougly separated by ~50 km. Figures shows a large interstation scatter between these two station even there is ~50 km distance between two stations (Mayeda *et al.*, 2003).

2.5 Seismic Moment, M_0 and Moment Magnitude, M_w

To circumvent the saturation problem, seismic moment, M_0, which is related to the physical property of earthquake source, is used for the quantification of earthquakes. Seismic moment is described as a driving force which has a particular direction in three dimensional space and causes a movement on two dimensional fault having its own direction. Although this characteristics of driving force make the determining of seismic moment difficult, seismologists utilize scalar moment in magnitude estimations. Considering that an earthquake is a result of the interaction between the opposite block of the crust on a fault, scalar seismic moment can explain the mechanical process which takes place during an earthquake. Scalar seismic moment can be obtained from direct field observations by ;

$$M_0 = \mu.u.A \qquad (2.7)$$

where M_0 is seismic moment, μ represents the rigidity or shear wave resistance which is a measure of material strength, u indicates average fault displacement and A defines the rupture area. Figure 2.2 presents a cartoon show of the relationship between fault area and moment magnitude.

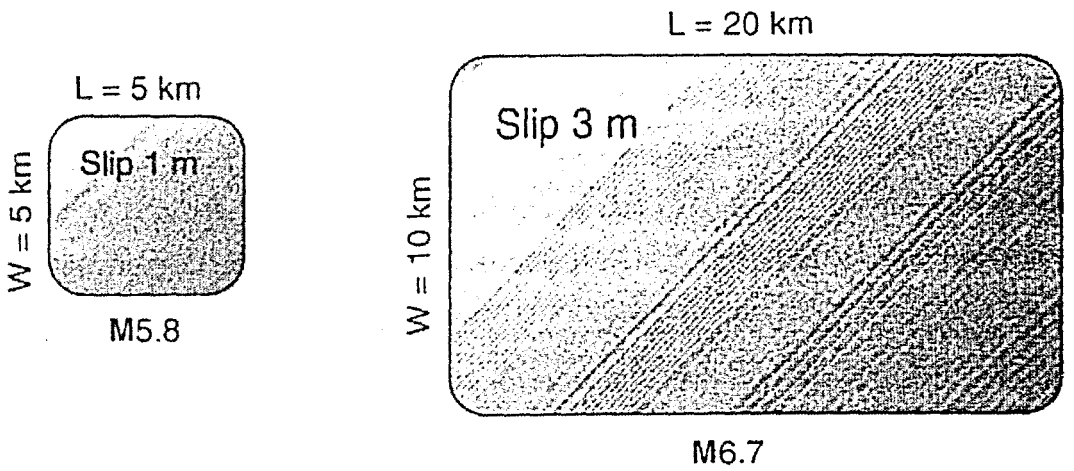

Figure 2.2 A cartoon illustration showing the effect of rupture area and amount of slip on seismic moment (Hough, S. E., 2002).

Brune (1970) suggested that the far-field source displacement spectrum was flat at low frequency and varied proportional with seismic moment, M_0. The analytic expression of source scaling is given by Aki and Richards (1980) within the following equation :

$$\Omega(\omega) = k.M_0 / [1 + (\omega/\omega_0)^2]^{\gamma/2} \qquad (2.8)$$

where $\Omega(\omega)$ indicates the source displacement amplitude, M_0 is the seismic moment, k is a constant which characterizes the proportionality between source displacement and seismic moment, ω is the angular frequency, ω_0 is the corner frequency and γ is related to the shape of the spectrum at high frequencies. Hanks and Thatcher (1972) also utilized the spectral amplitude of seismic waves to determine seismic moment, M_0. According to them, the relation between the seismic moment and spectral level of the long-period shear waves is given by :

$$M_0 = 4\pi.\rho.\upsilon_S^3.\Delta.\Omega_0 \qquad (2.9)$$

where M_0 is seismic moment, ρ is rock density, Δ is hypocentral distance, υ_S is shear-wave velocity and Ω_0 reprensents spectral level of low frequency shear waves.

Although seismic moment is the best way to size up the eatrhquakes source, it is difficult to report an earthquake size by directly seismic moment since seismic moment values show a great variation ranging from the moment of 1 to tens orders of magnitude. To avoid the great deal of numbers in reporting an earthquake size, Hanks and Kanamori (1979) introduced a new magnitude scale based on seismic moment which is defined by :

$$M_W = \log_{10}(M_0/1.5) - 10.7 \quad (\text{Mo in dyne-cm}) \qquad (2.10)$$

The moment magnitude scale has many advantages compared with the others mentioned in the paragraphs above. First of all, it is directly related to the physical properties of the source size and it never suffers from the saturation problem unlike the traditional direct phase amplitude-based magnitude scales. In other words, it represents the actual size of the source. Moreover, it is used for both deep and shallow earthquakes.

3.THE HISTORICAL BACKGROUND OF THE STUDIES ON CODA WAVES

The historical development of the studies on coda waves starts with the Aki's observations in 1960s. In 1969, Keiiti Aki examined the later portions of high frequency regional seismograms and he named these wavefield "coda waves" in order to identify the last part of seismograms following direct arrivals (Figure 3.1). According to his observations, unlike the direct waves that form the early portion of seismograms and have a decreasing amplitude with increasing distance, the overall amplitude of coda waves at all stations was showing some similarities that pointed out that the amplitude of coda waves did not depend on epicentral distance. He also encountered analogous spectral properties among the stations as well as similar coda amplitudes. Finally, he proposed that the incoherent scattered waves of local earthquakes, which resulted from the random heterogeneity, distributed uniformly in the Earth's lithosphere caused the coda waves on regional seismograms. Aki also suggested that the spectral content of coda waves could provide with a strong tool the seismologists to study on source excitation characteristics.

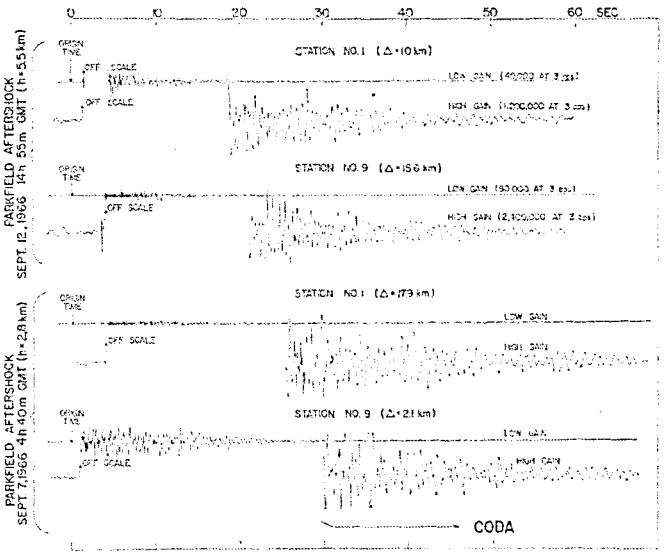

Figure 3.1 Waveforms from two aftershocks of the Parkfield earthquake recorded at two temporary stations of U.S.G.S. Coda waves, the later portion of seismograms, seem to have similar spectral shape, especially, on high gain traces (Aki, K., 1969).

Aki and Chouet (1975) analyzed the coda waves for some small local earthquakes, which occured at central California and western Japan by benefiting from the findings of previous studies on coda waves. They interpreted the coda waves as a backscattered waves from a number of heterogeneities distributed randomly in the earth's crust. They proposed two models which explains the generation of coda waves. The first model is the single backscattering model in which scattering process is weak. In this model, the loss of seismic energy due to the scattering is neglected. The second model is the diffusion model suggesting that seismic energy propagates by a diffusion process. In their study, they used both two models allowing a proper discrimination of source effect from scattering and attenuation effects (Figure 3.2). They also found that the coda waves were composed of backscattered surface waves at low frequencies less than 10 Hz. while they were made of backscattering body waves for the higher frequencies. These results were characteristic of Western Japan and Central California earthquakes. They also emphasized following facts about coda waves at epicentral distance of less than about 100 km:

1-) The spectral contents of later portion of a local earthquake seismogram are nearly the same for all recording stations while there are a significant differences among the spectra of the early part for the same earthquakes (Aki, 1956, 1969).

2-) The epicentral distance or azimuth do not affect on the total duration of a seismogram of a local earthquake at epicentral distance less than about 100 km (see Figure 3.3). Total duration of a seismogram, in this case, can be used effectively as a measure of earthquake magnitude (Bisztricsany, 1958; Soloviev, 1965; Tsumura,1967; Lee al., 1972).

3-) For the different local earthquakes, the power spectra of coda waves show a decreasing as a function of time (see Figure 3.3). Decay of coda waves power spectra are not related to the distance and the nature of the wave path between epicenter and station (Aki, 1969; 1975).

4-) For the earthquakes whose magnitudes are les than M=6 ,the temporal shape of narrowband coda waves is independent of magnitude (Aki, 1969; 1975).

5-) The excitation of coda waves depends on the local geology at the recording sites (Aki, 1969).

The other parameter that they introduced with their paper was coda Q (Qc), which was defining the non-dimensional measure of the decrease in amplitudes of coda waves during the wave propagation. They first considered that Qc only depended on the attenuation caused by anelasticity of the earth medium in the single-scattering model. In addition to anelastic loss, they took the energy loss resulted from scattering into account in diffusion theory. They measured Qc from the decay rate of coda at a certain frequency band and observed that this

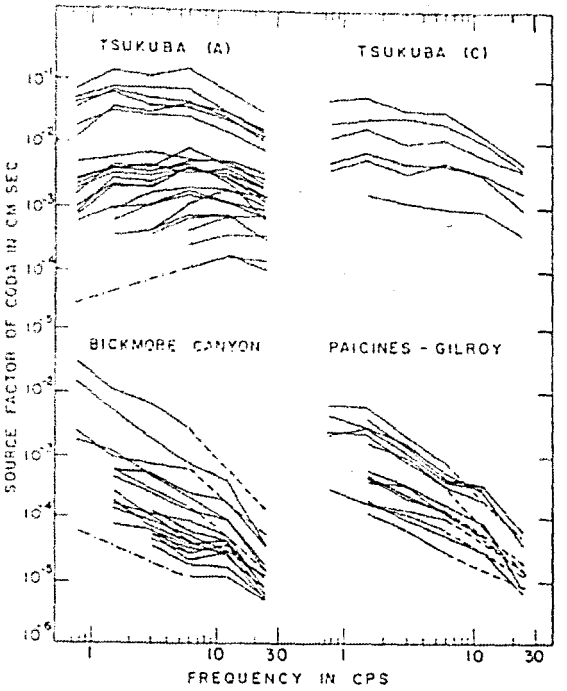

Figure 3.2 Source factors obtained from coda waves in a frequency range changing from 1 to 25 Hz at Tsukuba, Japan and Stone Canyon, California (Aki and Chouet, 1975).

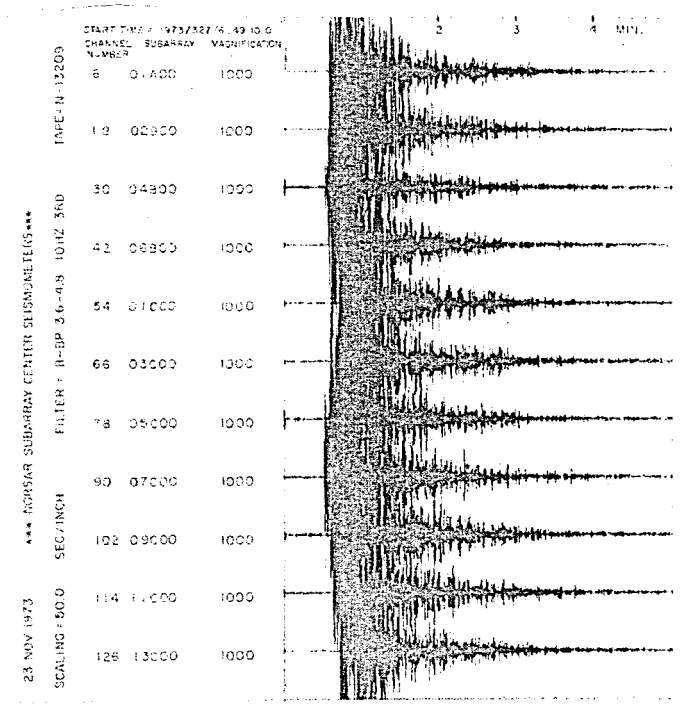

Figure3.3 Waveforms of a local earthquake recorded at a subarray of NORSAR. Epicentral distance is changing from a few kilometers to more than 100 km. The the shape of coda decay seems to be similar without depending on the different wave paths between the event source and receiver (Aki and Chouet, 1975).

decay rate was not related to the location of the events and recording site for the earthquakes occurring at an epicentral distance less than about 100 km.

Rautian and Khalturin (1978) analyzed the spectral content and differences among the coda waves in time domain. Their purposes were to show the dependence of the shape of coda envelopes due to the attenuation, site conditions and wave types composing the coda and to demonstrate that the spectral content of coda waves could be used for estimating source characteristics in different regions (Figure 3.4). They indicated the existence of two factors which affected on the spectral content of coda and the shape of coda decay with time. One of these two factors is related to the radiation pattern from the source to the receiver and it does not affect on decay with time. The other factor is based on the medium properties and it plays an important role in the decay of coda with time. They also suggested that the second factor determined the transformation of a radiated impulse into scattered waves. Following the study of Aki and Chouet (1975) which aimed to reveal the characteristics of coda waves from local earthquake seismograms recorded on the Earth, Nakamura, 1977 and Dainty and Toksöz, 1981 examined coda waves obtained from the lunar seismograms by applying the diffusion model. Dainty and Toksöz claimed that the diffusion model based on a strong scattering process would be only valid for the conditions under the moon's litosphere.

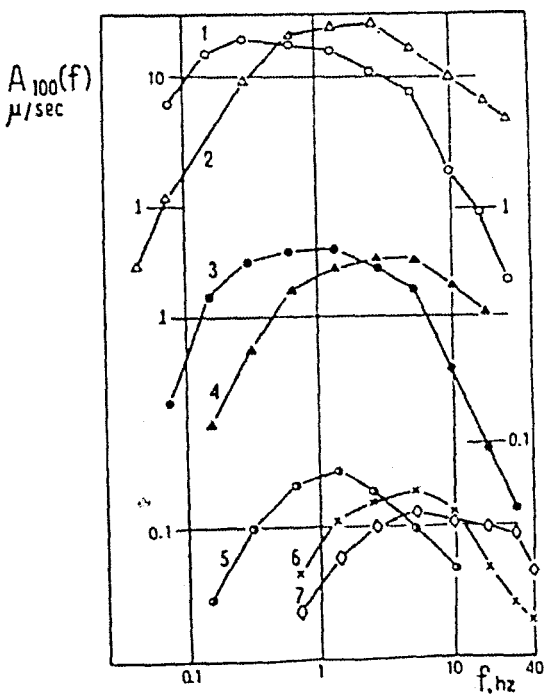

Figure 3.4 Coda source spectra found for the events recorded at different regions (Rautian and Khalturin, 1978).

Observational and theoretical studies on the attenuation of coda waves indicate that ,for a given region, Qc is the sum of the attenuation caused by anelastic energy loss, Qa and attenuation resulted from scattering, Qs. There are some models and approachs regarding scattering process which were developed in order to separate intrinsic Q (Qa) and scattering Q (Qs) from each other and estimate them as a function of frequency. Some of these models and approaches are Energy Flux Model (Frankel and Wennenberg, 1987), Radiative Transfer approach (Wu and Aki, 1988), Multiple Lapse Time Window analysis (Fehler *et al.*, 1992; Mayeda *et al.*, 1992). As the consequence of the researches using above approaches, it is obvious that Qc is a crucial parameter in that it provides with information about the crustal heterogeneities and characterizes the tectonic activity of a region however the results from the separation of Qa and Qs do not yield a reasonable relationship between intrinsic and scattering Q, Qa, Qs and coda Q, Qc.

There have been some studies made by Novello-Casanova *et al.*, 1985; Gusev and Lemzikov, 1985; Sato *et al.*, 1988; Jin and Aki, 1989, 1991; Frankel, 1991 which claimed that temporal and spatial variation in coda Q values would be a precursor of forthcoming seismic activity of a region. For instance, in 1989, Jin and Aki analyzed coda Q values measured from short period seismograms recorded at Riverside, California earthquakes during the period between 1933 and 1987 and they found that the Qc^{-1} values increased with increasing seismic b values which is defined by the ratio between the number of small to large earthquakes.

In addition to the studies of Qc, researchers used another observational approach called "Coda-Normalization Method" for separating the source effect which is controlled by the seismic source radiation from the recording site amplification on a seismogram. Source radiation is defined by the frequency dependence of seismic waves radiated from the source. The other influence appearing on a seismogram is the site amplification which is related to the near surface geology. Quantifying of these two effects as a function of frequency is quite important in seismic hazard assesments and sizing up the earthquakes. In fact, coda method provided with a robust and easy way to determine the seismic source radiation and site effect since it was purely emprical and did not require any initial knowledge of geology, velocity structure, source process, etc. The main idea in the basis of coda normalization method is that, at some lapse time, the coda energy does not vary in some volume surrounding the source. The results of the studies made by Aki and Chouet, 1975 and Ratuian and Khalturin, 1978

indicating similarities among the decay shapes which does not depend on the source-receiver distance also confirmed the starting point of the coda-normalization method.

The simple approach used in isolating site effect on a seismogram by using coda method is based on that the relative amplitudes of a signal recorded at two stations at the lapse time t_c which is quite large are considered to be the same in the case that there is not any local amplification caused by near-surface geology. Considering that two stations having different local geological characteristics, the relative amplitude of two stations for the same source can be measured by dividing the amplitude of the seismogram at one station by the amplitude at another one. In 1978, Tsujiura used the coda-normalization method to calculate the relative site amplification factors of coda waves and direct S-waves as a function of frequency. He aimed to find how the coda waves and direct S-waves were affected by the different site conditions for the same source. Finally, he observed the relative site amplification factors of two wave types (S-waves and coda waves) measured from station pairs were almost same in a frequency range from 0.75 to 24 Hz. This result strongly supported the idea that S-coda waves consisted of scattered S-waves. Later, Tucker and King (1984) also made a comparison of site amplification factors of coda waves and direct S arrivals. They observed similarities between the site factors of coda and direct S-waves as well as Tsujiura (1978). Phillips and Aki (1986) analyzed the digital data of over 90 local earthquakes recorded at 150 stations in Northern California to determine the frequency-dependent site amplification of each station of the array. In that study, they used an approach using multiple windows lapse times to analyze the data. Their approach was assuming that the site amplification at one station must be the same for the different earthquakes. In this method, the source radiation was regarded as the same for an earthquake recorded at all stations. They also assumed that the decay shapes of coda envelopes were independent of source-receiver distances and the conditions and recording site conditions. In conclusion, they proposed that the site factors could only vary with local geology of station sites without being affected by different earthquakes and window lapse times. Another study on determining the site amplification factors by using 15 stations in the Long Valley caldera region of Eastern Sierra Nevada was made by Mayeda *et al.,* (1991). In that study they used 154 local earthquakes in a magnitude range between 1.5 and 2.8. They selected a station, which had the granitic site as the reference station and calculated the amplification factors of each station relative to the reference site in six frequency bands between 1.5 and 15.0 Hz. They observed the amplifications at all station sites were five to 17 times larger than those measured at reference granite site at 1.5 and 3.0 Hz while the source

factor of each station relative to the reference one showed an inverse variation with higher frequencies. They attributed this to the effect of impedance contrast between the caldera fill and basement rock and high absorption in caldera region for higher frequencies. Their study indicated that the amount of the amplification might not be similar at sites having analogous surficial geology and emphasized that the absorption and impedance contrast due to the near surface geology could cause an unstable behavior in site amplifications at higher frequencies. Fehler *et al.,* (1992) determined site amplification factors of Kanto-Tokai region in Japan. They also compared the site factors that they found in that study with the magnitude residuals of local at different frequency bands. The results of comparison process at a centered frequency of 6.0 Hz was important in terms of pointing that one of the reasons of magnitude residuals obtained during magnitude estimations was the site effect since amplification factors showed a good agreement with magnitude residual values. In the same year, Koyanagi *et al.,* (1992) used the coda method to find the site factors of different sites in Hawaii by analyzing seismic data from Hawaiian Volcanò Observatory (HVO) network. They determined the site amplification factors by taking the ratios of S-coda amplitude spectra of 136 local earthquakes for a frequency band ranging from 1.5 to 15 Hz. According to their study, a similar frequency dependence of site factors existed among the stations however there were remarkable subsurface differences due to the underlying structure and lava flow characteristics. They proposed that such a behavior observed in the site amplifications, was related to what the frequency dependent site factors were affected by regional trends. They also studied on the relationship between the site amplification factors and earthquake magnitude residuals for the same events at different frequency ranges (1.5-15 Hz). This comparison of the site effects with independent determination of earthquake magnitude residuals resulted in a good agreement between 1.5 and 6.0 Hz. similar to previous studies (Fehler *et al.,* 1992 and Mayeda *et al.,* 1991).

Besides determining the recording site amplification factors, the coda-normalization method is used to quantify the seismic source radiation. Prior to the development of coda method to find out the source radiation and site effect, Aki (1967) investigated the relationship between the amplitude spectrum of seismic waves and source size. Finally he accomplishes to size up an earthquake using some spectral density curves depending on the frequency. The spectral density curves he obtained in that study yielded such displacement spectra that were flat at low frequencies and showing a decrease above a corner frequency.

Later on, the flat part in the displacement spectrum was utilized to calculate the seismic moment, which is a physical measure of earthquake size (Aki and Richards, 1980).

Recently, the amplitude spectrum of coda waves has been used to make an estimation of seismic moment rather than those obtained from direct arrivals. Since the coda waves sample some volume in which the seismic energy is distributed uniformly, the coda method does not requires any model or theory regarding source radiation and propagation effects in quantifying the size of earthquakes. This characteristic of coda waves allows us to determine an unbiased and stable size of a seismic source using the coda method. Biswas and Aki (1984) found an empirical relationship with the coda wave amplitudes measured at some lapse time after from the origin time and seismic moment by relating the time-dependent decay rate of coda amplitudes of two larger earthquakes in Alaska (Rampart and St. Elias) to their independent seismic moment estimations. In 1993, Mayeda used coda method to estimate the source sizes of some of Nevada Test Site (NTS) explosions. He measured the amplitudes of Lg-coda waves between 0.75 and 1.25 Hz. In that study, he showed that m_b obtained from Lg-coda waves at ~1 Hz were 3 to 4 times more stable than those obtained from direct Lg waves for the same stations and events (Figure 1.1). Mayeda and Walter (1996) used 2-D distant dependent scattered model to generate synthetic narrowband coda envelopes. They measured some coda amplitudes at each consecutive frequency band and finally they tied these non-dimensional coda amplitudes to an absolute scale, moment-rate spectra (Figure 1.3). Mayeda *et al.,* (2003) developed an empirical methodology based on the single scattering model of Aki and applied the method to the local and near regional events located along the Dead Sea rift. Their empirical method included S-to-coda transfer function effects and the distance dependent changes in coda envelopes shape both for local and regional epicentral distances. It also did not require the use of any theoretical assumption regarding coda excitation and scattering to correct the measurement for path effects. In that study, they measured the coda amplitudes of observed S-coda envelopes, which were band pass filtered in 14 frequency bands ranging from 0.02 to 8 Hz. Finally they tied the dimensionless coda amplitudes to an absolute scale namely, seismic moment rate spectra by making use of individually estimated seismic moment values of some reference events (Figure 3.5).

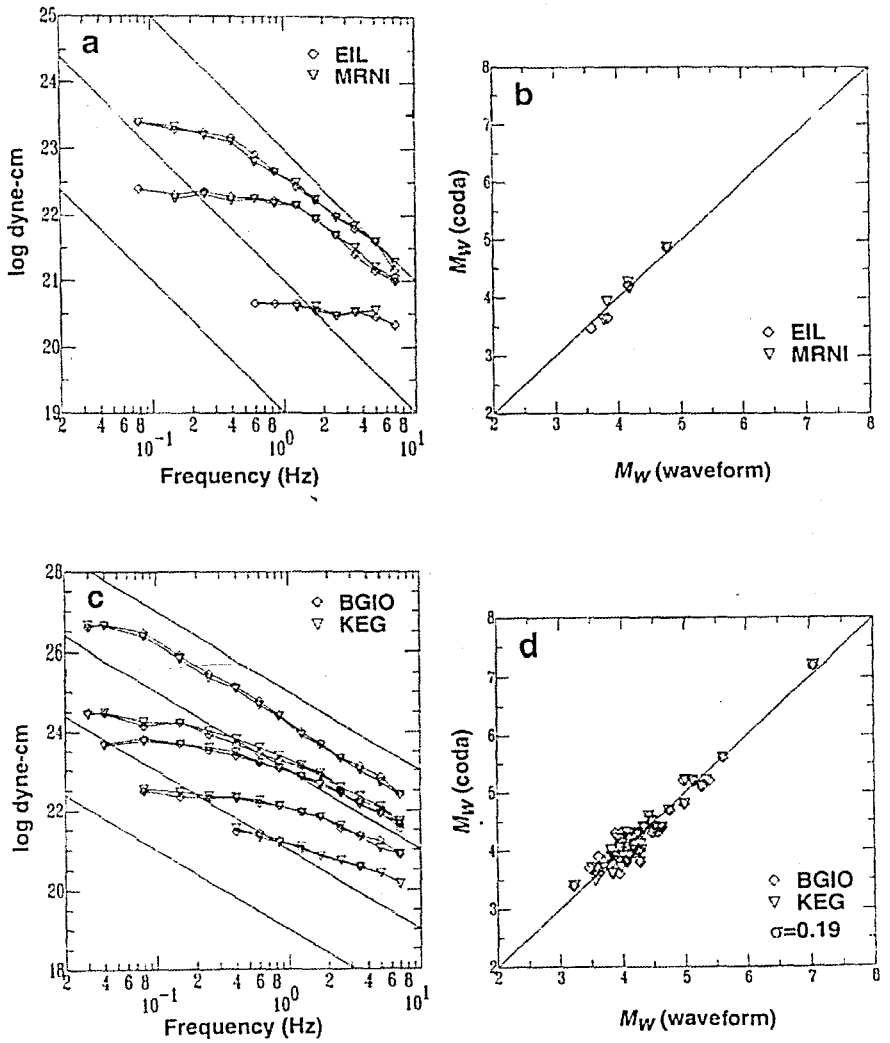

Figure 3.5 a) Some examples from coda amplitude-based source spectra for station EIL (diamonds) and MRNI (triangles), **b)** The relationship between coda derived moment magnitude estimations, M_W(coda) and individually derived moment magnitudes, M_W (waveform) of the same events for station EIL (diamonds) and MRNI (triangles), **c)** Coda derived source spectra of common events at BGIO (diamonds) and KEG (triangles), **d)** Another comparison relationship between coda derived moment magnitude estimations, M_W (coda) and individually derived moment magnitudes, M_W (waveform) of the same events for station BGIO (diamonds) and KEG (triangles) (Mayeda *et al.*, 2003).

4. THE SINGLE BACKSCATTERING MODEL

It is quite difficult to analyze high-frequency seismograms which are enormously influenced by lateral heterogeneities of the Earth's crust in order to determine the seismic source and wave path properties. For this purpose, the use of deterministic ways require the knowledge of well-modeled scattering and anelastic attenuation process of the Earth's litosphere along the wave path. On the other hand, the analysis of long-period surface waves controlled by the shallow part of Earth's crust is experienced successfully with deterministic approaches which assume the existence of a lateral homogeneous litosphere but it is insufficient for high-frequency wave analyses to be able to define crustal structure an seismic source characteristics (Aki, 1969).

As mentioned in previous chapters, with Aki's investigations showed that coda wave studies provide a robust and straightforward statistical approach in interpretation of crustal structure and determination of source parameters. In other words, coda waves analyses have brought easy and useful solutions along to some problems in analyzing high-frequency seismic waves.

In 1969, Aki first examined coda waves, the tail portion of high-frequency seismograms, and he proposed that seismic coda waves of local earthquakes are backscattering waves produced by a large number of heterogeneities distributed randomly and uniformly in the Earth's crust. According to him, numerous scatterers due to the lateral heterogeneities cause the superposition of primary waves to the extent of producing secondary waves on high-frequency seismograms. Later on Aki and Chouet (1975), made and extensive study on coda wave excitation of some small central California and western Japan earthquakes. In that study, they compared the duration of an earthquake considered to occur under the condition of an homogeneous Earth's litosphere with the observed signal duration of the same event. For this purpose, they used a simple way which is based on dividing the fault length by the rupture velocity in calculating the duration of an event. This process showed that the duration would be only a few seconds for an earthquake (M=6) with 10 km of the fault length. On the other hand, they observed that the duration of same event extended to a few hundred seconds on the seismogram. Thus, they attributed such a large difference between expected and observed signal duration to the scattered waves from a large number of heterogeneities in the Earth's crust as well as Aki (1969). They finally presented two theory in order to explain the

appearance of coda waves following direct arrivals such as P, S or surface waves on high frequency seismograms. These two theory are respectively the single backscattering model and diffusion model. In the single backscattering model, the scattering is aaumed to be a weak process which means the seismic energy loss due to the scattering can be neglected while in the latter, the seismic energy transfer is defined by a diffusion process. Aki and Chouet showed that both of two models were sufficient for the seperation of the source effect from attenuation and scattering effects on the spectra of coda waves.

Especially, the single scattering model has become an inspiring starting point for many researchers to design some statistical approaches in understanding the source, attenuation and site characteristics of the Earth's litosphere by using high-frequency seismograms. The basic idea in suggesting that a such statistical treatment can be devised by coda waves analyses depends on the fact that the coda portion of a seismogram is regarded as the results of same kind of averaging over many samples of heterogeneities. (Aki, 1969)

In our study, since we are benefiting from an emprical method based on the single scattering model in isolating the source size from site and attenuation effects, in this chapter, we will go into detail about the basis of the single backscattering model to have an insight into the the statistical techniques.

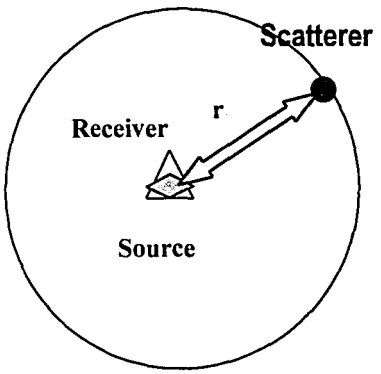

Figure 4.1 Basic illustration of single back scattering model. The single back-scattering model assumes that the source and receiver are located at the same place. Here r represents the distance from both source and receiver to the scatterer.

In the seismic scattering model, the seismic station and source are considered to be located at the same place (Figure 4.1). In this case, for a single scatter at a distance r, $\varnothing(\omega \backslash r)$ represents the Fourier transform of displacement caused by a wavelet, which is scattered backward, from this scatterer to the source. Considering that coda waves are made of the secondary waves from many scatterers due to the random distributed heterogeneities, N(r) indicates the number of scatterers within radius r of the station and N(r) in the zone limited by (r, r+Δr) is equal to (dN/dr). Δr. Since the secondary waves propagate with the same velocity, v as well as primary waves, the secondary waves scattered from the each heterogeneity in a distance range (r, r+Δr) will arrive at the station in the time interval (t, t+Δt), where t = 2r/v and Δt = 2Δr/v. Since Δt will be quite greater than t, which is the duration of a single backscattered wave as Δr is long enough, the total energy generated by each scattered wavelet arriving at the station in (t, t+Δt), is obtained from the multiplication of the power spectral density $P(\omega \backslash t)$ by Δt:

$$P(\omega \backslash t).\ \Delta t = \sum_{r < r_n < r+\Delta r} | \varnothing(\omega) |^2 = dN/dr.\Delta r.\ | \varnothing(\omega \backslash r) |^2 \qquad (4.1)$$

where r_n is the distance from the station to the nth scatterer. For the case where the scattering process happen to the body waves as primary waves, the density ,σ of scatterers is taken into account per unit volume. Thus, the number of scatterers within a spherical shell (r, r+Δr) is given by :

$$(dN \backslash dr).\ \Delta r = 4.\sigma.\pi.r^2.\ \Delta r \qquad (4.2)$$

Putting the equation (4.2) into the equation (4.1), we find the total energy of scattered body waves in a distance range (r, r+Δr) as the equation (4.3) :

$$P(\omega \backslash t).\ \Delta t = | \varnothing(\omega \backslash r) |^2 .4.\sigma.\pi.r^2.\ \Delta r \qquad (4.3)$$

On the other hand, considering the geometrical spreading, the amplitude spectra of the scattered waves which depend on travel distances is given by :

$$|\varnothing(\omega\backslash r)| = |\varnothing(\omega\backslash r_o)| . \left(\frac{r_0}{r}\right)^2 \qquad (4.4)$$

where r indicates the distance between station and scatterer and r_o is a reference distance.

Besides geometrical spreading, the anealastic attenuation which results in the transfer of seismic energy into the heat is added into (4.4), then the secondary wave intensity becomes:

$$|\varnothing(\omega\backslash r)| = |\varnothing(\omega\backslash r_o)| . \left(\frac{r_0}{r}\right)^2 . e^{-\omega t/2Q} \qquad (4.5)$$

where Q is the quality factor, the partial energy loss per 1 cycle is given by $2.\pi.Q^{-1}$ and attenuation of the scattered waves is defined by $(-\omega.t/Q)$, during the time period t.

Since $r = v.t/2$ and $\Delta r = \Delta t.v/2$, the power spectral density of coda waves

$$P(\omega\backslash t).\Delta t = |\varnothing(\omega\backslash r_0)|^2 .8. r_0^4 . \pi.\sigma.v^{-1}.t^{-2} . e^{-\omega t/Q} \qquad (4.6)$$

For the coda waves which are made of backscattered surface waves, the expression of power spectral density changes into the equation (4.7) :

$$P(\omega\backslash t).\Delta t = |\varnothing(\omega\backslash r_0)|^2 .2. r_0^2 . \pi.\sigma.t^{-1} . e^{-\omega t/Q} \qquad (4.7)$$

The general form of the power spectral density of coda waves both for body waves and surface waves is :

$$P(\omega\backslash t).\Delta t = S.t^{-m} . e^{-\omega t/Q} \qquad (4.8)$$

Here the constant term m is related to the geometrical spreading. S is called "source term" and depends on the size of earthquakes. The source term S includes both the effect of primary waves and secondary waves source. Aki and Chouet suggest that the secondary wave source must be common to all earthquakes as long as the composition of primary waves is the same

although the primary wave sources vary with earthquakes so that the difference in the source factor depends on the difference in the earthquake source.

Considering that the Fourier transform of a power spectrum is the autocorrelation function,

$$\varnothing(\tau) = \frac{1}{2\pi} \int_{-\infty}^{\infty} P(\omega \backslash t).e^{i\omega t}.d\omega \qquad (4.9)$$

for zero lag, where τ=0,

$$\varnothing(\tau) = \left[f^2(t)\right] = \frac{1}{2\pi} \int_{-\infty}^{\infty} P(\omega \backslash t).d\omega \qquad (4.10)$$

since $P(\omega \backslash t)$ will have a constant value, for a band pass filtered signal with ω_0 and ω_1 frequencies ($\omega_0 < |\omega| < \omega_1$), then

$$\left[f^2(t)\right] = 2.P.\Delta f \qquad (4.11)$$

where $\Delta f = (\omega_1 - \omega_0)/2\pi$

From 4.11, they find that twice the rms value will yield the analytic expression of coda amplitudes :

$$A(\omega \backslash t) = 2.[\ 2.P(\omega \backslash t).\Delta f\ ]^{1/2} \qquad (4.12)$$

After some arrangaments, they finally obtain the following form:

$$A(\omega \backslash t) = c.t^{-a}.e^{-\omega t/2Q} \qquad (4.13)$$

where c is the source factor at the frequency ω, a is a constant depending on geometrical spreading and Q represents the quality factor.

From 4.8 and 4.12, $c = 2.(2.\Delta f.S)^{1/2}$ and a=m/2. When the logarithm of both sides of equation 4.13 are taken, we get:

$$\log_{10} A(\omega \backslash t) = C - a.\log_{10} t - b.t \qquad (4.14)$$

Here C is represented by the logarithm of c and b is a parameter regarding the quality factor Q and given by $b = \frac{\pi.f}{Q}(\log e)$ (4.15)

Aki and Chouet finally achieved to define the coda amplitude as a combination of source factor, geometrical spreading and attenuation by analyzing coda waves. As seen from 4.15, the linear form of coda amplitude allows researchers to investigate separately these effects on high frequency seismograms.

5. METHODOLOGY OF REGIONAL MAGNITUDES BASED ON CODA-DERİVED MOMENT-RATE SPECTRA: AN APPLICATION TO TURKISH BROADBAND STATIONS.

5.1 Data

We used the waveform data obtained from three regional broad-band stations in Turkey respectively ISK, ISP and MALT broad-band stations. Our data set is divided into two parts because of the different operation periods of the regional broad-band stations.

The first dataset comprises well-located common events which occurred mostly throughout the Marmara and surrounding region during 1998 to 2001. It includes a large number of events which are the mainshocks and some aftershock sequences of the August 17, 1999, M_W 7.6, Izmit and November 12, 1999, M_W 7.2, Düzce earthqukes. We selected 182 common events to be processed which were recorded at three-component broad-band stations ISK and ISP in the distance range of ~30 to 1040 km (Figure 5.1). The magnitudes of these events ranges from the 4.0 M_d to the larger. We tested and verified the emprical distance corrections by using these events and then made a comparison between distance-corrected coda and corresponding direct wave measurements.

The second dataset used in this study includes the earthquakes which are mostly distributed all over Turkey compared with the events in the first dataset. We selected 137 common events observed by both ISP and MALT broad-band stations during the 2000 to 2002 in the distance range of ~30 to 1400 km (Figure 5.2). The magnitude range of these earthquakes are ranging from 3.2 to 6.5 according to the NEIC regional earthquake catalog. Source parameters of all earthquakes in both ISP-ISKB and ISP-MALT data set are given in Appendix A.

We applied the same emprical distance corrections for each station in each station pair. Thus, any amplitude scatter which could be observed between the stations in two station pairs can not be attributed to the gross path variations. The possible amplitude scatter can result from the the undesirable effect of the source radiation pattern, depth and random interference.

Figure 5.1 The distribution of selected 182 earthquakes in the ISP-ISKB data-set.

Figure 5.2 The distribution of 137 selected earthquakes in the ISP-MALT data-set.

5.2 Coda Calibration Method

In this chapter, the methodology will be defined including its procedures and results from applications to the earthquakes in our two data set. After collecting the regional broadband recordings of these earthquakes and removing the instrument response of each station (ISP, ISKB and MALT), we apply the following steps to calibrate each station.

1) Forming narrowband envelopes
2) Measuring the peak velocity of S-wave envelope
3) Fitting our narrowband observed coda envelopes with sytnthetics
4) Applying emprical distance corrections
5) Tiying the distance corrected and nondimensional coda amplitudes to an absolute scale using independently derived moments which were calculated by Orgulu (2001;2003) and taken from Harvard CMT catalogs.

The emprical procedure of the method used in this study accounts for all propagation, site, instrument and S-coda transfer function effects. At the final step, we use the coda-derived moment rate spectra in order to provide a stable, unbiased and unsaturated magnitude (moment magnitude, M_W) which is tied to a physical measure of earthquake size (i.e., seismic moment). To show the cosistence between our *coda derived moment magnitudes*, M_W(coda) and waveform modeled moment magnitudes, M_W(waveform), we make a comparison between these two type of magnitudes.

5.2.1. Forming Coda Envelopes

In the first step, an 8^{th} order, zero-phase (four poles, two passes) Butterworth filter is applied to two horizontal component of each broadband recording for 14 narrow and subsequent frequency bands ranging from 0.02 Hz. to 8.0 Hz. At that point, 14 frequency ranges are chosen by a such way that we can estimate M_W for the largest earthquake in our dataset and measure the coda amplitudes of smaller events at higher frequencies.

The following formulations are used to correct each horizontal component for noise and to form observed narrowband coda envelopes.

$$E(t\backslash f) = \log_{10}[\, e(t\backslash f)^2 - N \,]^{1/2} \qquad (5.1)$$

$$e(t\backslash f) = [\, v(t)^2 + h(t)^2 \,]^{1/2} \qquad (5.2)$$

where f is the center frequency, t is the time from the origin, v(t) is the band pass filtered seismogram which is corrected to ground velocity, h(t) is its corresponding Hilbert transform and N is the envelope of the noise preceding the event to be processed. In general, when we form the envelopes of the larger events which have a long coda and good signal to noise ratio, correcting the noise will not have an influence on our final results. However we obtain longer coda envelopes by applying noise correction procedure to small events.

After the noise correction, we take the logarithm of the envelopes, average and smooth two horizontal components. Figure 5.3, 5.4 and 5.5 show examples of two horizontal components recorded at stations ISKB, ISP and MALT and their corresponding coda envelopes at obtained at 14 frequency bands. We take note that the vertical component can be used during the formation of coda envelopes. However it is prefereable to utilize two horizontal components than the vertical components since the signal to noise ratios of S waves are better on horizontal components. Using of two horizontal components also allows us to obtain averaged and smoothed narrowband coda envelopes at each frequency band.

a

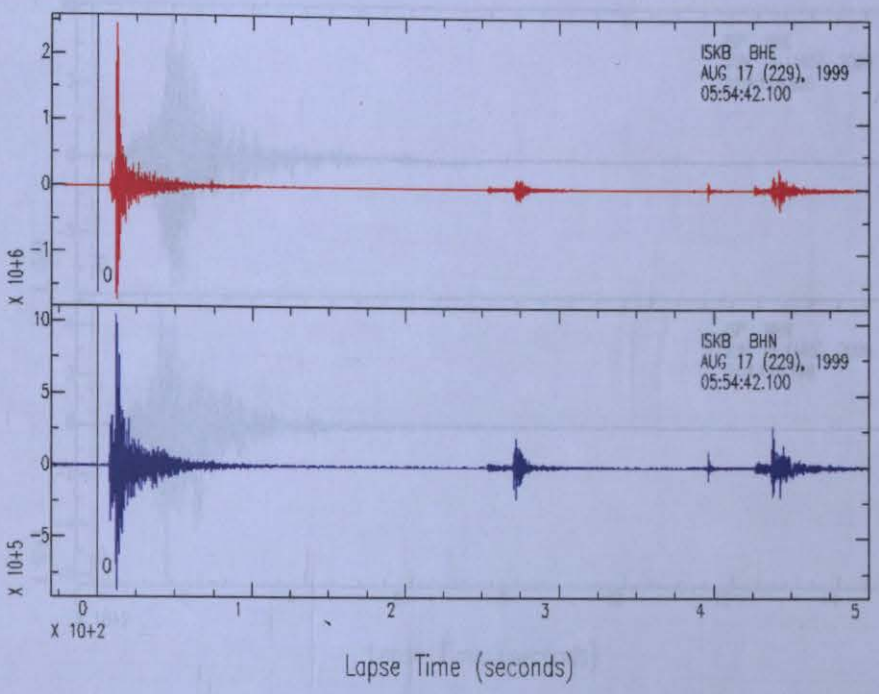

b

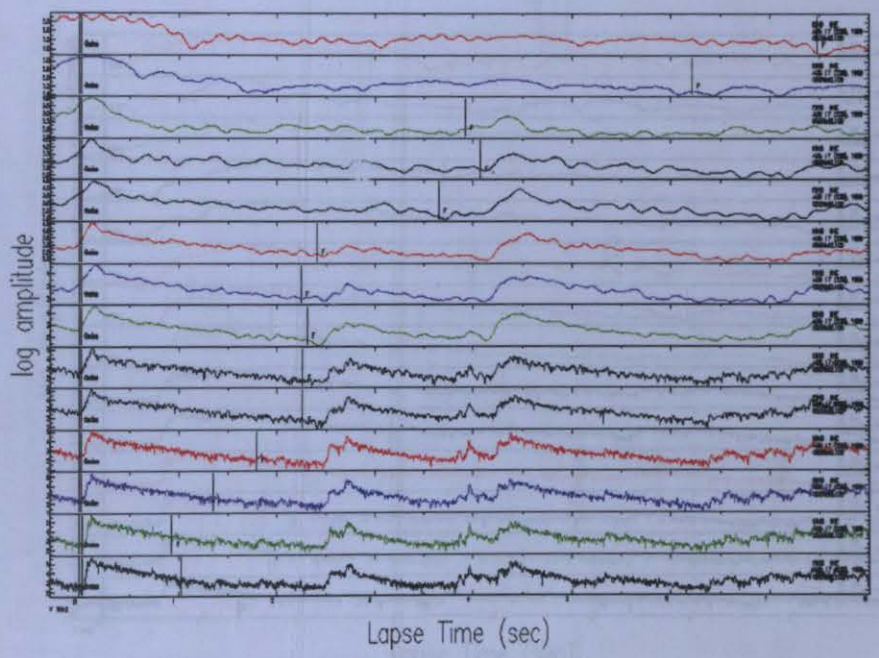

Figure 5.3 a) An example from two horizontal components recorded at ISKB and used in forming narrow band coda observed envelopes, **b)** The narrowband observed coda envelopes of these two horizontal components at 14 subsequent frequency band ranging between 0.02 and 8.0 Hz.

a

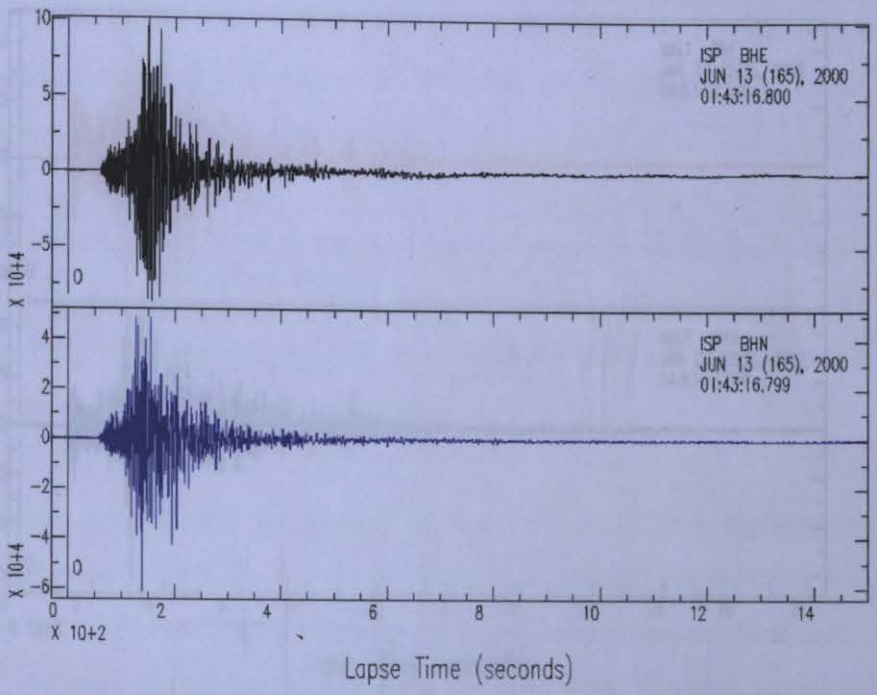

b

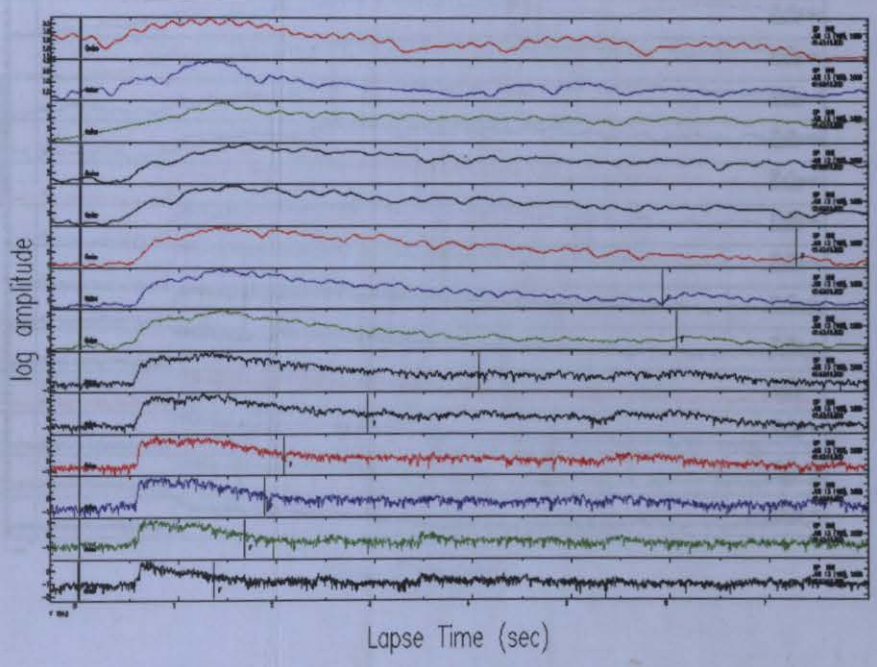

Figure 5.4 a) An example from two horizontal components recorded at ISP and used in forming narrow band coda observed envelopes, **b)** The narrowband observed coda envelopes of these two horizontal components at 14 subsequent frequency band ranging between 0.02 and 8.0 Hz.

a

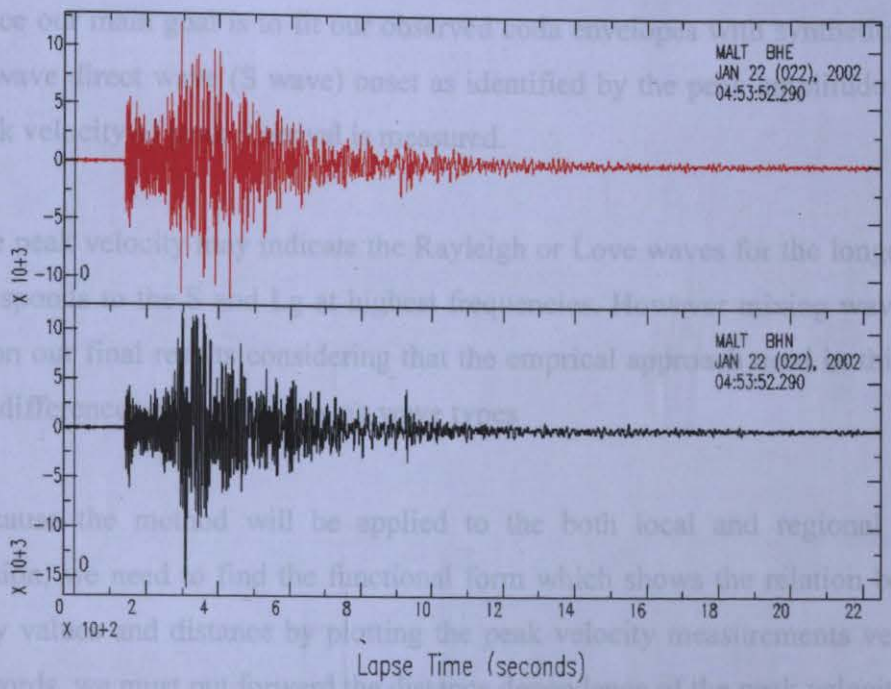

b

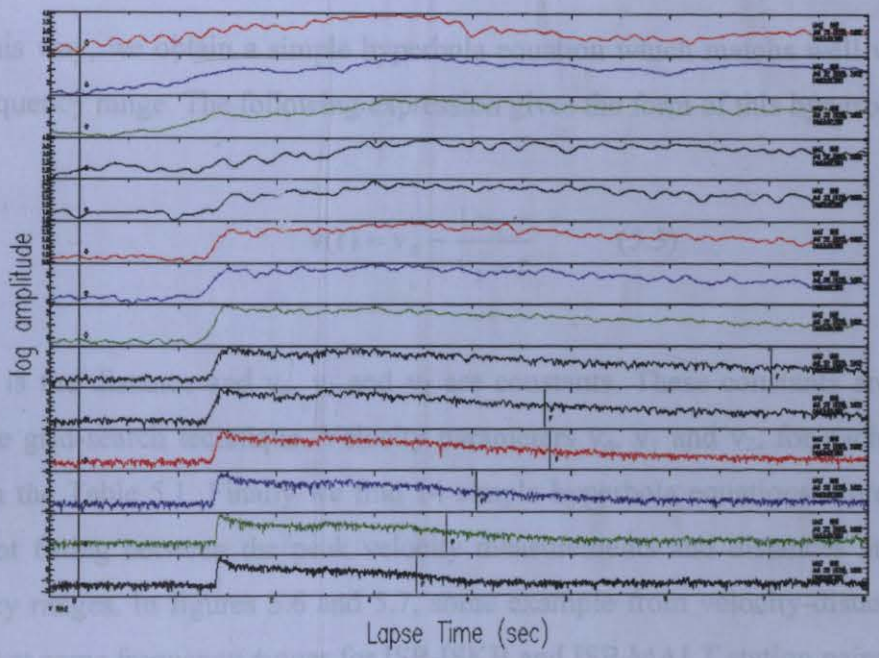

Figure 5.5 a) An example from two horizontal components recorded at MALT and used in forming narrow band coda observed envelopes, **b)** The narrowband observed coda envelopes of these two horizontal components at 14 subsequent frequency band ranging between 0.02 and 8.0 Hz.

5.2.2 Measuring the peak S wave velocity

Since our main goal is to fit our observed coda envelopes with synthetics that start at the direct wave direct wave (S wave) onset as identified by the peak amplitude of the envelope, the peak velocity of peak S arrival is measured.

The peak velocity may indicate the Rayleigh or Love waves for the longest periods while it corresponds to the S and Lg at highest frequencies. However mixing wave types does not affect on our final results considering that the emprical approach used in this study accounts for the differences caused by mixing wave types

Because the method will be applied to the both local and regional earthquakes for calibration, we need to find the functional form which shows the relation between our peak velocity values and distance by plotting the peak velocity measurements versus distance. In other words, we must put forward the distance dependence of the peak velocities.

In this way, we obtain a simple hyperbola equation which matchs well with our data for each frequency range. The following expression gives the form of this hyperbola :

$$v(r) = v_0 - \frac{v_1}{v_2 + r} \qquad (5.3)$$

where r is the distance and v_o, v_1 and v_2 are constants. These constants are determined by using the grid-search technique. Velocity parameters v_o, v_1 and v_2, for each station pair are given on the Table 5.1. Finally we find 14 simple hyperbola equations representing the best consistent fitting between the peak velocity measurements and distances at 14 narrowband frequency ranges. In figures 5.6 and 5.7, some example from velocity-distance relationships obtained at some frequency ranges for ISP-ISKB and ISP-MALT station pairs are given.

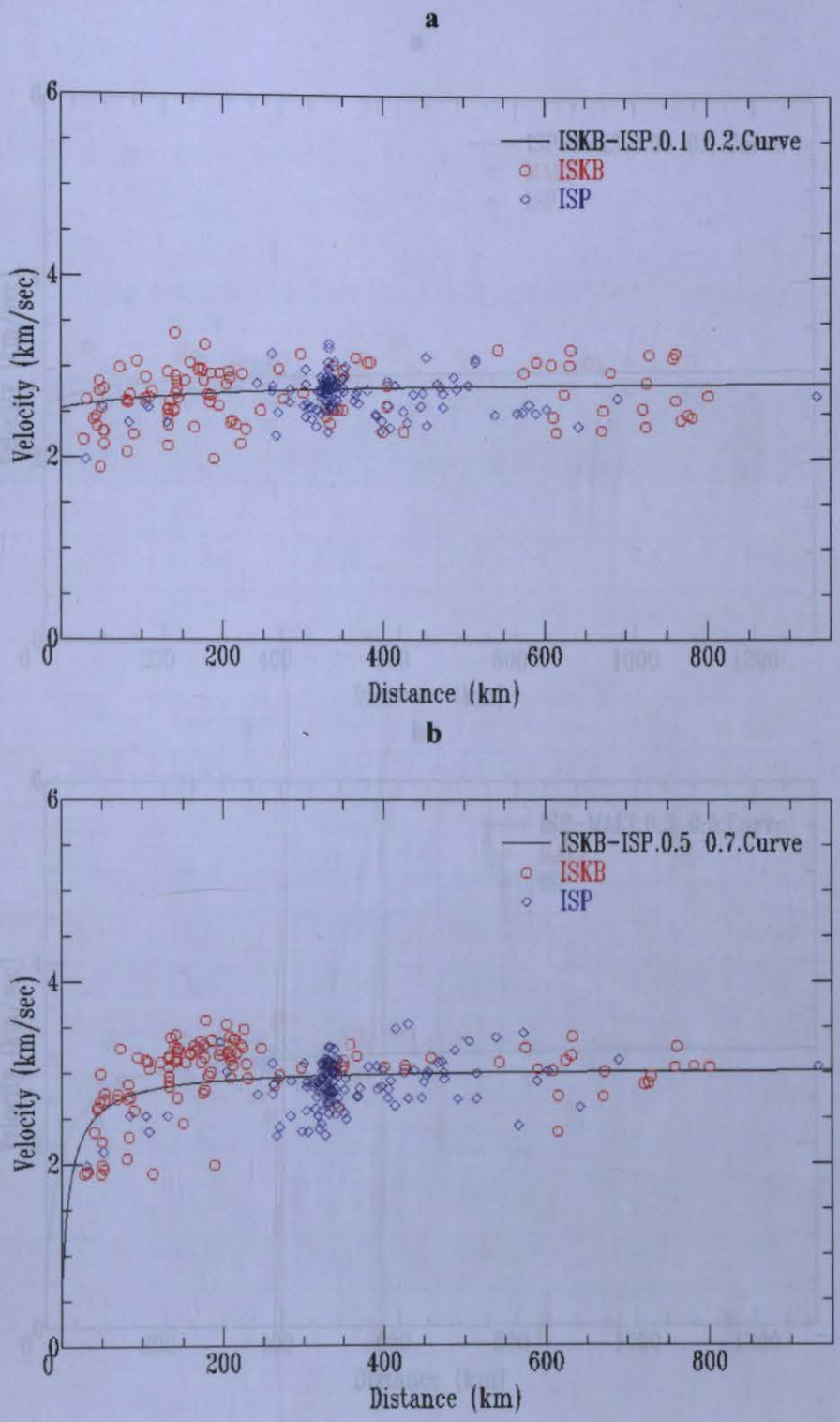

Figure 5.6 The peak velocities plotted versus distance at some frequency bands. **a**) The peak velocities as a function of distance at 0.1-0.2 Hz for the events recorded at ISP and ISKB stations, **b**) The peak velocities as a function of distance at 0.5-0.7 Hz for the events recorded at ISP and ISKB stations.

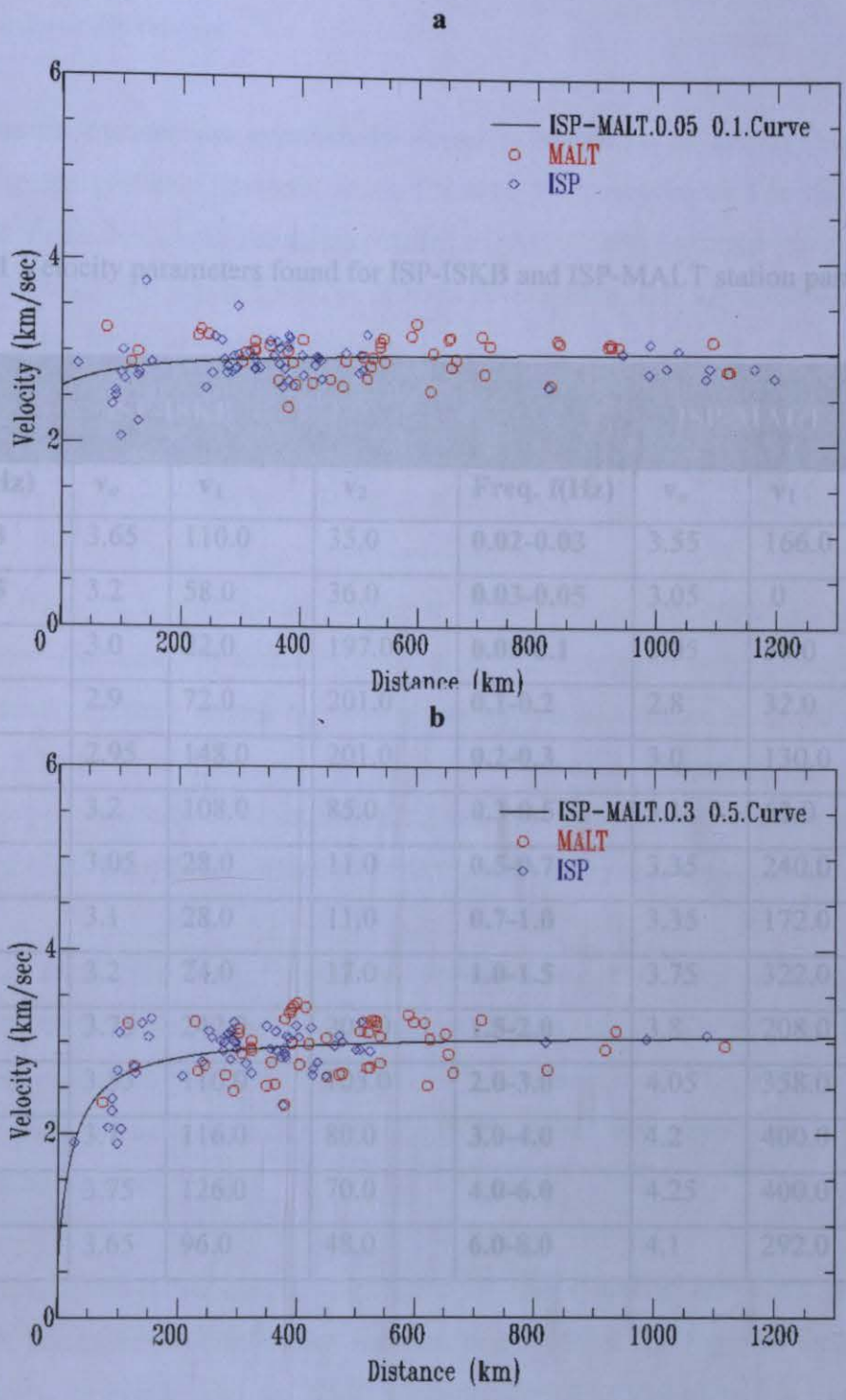

Figure 5.7 The peak velocities plotted versus distance at some frequency bands. **a**) The peak velocities as a function of distance at 0.05-0.1 Hz for the events recorded at ISP and MALT stations, **b**) The peak velocities as a function of distance at 0.3-0.5 Hz for the events recorded at ISP and MALT stations.

Table 5.1 Velocity parameters found for ISP-ISKB and ISP-MALT station pairs.

ISP-ISKB				ISP-MALT			
Freq. f(Hz)	v_0	v_1	v_2	**Freq. f(Hz)**	v_0	v_1	v_2
0.02-0.03	3.65	110.0	35.0	**0.02-0.03**	3.55	166.0	3.63
0.03-0.05	3.2	58.0	36.0	**0.03-0.05**	3.05	0	1.0
0.05-0.1	3.0	22.0	197.0	**0.05-0.1**	3.05	58.0	130.0
0.1-0.2	2.9	72.0	201.0	**0.1-0.2**	2.8	32.0	41.0
0.2-0.3	2.95	148.0	201.0	**0.2-0.3**	3.0	130.0	74.0
0.3-0.5	3.2	108.0	85.0	**0.3-0.5**	3.1	62.0	24.0
0.5-0.7	3.05	28.0	11.0	**0.5-0.7**	3.35	240.0	164.0
0.7-1.0	3.1	28.0	11.0	**0.7-1.0**	3.35	172.0	92.0
1.0-1.5	3.2	24.0	17.0	**1.0-1.5**	3.75	322.0	201.0
1.5-2.0	3.75	242.0	201.0	**1.5-2.0**	3.8	208.0	74.0
2.0-3.0	3.55	110.0	103.0	**2.0-3.0**	4.05	358.0	201.0
3.0-4.0	3.7	116.0	80.0	**3.0-4.0**	4.2	400.0	201.0
4.0-6.0	3.75	126.0	70.0	**4.0-6.0**	4.25	400.0	193.0
6.0-8.0	3.65	96.0	48.0	**6.0-8.0**	4.1	292.0	173.0

5.2.3 Synthetic Envelopes

In essence, the emprical approach developed by Mayeda *et al.* (2003) simply depends on generating the synthetic envelope forms for each frequency band. For this purpose, they benefited from the single scattering model of Aki (1969) in order to find an analytic expression which represents the shape of coda envelopes at both local and regional distances and they found the following formulation,

$$A_c(f, t\backslash r) = W_0(f) \cdot S(f) \cdot T(f) \cdot D(r,f) \cdot H\left[t - \frac{r}{v(r)}\right] \cdot \left[t - \frac{r}{v(r)}\right]^{-\gamma(r)} \cdot \exp\left[-b(r) \cdot \left(t - \frac{r}{v(r)}\right)\right] \quad (5.4)$$

where $W_0(f)$ is the S wave source amplitude, S(f) is the site response, T(f) is the S-to-coda transfer function caused by scattering conversion, D(r, f) represents the geometrical spreading and attenuation effects caused by both scattering and absorption, H is the Heaviside step function, t is the time from the origin, r is the distance in kilometers, v(r) is the distance dependent peak velocity of direct arrival (S wave) in km/sec, $\gamma(r)$ and b(r) are the distance dependent coda shape factors which controls the coda decay, f is the center frequency.

In this study, the same formulation described above is used to form our synthetic envelopes. An important point to be mentioned here is that the distance and time dependent parameters in the last part of the equation (5.4) are related to the shape of the coda envelope while the path attenuation term, D(r, f) controls the overall amplitude level of the envelope as a function of distance.

The reason why the analytic expression of the synthetic envelopes includes distant dependent parameters is that it must account for both local and regional earthquakes. Since the empirical approach does not assume any scattering model in which the attenuation is explained, it employs a distance dependent relation allowing for the attenuation and geometrical spreading which could be caused by scattering, absorption, leakage out of the waveguide, etc.

5.2.4. Finding Coda Shape Parameters

To summarize up to this point, first observed narrowband coda envelopes are formed and then the peak velocities of direct arrival (S wave) are measured as a function of distance. Now, we need to find coda shape parameters $\gamma(r)$ and $b(r)$ in order to put into the analytic expression of synthetic envelopes (Equation 5.4).

In application, the first terms W, S, T and D on the right hand side of the equation (5.4) are ignored to find the parameters controlling the coda decay since they are only related to the source, path, site and transfer function effects. When the $\log_{10}$ of the both sides of the equation (5.4) is taken, we obtain the following form,

$$\log_{10}\left[A_c(f,t/r)\cdot\left(t-\frac{r}{v(r)}\right)^{\gamma(r)}\right]=\log_{10}\left[H\left(t-\frac{r}{v(r)}\right)\right]-b(r)\cdot\left(t-\frac{r}{v(r)}\right)\cdot\log_{10}(e) \qquad (5.5)$$

Since $\left(t-\frac{r}{v(r)}\right)$ in equation 5.5 corresponds to the time at the distance, r, equation 5.5 can be easily simplified into equation 5.6,

$$\log_{10}\left[A_c(f,t/r)\cdot t^{\gamma(r)}\right]=\log_{10}A_0-b(r)\cdot t\cdot\log_{10}(e) \qquad (5.6)$$

where A_0 represents S-wave source, S-to-coda transfer function and site effects. From the equation 5.6, it is obvious that the right-hand side of the equation 5.6 becomes a linear form when we take the logarithm of both sides. To able to calculate b and γ value of each event for each frequency band, a grid search technique is used. The use of the grid search approach allows us to reduce two variables, γ and b in equation 5.6 to only one. For this purpose, firstly, γ is varied from 0 to 2 in increments of 0.1 and for each γ, corresponding slope of the linear form $\left(b(r)\cdot\log_{10}(e)\right)$ are measured. Finally, desired γ and b values are selected from among those giving the lowest residual at the end of the fitting process between observed and synthetic envelopes.

For the earthquakes recorded at both ISP-ISKB and ISP-MALT station pairs, we observed, especially, at low frequencies (below ~0.7) b values did not change with distance

and it exhibited a typical constant behavior however we encountered a slight distance dependency of *b* parameter above this frequency range. Beside this, we also realized that *b* showed a weak change with the frequency. For instance, b values obtained for the events in ISP-ISKB data set are quite close to 0 (~-5.5 $.10^{-7}$ at lowest frequency band, 0.02-0.03) and begin to slightly decrease with increasing frequencies approaching toward -0.21. On the other hand, b values calculated for the earthquakes in ISP-MALT data set indicated significantly similar distance and frequency dependent behavior to those found for ISP-ISKB station pair. In Appendix B. distance-dependent b values, which were observed from both ISP-ISKB and ISP-MALT, station pairs at some frequency bands are given. Addition to the variations of b with time and frequency, we looked at gamma, γ values in the same manner to be able to see changes in γ with frequency and distance. The most significant characteristic of γ observed at both ISP-ISKB and ISP-MALT station pairs was that γ was showing a decreasing behavior with distance. For instance, γ values found for ISKB station pairs at 0.1-0.2 Hz. are nearly 0.9 at distances between 100 and 200 km and start to decrease to ~0.1 at the distance of 800 km. A similar relationship between γ and distance was obtained for ISP and MALT stations. Unlike b parameters, γ obtained at ISP, ISKB and MALT stations was not changing remarkably with frequency. The distance dependency of γ values at some frequency bands for ISP-ISKB and ISP-MALT is shown in Appendix B.

After fixing γ and b, we find two simple hyperbola forms which give a distance dependence relation of coda shape factors γ and b for each frequency ranges,

These hyperbola forms are given in the below:

$$b(r) = b_0 - \frac{b1}{b2 + r} \qquad (5.7)$$

$$\gamma(r) = \gamma_0 - \frac{\gamma_1}{\gamma_2 + r} \qquad (5.8)$$

where r is the distance and b_0, b_1, b_2, γ_0, γ_1 and γ_2 are constants. Table 5.2 and 5.3 show the constant parameters of these hyperbola equations we found at each frequency band for two ion pairs (ISP-ISKB, ISP-MALT).

Table 5.2 b and gamma parameters for ISP-ISKB.

Freq. f (Hz)	b_0	b_1	b_2	γ_1	γ_2	γ_3
0.02-0.03	0	0.16	500.0	0.6	-72.0	52.0
0.03-0.05	0	0.32	462.0	0.5	0	1.0
0.05-0.1	-0.000525	0	0.0001	0.3	-72.0	101.0
0.1-0.2	-0.00105	0.02	500.0	0.4	-39.0	101.0
0.2-0.3	-0.0021	0.12	500.0	0.1	-74.0	77.0
0.3-0.5	-0.00315	0.2	500.0	0.1	-72.0	38.0
0.5-0.7	-0.00525	0.06	3.0001	0.1	-62.0	51.0
0.7-1.0	-0.0063	0.14	9.0001	0.1	-69.0	101.0
1.0-1.5	-0.0084	0.08	4.0001	0.1	-67.0	57.0
1.5-2.0	-0.007875	0.2	9.0001	0.2	-42.0	101.0
2.0-3.0	-0.008925	0.08	500.0	0.1	-76.0	40.0
3.0-4.0	-0.009975	0	0.0001	0.1	-47.0	25.0
4.0-6.0	-0.00945	0.2	95.0001	0.1	-84.0	93.0
6.0-8.0	-0.0063	3.82	482.0	0.5	0	1.0

Table 5.3 b and gamma parameters for ISP-MALT.

Freq. f (Hz)	b_0	b_1	b_2	γ_1	γ_2	γ_3
0.02-0.03	0	0.26	500.0	0.4	-100.0	63.0
0.03-0.05	0	0.28	500.0	0.4	-44.0	100.0
0.05-0.1	-0.000525	0	0.0001	0.3	-43.0	59.0
0.1-0.2	-0.00105	0.04	500.0	0.2	-97.0	101.0
0.2-0.3	-0.0021	0	0.0001	0.1	-100.0	101.0
0.3-0.5	-0.00315	0.1	159.0	0.1	-75.0	78.0
0.5-0.7	-0.00525	0.08	90.0001	0.2	-42.0	89.0
0.7-1.0	-0.00735	0	0.0001	0.2	-41.0	75.0
1.0-1.5	-0.008925	0.04	52.0001	0.3	-36.0	101.0
1.5-2.0	-0.0063	2.74	495.0	0.4	0	1.0
2.0-3.0	-0.012075	0.2	220.0	0.5	0	1.0
3.0-4.0	-0.013125	0.16	16.0001	0.4	0	1.0
4.0-6.0	-0.01365	0.16	13.0001	0.4	0	1.0
6.0-8.0	-0.0063	1.16	49.0001	0.2	0	1.0

5.2.5. Raw Coda Amplitude Measurements and the Application of the Empirical Distance Corrections to the Measurements

To measure the raw coda amplitudes, we need first to form our synthetics by employing the distant dependent velocity values and coda shape parameters found as a function of distance and frequency into the equation (5.4). We also take the $\log_{10}$ of equation (5.4) to be able to make a consistent comparison between observed and synthetic envelopes. The amount of the difference between two kinds of envelopes, which is obtained by a DC shift process, determines the raw coda amplitudes for each earthquake at 14 frequency ranges. In fact these amplitude values are similar to those obtained from direct waves provided that a distance correction is made. Because any scattering model in which an attenuation mechanism is built is not assumed by the methodology, our raw coda amplitudes still need to be corrected for the distance. Mayeda *et al.*, 2003 realized that the classical attenuation relationship did not fit simultaneously coda waves at local and regional distances. They suggested that the coda amplitudes would show a homogeneous behavior, at least, up to a critical distance and then begin to decay gradually. Finally they developed the following relationship between coda wave amplitudes and distance.

$$P(f,r)=\left[1+\left(\frac{r}{p_2}\right)^{p_1}\right]^{-1} \qquad (5.9)$$

where P is the source-normalized coda amplitude, r is the epicentral distance, f is the center frequency, and p1 and p_2 are the constants. In fact this empirical form does fit adequately the coda at local and regional distances. In this step, the raw coda amplitudes of common events recorded at two stations in a station pair are selected and then they are fitted the above functional form (see Mayeda *et al.*, 2003). With the use of a grid-search technique, the best p_1 and p_2 constants that minimize the inter-station standard deviation are determined and for each frequency band best fitting empirical relations between coda amplitudes and distance are found. Next, each frequency dependent distance-amplitude relation is considered as a model to remove the distance effect on the amplitudes. The model obtained for each frequency band is simultaneously applied to the raw coda amplitudes measured from two stations in a station-pair in order to find distance-corrected coda amplitudes. Table 5.4 and 5.5 includes the

constants, p_1 and p_2 of all models describing the coda amplitudes as a function of distance for ISP-ISKB and ISP-MALT station pairs. Figures 5.8 and 5.9 show some example models at different frequency bands for ISP-ISKB and ISP-MALT station pairs.

Table 5.4 p_1 and p_2 for ISP-ISKB

Freq. F (Hz.)	p_1	p_2
0.02-0.03	1.5	190
0.03-0.05	1.0	490
0.05-0.1	1.0	390
0.1-0.2	1.5	390
0.2-0.3	2.0	290
0.3-0.5	2.0	290
0.5-0.7	3.0	290
0.7-1.0	3.0	190
1.0-1.5	3.5	190
1.5-2.0	4.0	290
2.0-3.0	10.0	190

Table 5.5 p_1 and p_2 for ISP-MALT

Freq. f (Hz.)	p_1	p_2
0.02-0.03	0	0
0.03-0.05	7.5	1290
0.05-0.1	2.5	1690
0.1-0.2	1.5	790
0.2-0.3	2.5	590
0.3-0.5	2.5	290
0.5-0.7	3.0	290
0.7-1.0	4.0	390
1.0-1.5	4.5	290
1.5-2.0	0	0
2.0-3.0	4.5	190

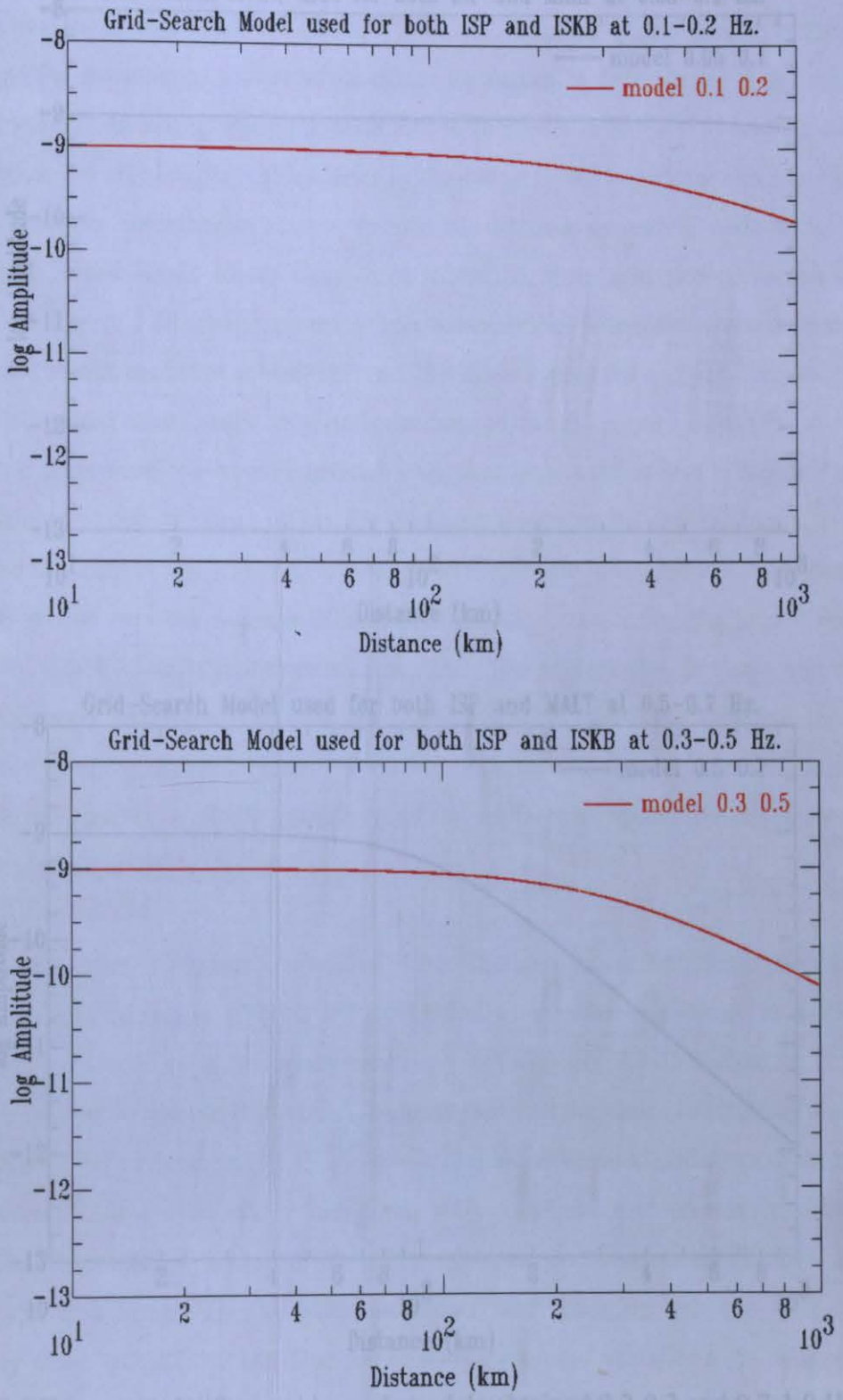

Figure 5.8 Two examples from grid search models obtained 0.2-0.3 and 0.7-1.0 Hz for ISP-ISKB stations pair.

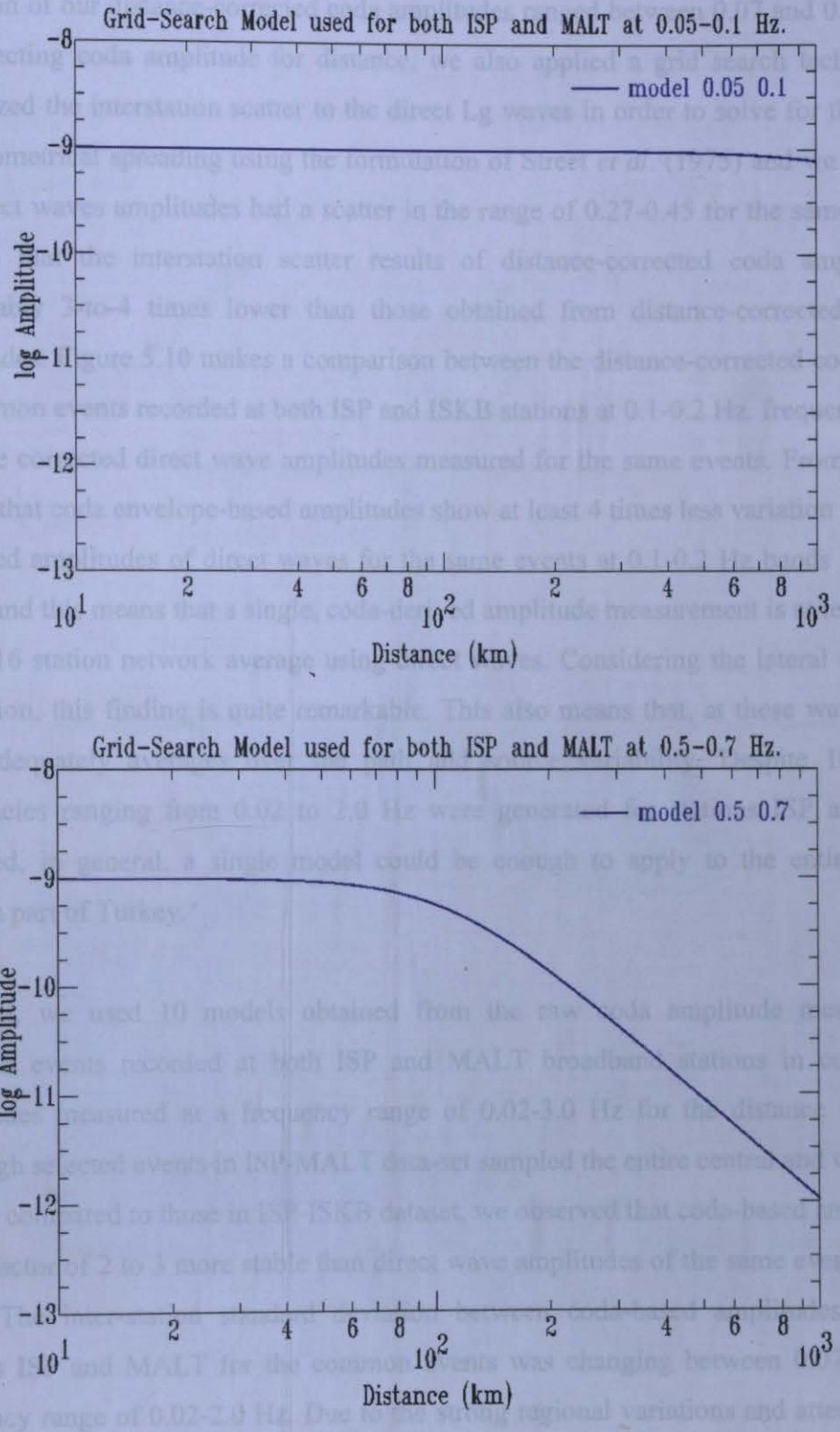

Figure 5.9 Two examples from grid search models obtained 0.2-0.3 and 0.7-1.0 Hz for ISP-MALT stations pair.

After applying the distance corrections to the raw coda amplitudes for the frequencies 0.02 and 2.0 Hz, we looked at the consistency between distance corrected amplitude measurements of common events at stations ISP and ISKB. The interstation standard

deviation of our distance-corrected coda amplitudes ranged between 0.07 and 0.2. In addition to correcting coda amplitude for distance, we also applied a grid search technique, which minimized the interstation scatter to the direct Lg waves in order to solve for the attenuation and geometrical spreading using the formulation of Street *et al.* (1975) and we observed that the direct waves amplitudes had a scatter in the range of 0.27-0.45 for the same events. This showed that the interstation scatter results of distance-corrected coda amplitudes were remarkably 3-to-4 times lower than those obtained from distance-corrected direct wave amplitudes. Figure 5.10 makes a comparison between the distance-corrected coda amplitudes of common events recorded at both ISP and ISKB stations at 0.1-0.2 Hz. frequency bands and distance corrected direct wave amplitudes measured for the same events. From figures 5.10, we see that coda envelope-based amplitudes show at least 4 times less variation than distance-corrected amplitudes of direct waves for the same events at 0.1-0.2 Hz bands as well as the others and this means that a single, coda-derived amplitude measurement is at least equivalent to a 9-16 station network average using direct waves. Considering the lateral complexity of the region, this finding is quite remarkable. This also means that, at these wavelengths, the coda adequately averages over the path and source variability. Despite 10 models for frequencies ranging from 0.02 to 2.0 Hz were generated for stations ISP and ISKB, we observed, in general, a single model could be enough to apply to the entire central and western part of Turkey.

Next, we used 10 models obtained from the raw coda amplitude measurements of common events recorded at both ISP and MALT broadband stations in correcting coda amplitudes measured at a frequency range of 0.02-3.0 Hz for the distance (Figure 5.12). Although selected events in ISP-MALT data-set sampled the entire central and western part of Turkey compared to those in ISP-ISKB dataset, we observed that coda-based amplitudes were still a factor of 2 to 3 more stable than direct wave amplitudes of the same events (see Figure 5.11). The inter-station standard deviation between coda-based amplitudes measured at stations ISP and MALT for the common events was changing between 0.07 and 0.2 in a frequency range of 0.02-2.0 Hz. Due to the strong regional variations and attenuation effect, which probably require 2-D corrections to be made, we could not measure coda amplitudes for the higher frequency ranges such as 2.0-3.0 and above this frequency range.

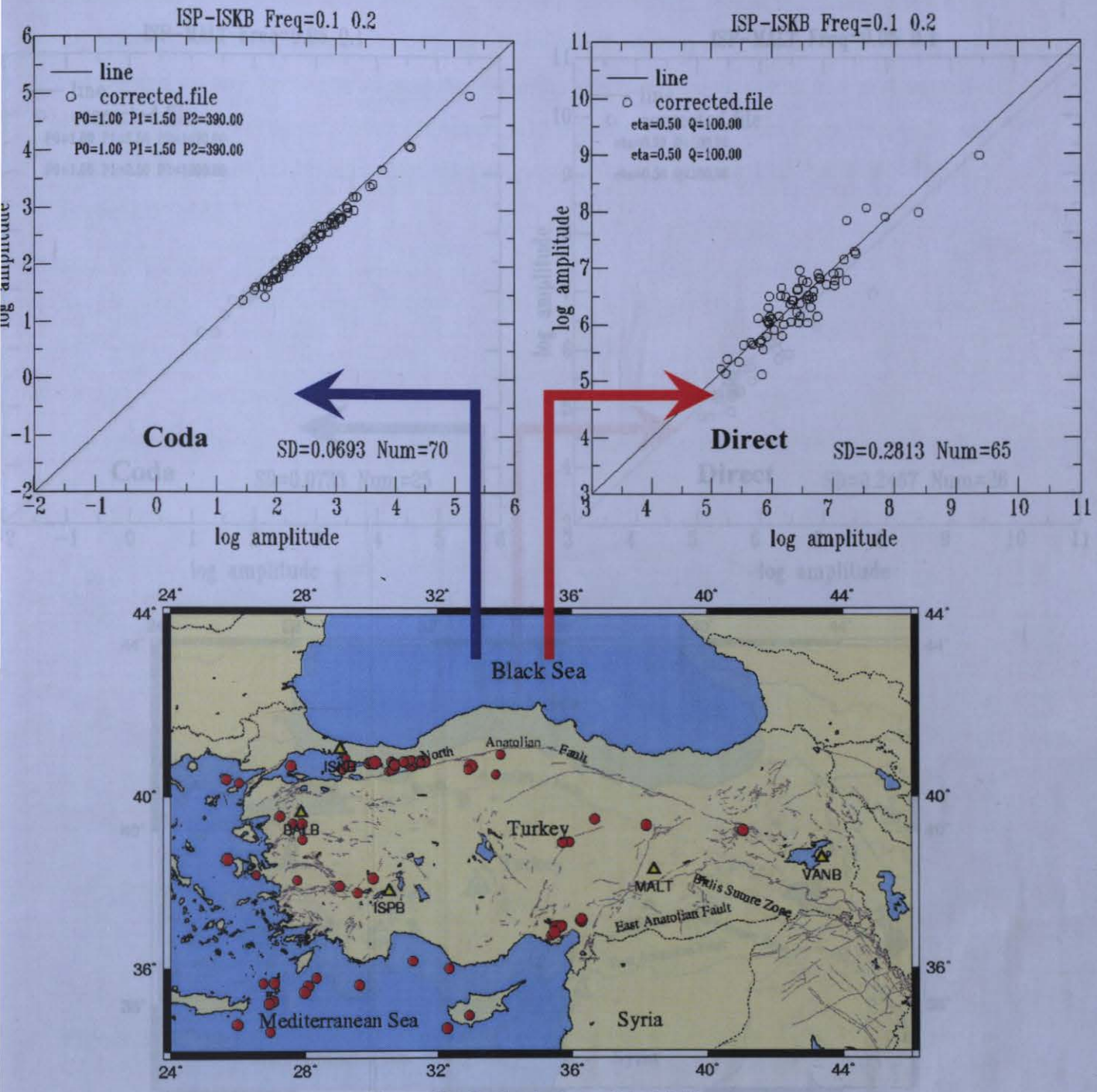

Events distribution between 0.1_0.2 Hz.

Figure 5.10 Comparison of distance-corrected coda amplitudes at 0.1-0.2 Hz with the amplitudes of direct Lg arrival for ISP-ISKB. Inter-station standard deviation results show that coda amplitudes at this frequency band are 4 times more stable than distance corrected direct waves for the common events whose locations are shown on the map.

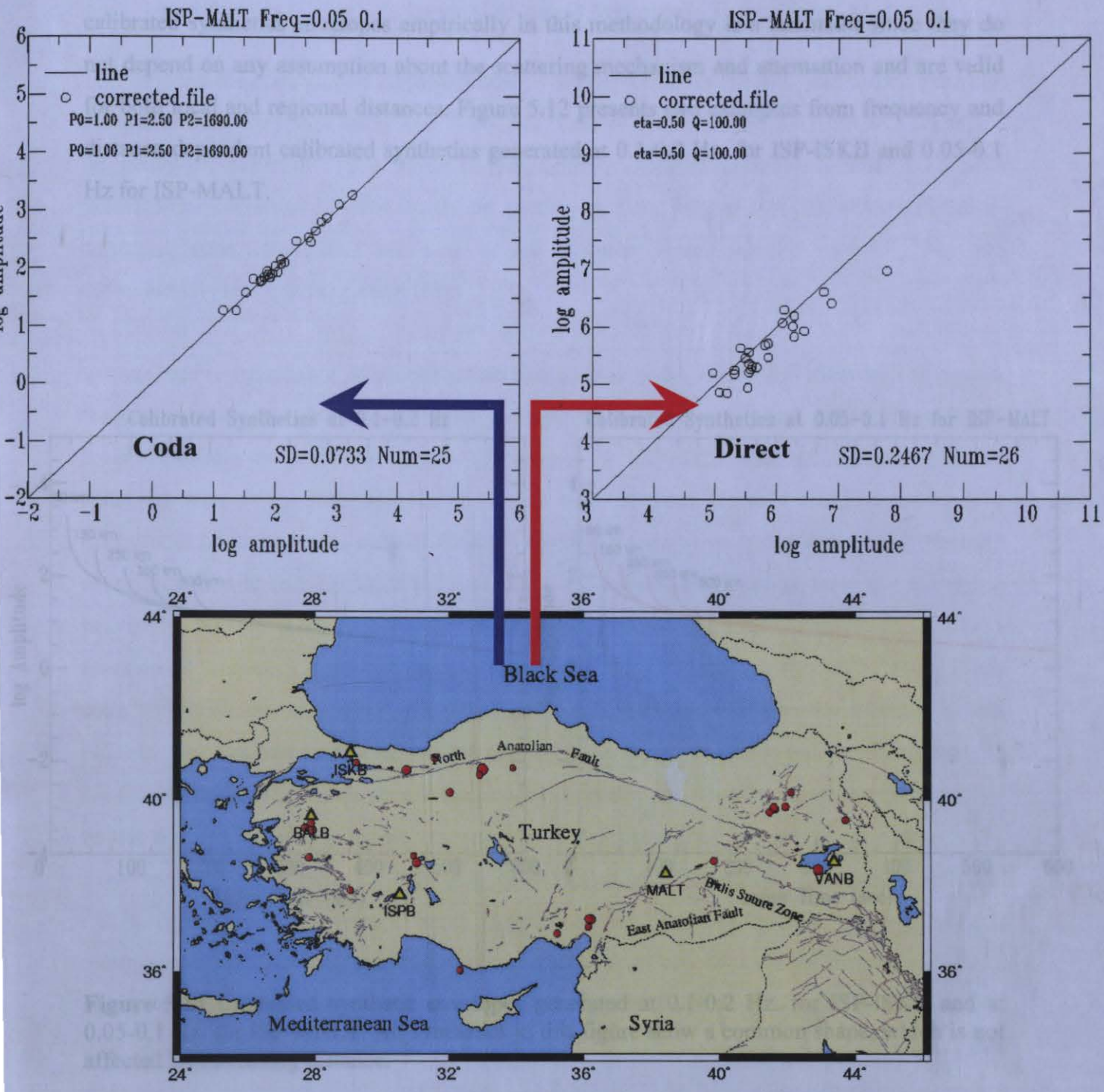

Events distribution between 0.05_0.1 Hz.

Figure 5.11 Comparison of distance-corrected coda amplitudes at 0.05-0.1 Hz with the amplitudes of direct Lg arrival for ISP-MALT. Inter-station standard deviation results showthat coda amplitudes at this frequency band are 3 times more stable than distance corrected direct waves for the common events whose locations are shown on the map.

After all parameters such as velocities and coda shape factors and path corrections were determined, we can now generate synthetic envelopes for a hypothetical source. Considering

the previous studies on coda waves (e.g., Mayeda and Walter, 1996), the generation of the calibrated synthetics envelopes empirically in this methodology is a landmark since they do not depend on any assumption about the scattering mechanism and attenuation and are valid for both local and regional distances. Figure 5.12 presents two examples from frequency and distance-dependent calibrated synthetics generated at 0.1-0.2 Hz. for ISP-ISKB and 0.05-0.1 Hz for ISP-MALT.

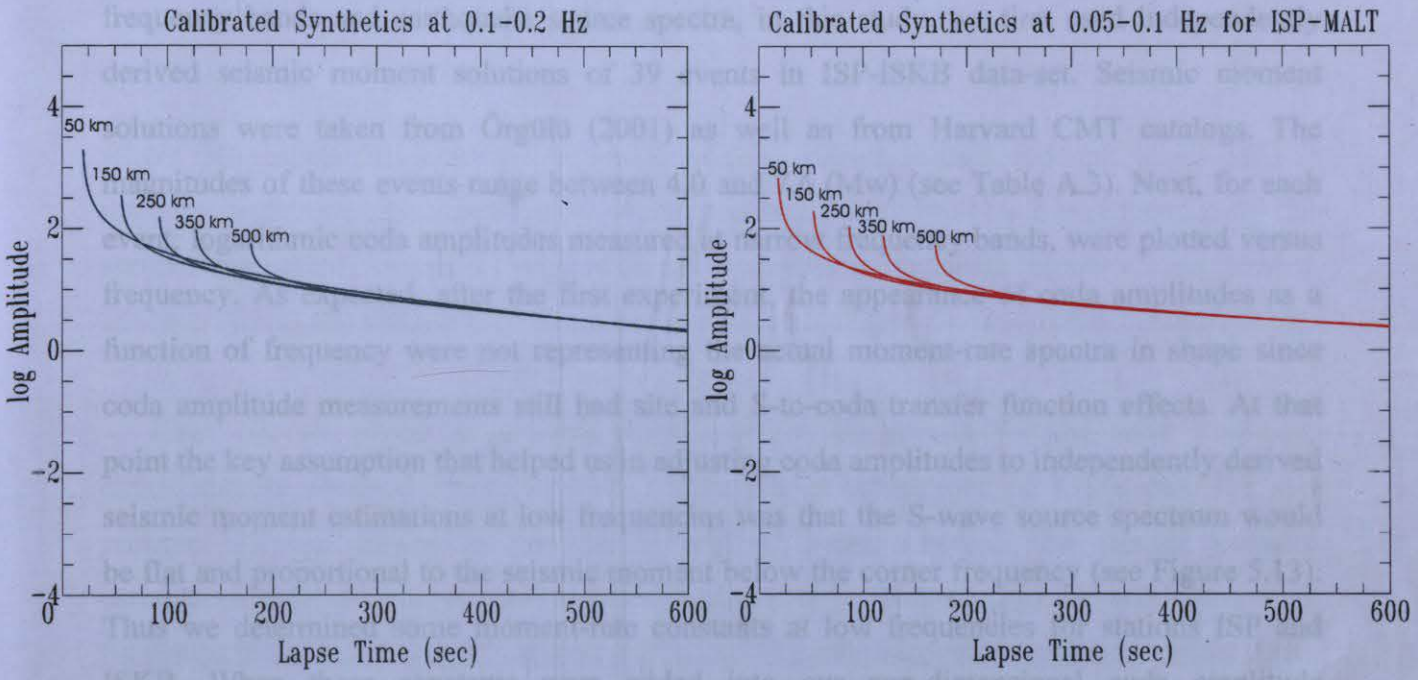

Figure 5.12 Calibrated synthetic envelopes generated at 0.1-0.2 Hz. for ISP-ISKB and at 0.05-0.1 Hz. for ISP-MALT. All synthetics in this figure show a common shape, which is not affected by increasing distance.

5.2.6. Tying the Distance Corrected Dimensionless Coda Amplitudes to an absolute scale and Results from Coda Derived Moment Magnitude Estimations, M_W(coda)

Although the coda amplitude measurements are corrected for the path and source radiation pattern effects, they still carry the S-to-coda transfer function and site effects. These are frequency-dependent effects and must be removed from the measurements in order to obtain a moment-rate spectrum. In other words, by making frequency dependent corrections, distance-corrected coda amplitudes are tied to an absolute scale, seismic moment, M_0 and consequently, moment magnitude, M_W.

In order to establish a relationship between coda-derived amplitudes measured at narrow frequency bands and earthquake source spectra, in this study, we first used independently derived seismic moment solutions of 39 events in ISP-ISKB data-set. Seismic moment solutions were taken from Örgülü (2001) as well as from Harvard CMT catalogs. The magnitudes of these events range between 4.0 and 7.6 (Mw) (see Table A.3). Next, for each event, logarithmic coda amplitudes measured at narrow frequency bands, were plotted versus frequency. As expected, after the first experiment, the appearance of coda amplitudes as a function of frequency were not representing the actual moment-rate spectra in shape since coda amplitude measurements still had site and S-to-coda transfer function effects. At that point the key assumption that helped us in adjusting coda amplitudes to independently derived seismic moment estimations at low frequencies was that the S-wave source spectrum would be flat and proportional to the seismic moment below the corner frequency (see Figure 5.13). Thus we determined some moment-rate constants at low frequencies for stations ISP and ISKB. When these constants were added into our non-dimensional coda amplitude measurements, they made uncorrected coda amplitudes at low frequencies roughly similar to independently derived seismic moment solutions. The smaller earthquakes in our dataset were used as empirical Green's function events in order to make corrections at higher frequencies since source spectra of small events could be considered to have approximately a constant level up to 8 Hz. The use of smaller events, in this way, would allow us to produce earthquake source spectra of much smaller events to be waveform modeled once we fixed the best moment-rate constants for higher frequencies. For ISP-ISKB station pair, we could determine some moment rate constants in a frequency range between 0.02 and 2.0 Hz owing to the geological complexities that prevented us from measuring coda amplitudes at higher frequencies. The application of the best moment-rate constants to the distance corrected

amplitudes of previously selected 39 events in ISP and ISKB dataset resulted in absolute source spectra in units of dyne-cm. These new coda-based source spectra obtained at two stations, ISP and ISKB also showed a consistent behavior almost for all events. Some example source spectra found for the events in ISP-ISKB dataset are given in Figure 5.14. Next we estimated coda-derived seismic moment values by averaging the two lowest frequency measurements. After determining coda-derived seismic moments of 39 earthquakes, we used the following relationship between seismic moment, M_0 and moment magnitude, M_W which was developed by Hanks and Kanamori (1979) in calculating M_W(coda) of each event.

$$M_W = \frac{2}{3}\log_{10}(M_0) - 10.7 \qquad (5.10)$$

where Mw represents moment magnitude and M_0 shows seismic moment. Coda-derived moment magnitudes, M_W(coda) of 39 events can be seen on Table A.3 in Appendix A. The comparison made between M_W(coda) and waveform modeled moment magnitudes, M_W(waveform) showed a good correspondence with a standard deviation of 0.2 (Figure 5.15).

Later on, we aimed to generate some moment-rate spectra for the coda amplitude measurements obtained from ISP-MALT data set in estimations of M_W(coda). For this purpose, 49 earthquakes in ISP-MALT data set were selected. The seismic moment estimations these 49 events were made by Örgülü (2003). Compared to 39 earthquakes used for the calibration of ISP-ISKB station pair, these 49 earthquakes were sampling almost entire region of Turkey. The magnitudes of these 49 earthquakes are between M_W 3.9 and 6.3 (see Table A4 in Appendix A). Likewise, we followed the same technique in finding frequency dependent source moment-rate constants for ISP-MALT station pair. After we applied these moment-rate constants to uncorrected coda amplitudes at each frequency, we observed that resultant coda-based moment rate spectra generated at each station for a given event showed a good agreement (Figure 5.16). These source spectra were then used to calculate M_W(coda) of the events for entire data set. Table A4 presents coda-derived moment magnitudes, M_W(coda) of selected 54 earthquakes in ISP-MALT dataset. Similar to the results from ISP-ISKB dataset, moment magnitudes, M_W(coda) estimated from the long-period levels of coda-derived source spectra indicated a consistent relation with independently derived moment magnitudes from long-period waveform modeling M_W(waveform) (Figure 5.17).

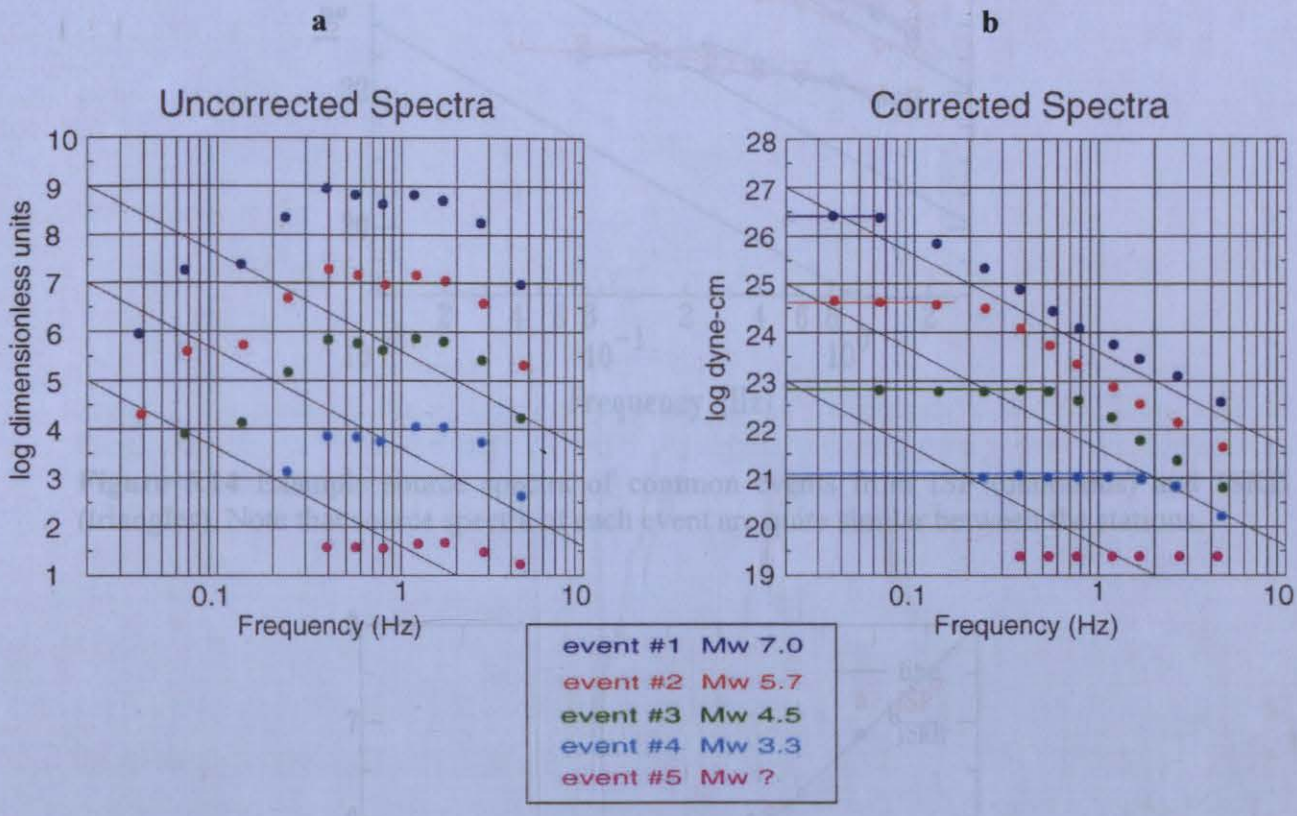

Figure 5.13 Cartoon illustration that shows how to tie non-dimensional coda amplitudes to an absolute scale. **a)** Distance-corrected coda amplitudes of some events whose magnitudes range between Mw=3.3 and Mw=7.0. As expected, after the first experiment, the appearance of coda amplitudes as a function of frequency does not represent the actual moment-rate spectra in shape since coda amplitude measurements still had site and S-to-coda transfer function effects **b)** The shape of source spectra after the application of moment-rate constants to coda amplitudes at each frequency band. Solid lines show the spectral level which corresponds seismic moment at low frequencies (Mayeda *et al.*, 2003).

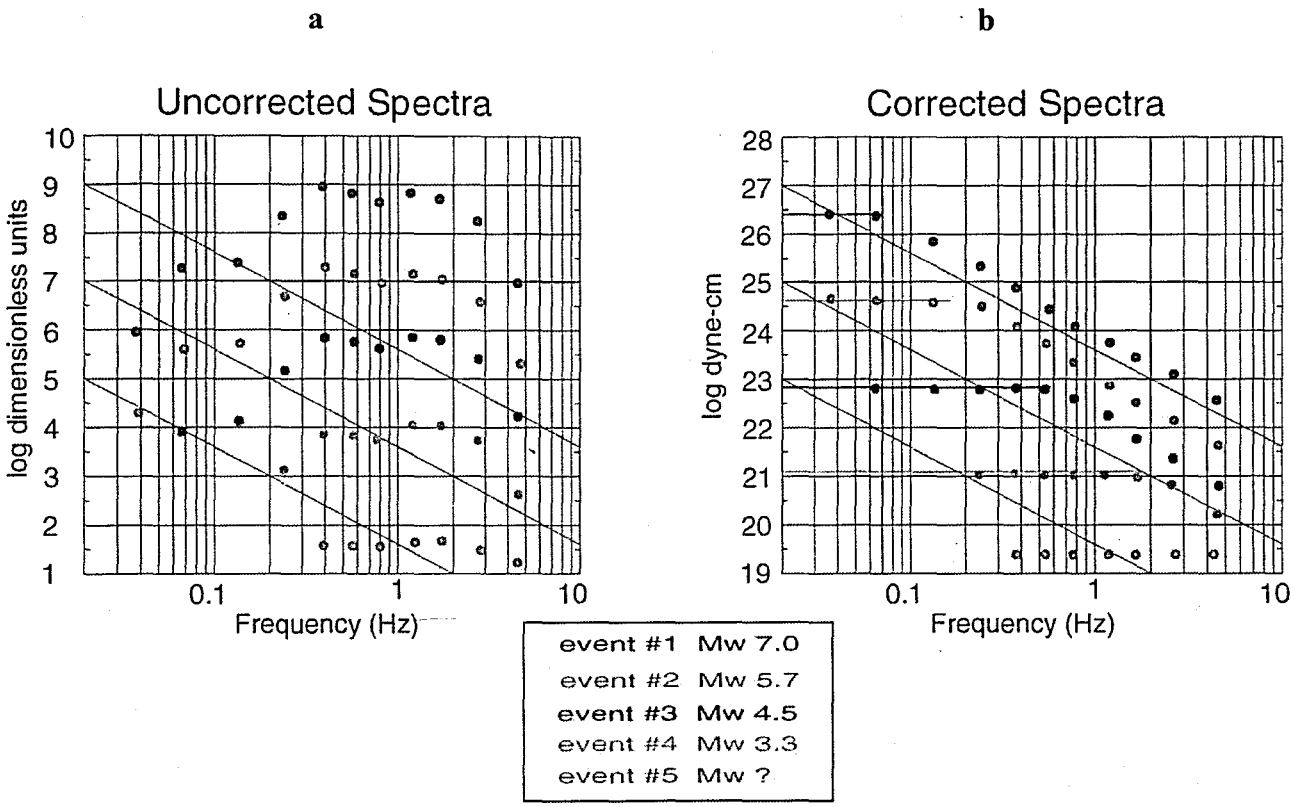

Figure 5.13 Cartoon illustration that shows how to tie non-dimensional coda amplitudes to an absolute scale. **a)** Distance-corrected coda amplitudes of some events whose magnitudes range between Mw=3.3 and Mw=7.0. As expected, after the first experiment, the appearance of coda amplitudes as a function of frequency does not represent the actual moment-rate spectra in shape since coda amplitude measurements still had site and S-to-coda transfer function effects **b)** The shape of source spectra after the application of moment-rate constants to coda amplitudes at each frequency band. Solid lines show the spectral level which corresponds seismic moment at low frequencies (Mayeda *et al.*, 2003).

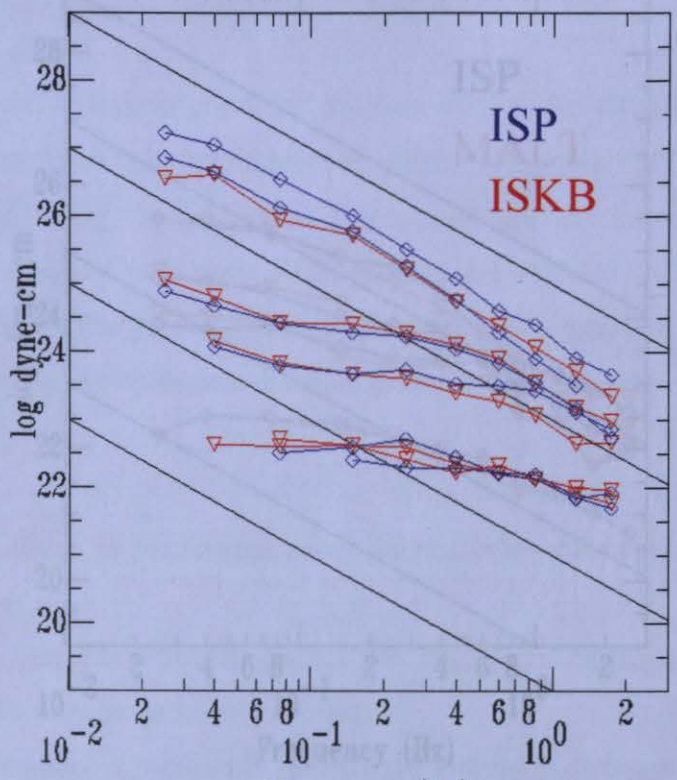

Figure 5.14 Example source spectra of common events from ISP (diamonds) and ISKB (triangles). Note that source spectra of each event are quite similar between the stations.

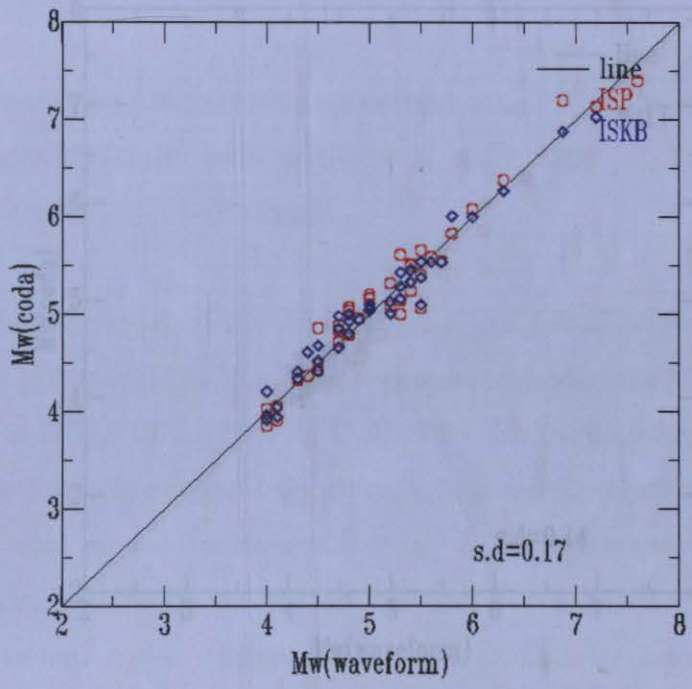

Figure 5.15 Comparison of M_W(coda) of 39 events estimated at stations ISP (circles) and ISKB (diamonds) with those obtained from long-period waveform modeling. There is a good correspondence with a standard deviation of 0.17 between two types of moment magnitude.

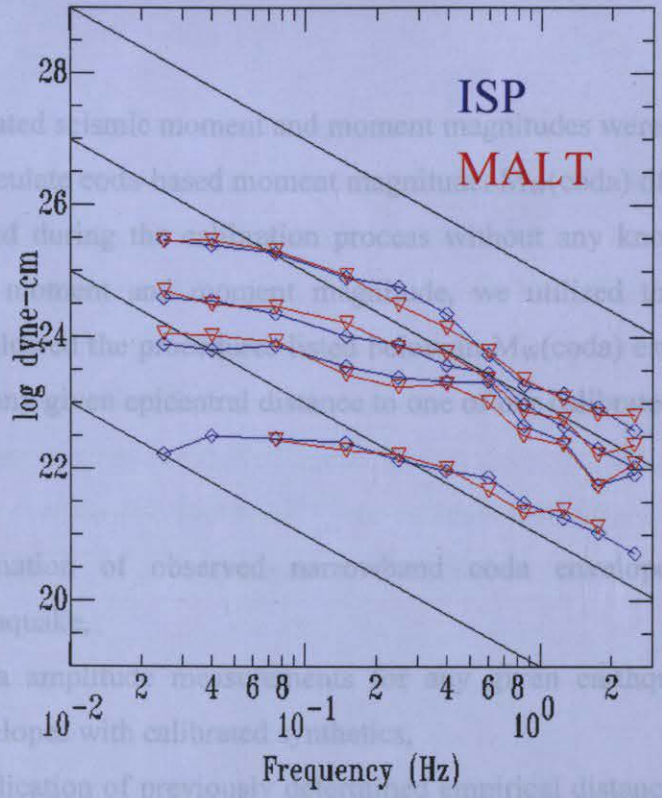

Figure 5.16 Examples source spectra obtained at ISP (diamonds) and MALT (triangles). Similar to the examples shown in Figure 5.14, source spectrum of a given event indicates a well agreement between stations.

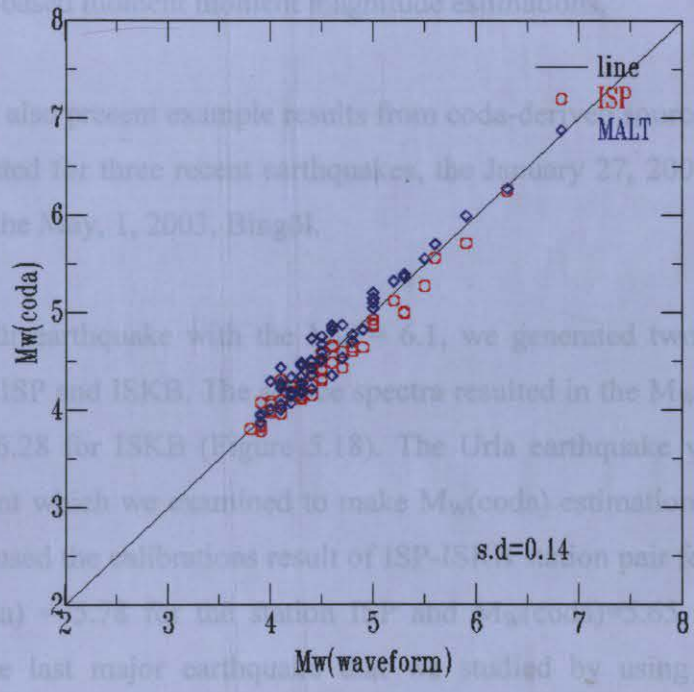

Figure 5.17 Comparison of coda derived moment magnitudes, M_W(coda) of 49 events estimated at ISP (circles) and MALT (diamonds) with those estimated from long-period waveform modeling. Our M_W(coda)'s are in a good agreement with M_W(waveform)'s.

With the use of moment rate constants, we have computed coda-derived source spectra and then obtained coda-derived moment magnitudes [$M_W(coda)$] of selected earthquakes whose

previously estimated seismic moment and moment magnitudes were used as reference scales . To be able to calculate coda-based moment magnitude, M_W(coda) of a new earthquake, which we have not used during the calibration process without any knowledge of independently derived seismic moment and moment magnitude, we utilized these frequency-dependent constants and followed the procedures listed below in M_W(coda) estimation of an earthquake that occurred at any given epicentral distance to one of our calibrated stations (ISP, ISKB and MALT) :

i) Formation of observed narrowband coda envelopes only for any given earthquake,

ii) Coda amplitude measurements for any given earthquake by fitting observed envelopes with calibrated synthetics,

iii) Application of previously determined empirical distance corrections to raw coda amplitudes of new earthquake at each frequency band,

iv) Transformation from distance corrected coda amplitudes to an absolute scale, source spectra by using previously determined best moment rate constants,.

v) Coda-based moment moment magnitude estimations,

In this chapter, we also present example results from coda-derived source spectra and moment magnitudes estimated for three recent earthquakes, the January 27, 2003, Pülümür and April 4, 2003, Urla and the May, 1, 2003, Bingöl.

For the Pülümür earthquake with the M_W = 6.1, we generated two coda-derived source spectra at stations ISP and ISKB. The source spectra resulted in the M_W(coda) = 6.36 for ISP and M_W(coda) = 6.28 for ISKB (Figure 5.18). The Urla earthquake with the M_W = 5.7 is another major event which we examined to make M_W(coda) estimations after the calibration study. We, again, used the calibrations result of ISP-ISKB station pair for this earthquake and found an M_W(coda) = 5.78 for the station ISP and M_W(coda)=5.65 for the station ISKB (Figure 5.19). The last major earthquake that we studied by using the coda magnitude methodology is the Bingöl earthquake with the M_W = 6.4. For this event, coda-derived source spectra computerized by using the calibration results of ISP-ISKB station pair indicated the M_W(coda) = 6.62 at station ISP and M_W(coda)=6.52 at station ISKB. In addition to M_W(coda) estimates by using the calibration parameters found for ISP-ISKB station pair, we calculated coda-derived moment magnitude of the Bingöl earthquake from the ISP-MALT calibration

results. Since we could not find any data recorded at station MALT due to the lack of data, we only estimated a moment magnitude value for the station ISP. The source spectrum of the Bingöl earthquake at the station ISP gave us the M_W(coda) as 6.43 (Figure 5.20). For all of three cases, we could not make M_W(coda) estimates for MALT since there was not available data recorded at this station. Thus, we turned our attention to another earthquake which we have not included the calibration process. Finally, we dealt with the M_W=5.4 earthquake of June 13, 2000 that occurred in the Mediterranean Sea. Later on, we generated its coda-derived source spectra at stations ISP and MALT and estimated the M_W(coda)=5.38 at from MALT and M_W(coda)=5.39 from ISP by using the calibration parameters found for ISP-MALT station pair (Figure 5.21).

Figure 5.18 a) the location of the Pülümür earthquake (red star) of January 27, 2003, recorded at stations ISP and ISKB.

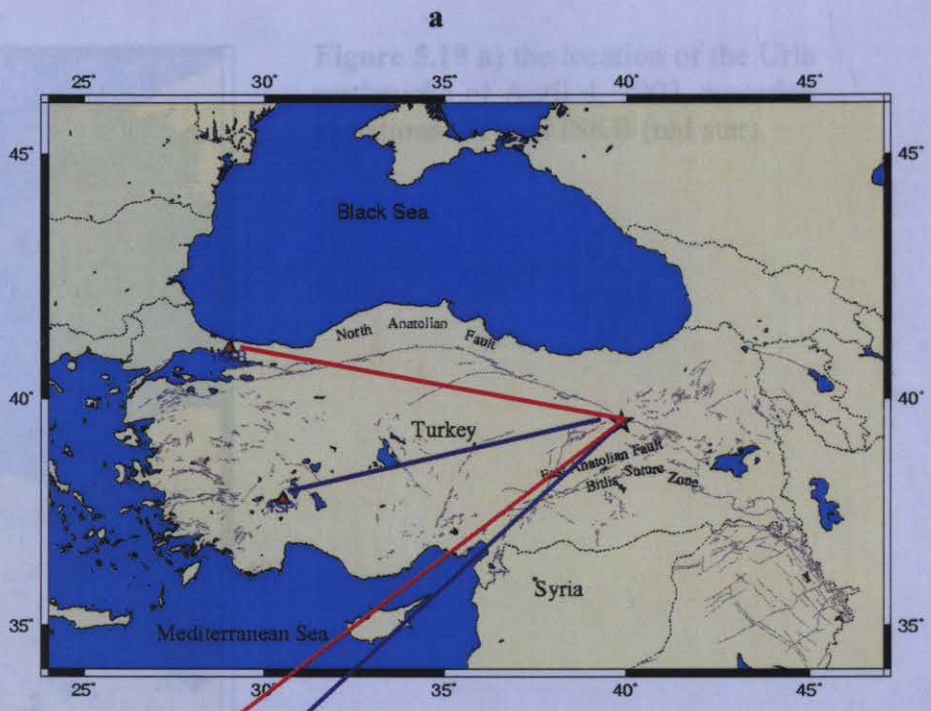

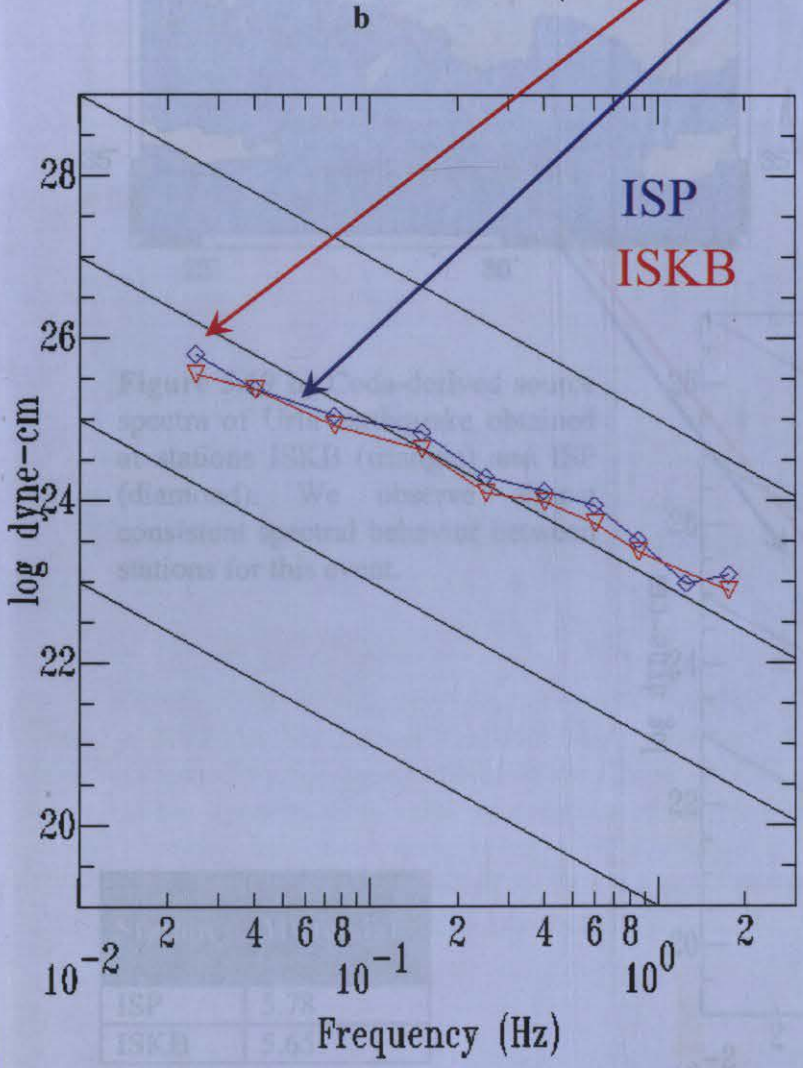

Figure 5.18 b) Resultant coda based source spectra obtained at ISP (diamonds) and ISKB (triangles). Similarity between spectra at different stations is important in terms of showing the stability of coda methodology.

Station	Mw(coda)
ISP	6.36
ISKB	6.28

Figure 5.19 a) the location of the Urla earthquake of April 4, 2003, recorded at stations ISP and ISKB (red star).

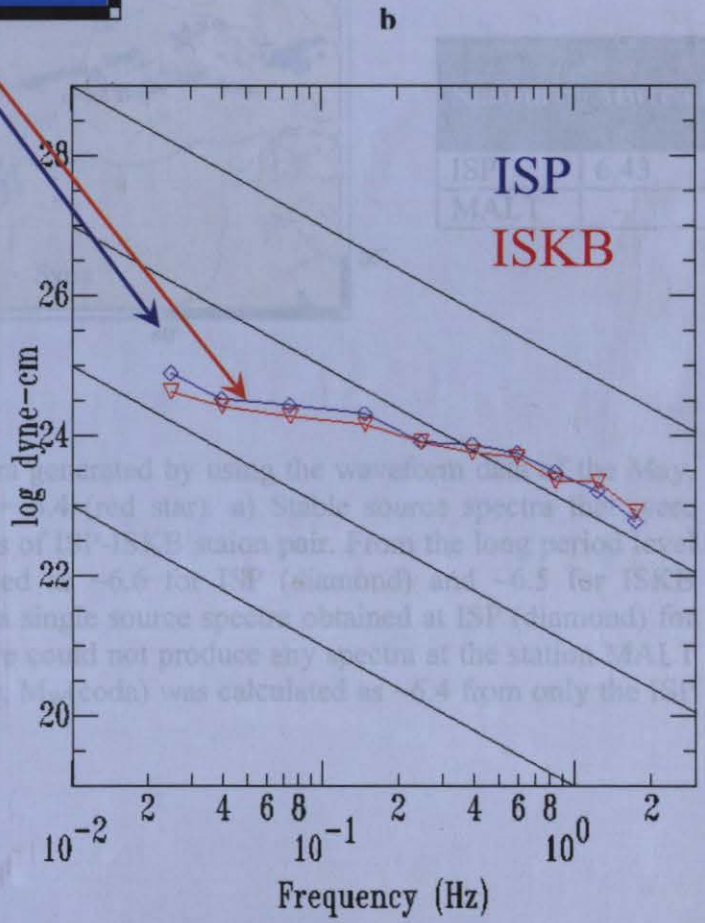

Figure 5.19 b) Coda-derived source spectra of Urla earthquake obtained at stations ISKB (triangle) and ISP (diamond). We observe almost consistent spectral behavior between stations for this event.

Station	Mw(coda)
ISP	5.78
ISKB	5.65

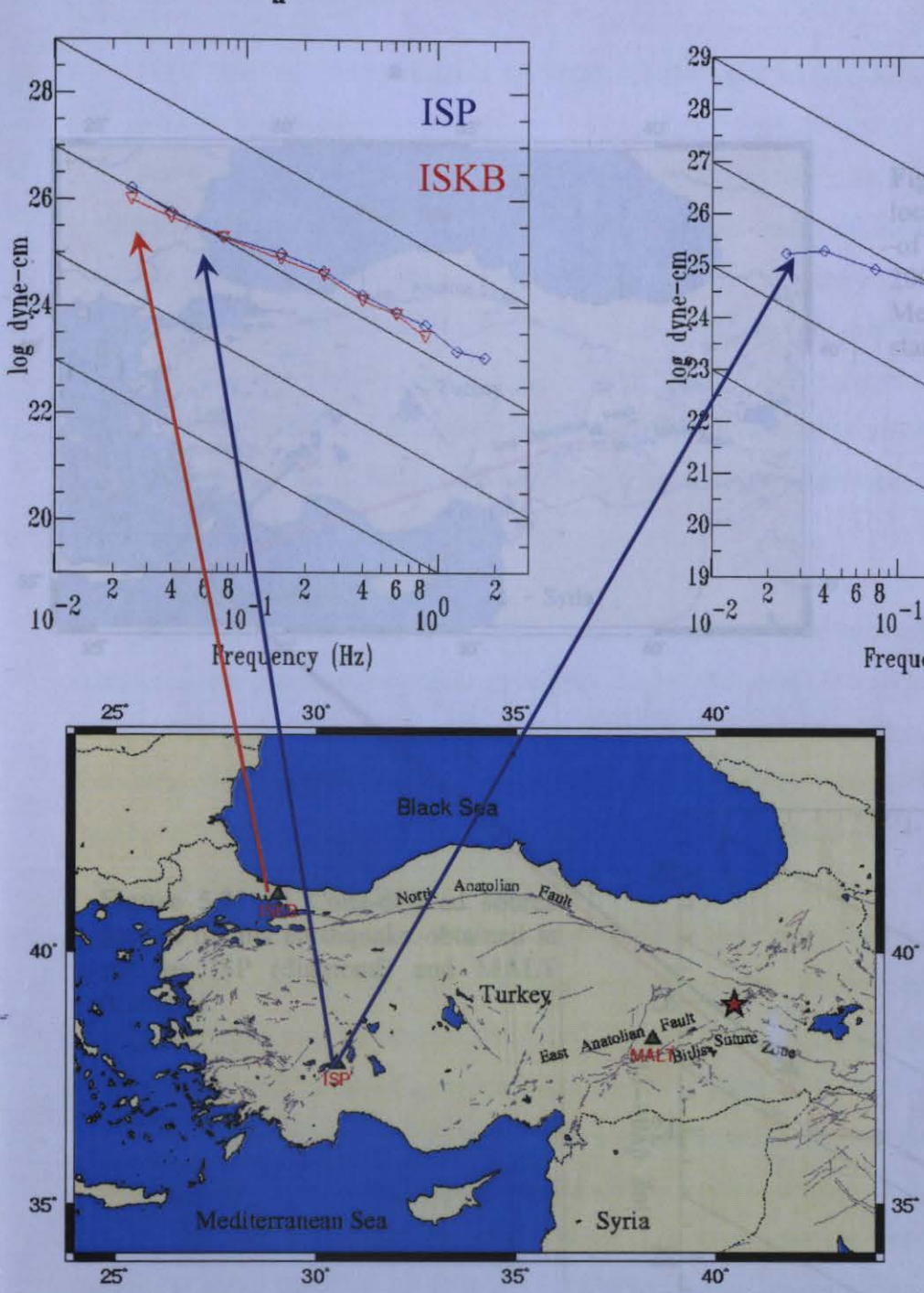

Station	Mw(coda)
ISP	6.62
ISKB	6.52

Station	Mw(coda)
ISP	6.43
MALT	-

Figure 5.20 Coda-derived source spectra generated by using the waveform data of the May, 1, 2003, Bingol earthquake with M_W = 6.4 (red star). **a)** Stable source spectra that were computed by the coda-calibration results of ISP-ISKB staion pair. From the long period level of the spectra, M_W(coda) was estimated as ~6.6 for ISP (diamond) and ~6.5 for ISKB (triangle). **b)** For the same earthquake, a single source spectra obtained at ISP (diamond) for the ISP-MALT station pair. Note that we could not produce any spectra at the station MALT for the lack of data. For this station pair, M_W(coda) was calculated as ~6.4 from only the ISP station.

a

Figure 5.21 a) the location of the $M_W = 5.4$ of earthquake June, 13 2000 that occurred in the Mediterranean Sea (red star).

b

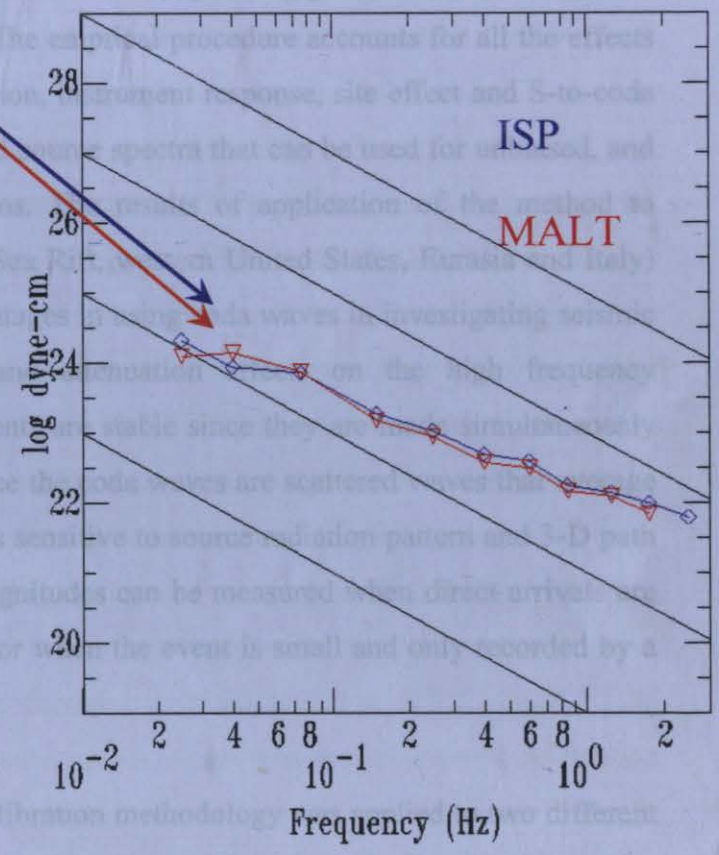

Figure 5.21 b) Coda-derived source spectra of this earthquake obtained at stations ISP (diamond) and MALT (triangle).

Station	Mw(coda)
ISP	5.39
MALT	5.38

6.DISCUSSION AND CONCLUSION

As a source parameter, magnitude plays an important role in seismology since it is necessary for establishing accurate seismicity catalogs, assessing the seismic hazard potential of a region (b-value), determining the source size (seismic moment, energy, and stress drop), and estimating nuclear explosion yield. However, the comparison of different relative magnitude scales ($m_b(P_g)$, $mb(P_n)$, $m_b(L_g)$, M_S, Ml, M_d, etc.) generally causes confusion for seismological studies due to their inconsistency and instability among each other. None of them represents the actual source size except for moment magnitude, (M_W), which is directly related to the faulting dimension.

Recently, a new magnitude calibration methodology has been used for stable local and regional estimates using coda envelopes large and small-to-moderate sized events. The methodology is a purely empirical approach with the goal of obtaining stable seismic source spectra which can then be used to compute moment magnitudes [M_W(coda)] from regional coda envelopes using broadband stations. The emprical procedure accounts for all the effects on coda amplitudes related to the propagation, instrument response, site effect and S-to-coda transfer function. The result is coda-derived source spectra that can be used for unbiased, and unsaturated moment magnitude estimations. The results of application of the method to different regions of the world (i.e., Dead Sea Rift, western United States, Eurasia and Italy) have shown that there are significant advantages in using coda waves in investigating seismic source characteristics as well as site and attenuation effects on the high frequency seismograms. First of all, coda measurements are stable since they are made simultaneously over a large portion of a seismogram. Since the coda waves are scattered waves that average over the entire focal sphere, they are not as sensitive to source radiation pattern and 3-D path heterogeneity. Moreover, coda-derived magnitudes can be measured when direct arrivals are clipped (i.e., when the event is large) and/or when the event is small and only recorded by a few stations.

In this study, this empirical regional calibration methodology was applied to two different datasets in Turkey consisting of earthquakes that occurred in a tectonically complex region with dominant lateral heterogeneities. During the calibration process two different datasets were compiled from three Turkish broadband stations (ISP, ISK, and MALT) to obtain stable moment magnitude estimates. The events in the first dataset (ISP-ISK) are distributed mostly

over the western Anatolia region while the second dataset (ISP-MALT) samples the entire country. For both datasets, in a frequency range between 0.02 and 1.0 Hz, the interstation scatter of distance corrected-coda amplitudes varies from 0.07 to 0.15, in good aggreement with results obtained from previous applications of the methodology to the western United States and Dead Sea Rift regions (e.g., Mayeda and Walter, 1996; Mayeda et al., 2003). This is a quite remarkable and encouraging result suggesting that the method can be easily applicable for even much larger and complex regions spanning distances ranging between local to far-regional distances. On the other hand, compared to the direct waves (i.e., L_g , P_g,, and surface waves), we observed a considerable reduction in the interstation scatter results by a factor of 3-to-4 when the envelopes of coda waves were used. For this region, this appears to be a robust methodology for frequencies at least up to 1 Hz because the coda waves provide roughly 3-to-4 times more stable amplitude measurements relative to the direct waves. In other words, a single coda measurement is approximately equivalent to a 9-to-16 station network average using direct waves. Observational results with regard to the standard deviation between distance-corrected coda amplitude measurements at different pairs of stations also showed that even a single, frequency dependent coda atenuation function was enough to explain the coda envelope amplitude over the entire country.

After correcting our coda amplitudes for propagation effects, we tied our non-dimensional measurements to an absolute scale using independently derived moments. In other words, we transformed distance corrected coda amplitudes into a source spectrum by making frequency dependent corrections for both the site and S-to-coda transfer function effects. The validation of this empirical approach is proven by observing identical spectra for the same event at two stations separated by roughly 500 km. The stable source spectra also confirm that the coda is averaging over any source radiation pattern as well as any lateral crustal heterogeneity. As a final validation, these selected source spectra were used to estimate coda-derived moment magnitudes, M_W (coda). Upon comparing our M_W(coda)'s with those from long-period waveform modeling, M_W(waveform), we observed a standard deviation of 0.17 for ISP-ISK and 0.14 for ISP-MALT. These results are comparable to previous applications of the method in other parts of the world. These observations prove the stability of coda waves at regional distances and furthermore can be used for small events that cannot be reliably waveform modeled due to poor signal to noise ratio for long period surface waves.

As a conclusion, we used a newly developed regional magnitude methodology based on coda envelopes to estimate stable source spectra and hence moment magnitudes for earthquakes in Turkey. We calibrated and tested the broadband stations ISK, ISP and MALT and our results strongly suggest that they can be used to estimate M_W (coda) for waveforms that are clipped and/or too small to be waveform modeled. With the use of the calibration results, we succesfully estimated M_W(coda)'s of three recent earthquakes, the January 27, 2003, Pülümür and April 4, 2003, Urla and the May, 1, 2003, Bingöl, that occurred in Turkey. We also proved that; a) the application of the methodology is successful in a tectonically complex and laterally heterogeneous region, b) it is convenient for a sparse local and regional seismic networks, c) the magnitude estimation is unbiased, c) it is transportable and universal, d) it does not saturate, e) it is insensitive to source radiation pattern. With the use of calibration results, we are able to estimate M_W (coda) for events that are even too small to be waveform modeled due to the poor signal-to-noise ratio.

REFERENCES

1. Aki, K., Correlogram analyses of seismogram by means of a simple automatic computer, *J. Phys. Earth.* 4, 71-79, 1956.

2. Aki, K., Scaling law of the seismic spectrum, *J. Geophys. Res.*, 72, 1217-1231, 1967.

3. Aki, K., Analysis of seismic coda of local earthquakes as scattered waves, *J. Geophys. Res.*, 74, 615-631, 1969.

4. Aki, K., and B. Chouet, Origin of coda waves: Source, attenuation and scattering effects, *J. Geophys. Res.*, 80, 3322-3342, 1975.

5. Aki, K., and P. G. Richards, Quantitative Seismology: Theory and Methods, Vol.2, *W. H. Freeman and Co., San Francisco*, 932 pp., 1980.

6. Biswas, N. N., and K. Aki, Characteristics of coda waves: Central and south central Alaska, *Bull. Seism. Soc. Am.*, 74, 493-507, 1984.

7. Bisztricsany, E., A new method for the determination of magnitude of earthquakes, *Geofiz. Kozlemen*, 7, 69-96, 1958.

8. Brune, J. N., Tectonic stress and the spectra of seismic shear waves from earthquakes, *J. Geophys. Res.*, 75, 4997-5009, 1970.

9. Dainty, A., and M. N. Toksöz, Seismic codas on the earth and the moon: A comparison, *Phys. Earth Planet. Inter.*, 26, 250-260, 1981.

10. Fehler, M., M. Hoshiba, H. Sato, and K. Obara, Separation of scattering and intrinsic attenuation for the Kanto-Tokai region, Japan, using measurements of S-wave energy versus hypocentral distance, *Geophys. J. Int.*, 108, 787-800, 1992.

11. Frankel, A., and L. Wennerberg, Energy-flux model of seismic coda: Separation of scattering and intrinsic attenuation, *Bull. Seism. Soc. Am.*, 77, 1123-1251, 1987.

12. Frankel, A., Review for "Observational and physical basis for coda precursors (Jin, A., and K. Aki)", in E*valuation of Proposed Earthquake Precursors* (ed. M. Wyss), pp. 51-53, AGU, Washington D. C., 1991.

13. Gusev, A. A., and V. K. Lemzikov, Properties of scattered elastic waves in the lithosphere of Kamchatka: Parameters and temporal variations, *Tectonophysics*, 112, 137-153, 1985.

14. Gutenberg, B., and C. F. Richter, Earthquake magnitude, intensity, energy, and acceleration, *Bull. Seism. Soc. Am.*, 32, 163-191, 1942.

15. Hanks, T. C., and W. Thatcher, A graphical representation of seismic source parameters, *J. Geophys. Res.*, 77, 4393-4405, 1972.

16. Hanks, T. C., and H. Kanamori, A moment magnitude scale, *J. Geophys. Res.*, 84, 2348-2350, 1979.

17. Hartse, H. E., W. S. Phillips, M. C. Fehler, and L. S. House, Single-Station Discrimination Using Coda Waves, *Bull. Seism. Soc. Am.*, 85, 1464-1474, 1995.

18. Hough, S. E., Earthshaking Science, *Princeton University Press*, 238 pp., 2002.

19. Jin, A., and K. Aki, Spatial and temporal correlation between coda Q^{-1} and seismicity and its physical mechanism, *J. Geophys. Res.*, 9414041-14059, 1989.

20. Jin, A., and K. Aki, Observational and physical basis for coda precursors, in E*valuation of Proposed Earthquake Precursors* (ed. M. Wyss), pp. 33-46, AGU, Washington D. C., 1991.

21. Koyanagi, S., K. Mayeda, and K. Aki, Frequency-dependent site amplification factors using the S-wave coda for the Island of Hawaii, *Bull. Seism. Soc. Am.*, 82, 1151-1185, 1992.

22. Lee, W. H. K., J. C. Roller, P. G. Bauer, and J. D. Johnson, Catalog of earthquakes along the San Andreas fault systemin central California for the year 1969, *U. S. Geol. Survey, Open-file Report*, 48 pp., 1972.

23. Mayeda, K., S. Koyanagi, and K. Aki, Site amplification from S-wave coda in the Long Valley Caldera region, California, *Bull. Seism. Soc. Am.*, 81, 2194-2213, 1991.

24. Mayeda, K., S. Koyanagi, M. Hoshiba, K. Aki, and Y. Zeng, A comparative study of scattering, intrinsic, and coda Q^{-1} for Hawaii Long Valley and central California between 1.5 and 15 Hz, *J. Geophys. Res.*, 97, 6643-6659, 1992.

25. Mayeda, K., m_b(Lg Coda): A stable single station estimator of magnitude, *Bull. Seism. Soc. Am.*, 83, 851-861, 1993.

26. Mayeda, K., and W. R. Walter, Moment, energy, stress drop, and Source spectra of western United States earthquakes from regional coda envelopes, *J. Geophys. Res.*, 101, 11195-11208, 1996.

27. Mayeda, K., A. Hofstetter, J. O'Boyle, W. R. Walter, Stable and Transportable Regional Magnitudes Based on Coda-Derived Moment-Rate Spectra, *Bull. Seism. Soc. Am.*, 93, 224-239, 2003.

28. Nakamura, Y., Seismic energy transmission in an intensively scattering enviroment, *J. Geophys.*, 43, 389-399, 1977.

29. Novelo-Casanova, D. A., E. Berg, V. Hsu, E. Helsley, Time-space variations of seismic S-wave coda attenuation Q_c^{-1} and magnitude distribution (b-value) for the Petatlan earthquake, *Geophys. Res. Lett.*, 12, 789-792, 1985.

30. Örgülü, G., and M. Aktar, Regional Moment Tensor Inversion for Strong Aftershocks of the August 17, 1999 Izmit Earthquake (M_W-7.4), 28, 371-374, 2001.

31. Örgülü, G., Analysis regional moment tensor inversion method and its applications to the Izmit, Düzce earthquake sequences and eastern Anatolian earthquakes, Ph. D. Thesis, Bogazici University, Istanbul, Turkey, 2001.

32. Örgülü, G., Seismic moment and moment magnitude study at LLNL, USA in 2003, in terms of project report, (unpublished).

33. Rautian, T. G., and V. I. Khalturin, The use of the coda for determination of the earthquake source spectrum, *Bull. Seism. Soc. Am.*, 68, 923-948, 1978.

34. Richter, C. F., An instrumental earthquake magnitude scale, *Bull. Seism. Soc. Am.*, 25, 1-32, 1935.

35. Richter, C. F., Elementary seismology, *San Francisco: Freeman*, 1958.

36. Sato, H., A. M. Shomahmadov, V. I. Khalturin, and T. G. Rautian, Temporal change in spectral coda attenuation Q^{-1} associated with the K=13.3 earthquake of 1983 near Garm, Tadjikistan region in Soviet central Asia, *Zisin*, 41, 39-46, 1988.

37. Soloviev, S. L., Seismicity of Sakhalin, *Bull. Earthq. Res. Inst.*, Tokyo Univ., 43, 95-102, 1965.

38. Street, R. L., R. Herrmann, and O. Nuttli, Spectral characteristics of the Lg wave generated by central United States earthquakes, *Geophys. J. R. Astron. Soc.*, 41, 51-63, 1975.

39. Tsujiura, M., Spectral analysis of the coda waves from local earthquakes, *Bull. Earthq. Inst. Univ. Tokyo.*, 53, 1-48, 1978.

40. Tsumura, K., Determination of earthquake magnitude from total duration of oscillation, *Bull. Earthq. Res. Inst.*, Tokyo Univ., 15, 7-18, 1967.

41. Tucker, B., and J. King, Dependence of sediment-filled valley response on input amplitude and valley properties, *Bull. Seism. Soc. Am.*, 74, 153-165, 1984.

42. Wu, R. S., and K. Aki, Multiple scattering and energy transfer of seismic waves-Separation of scattering effect from intrinsic attenuation, II. Application of the theory to Hindhu-Kush region, *Pure Appl. Geophys.*, 128, 49-80, 1988.

APPENDIX A:

The list of events

Table A.1 Events recorded at both stations ISP and ISKB.

Date	Origin time	Lat.	Lon.	Depth	Magnitude
1998 01 05	20:48:28.8	38.89	25.97	10	4.1
1998 02 24	15:11:37.1	36.24	28.03	0	4.3
1998 02 25	06:58:01.5	37.79	29.56	10	4.2
1998 03 05	01:45:08.9	39.55	27.25	7	4.4
1998 03 05	01:55:26.7	39.53	27.25	5	4.4
1998 03 09	11:21:16.2	35.78	28.34	36	4.8
1998 04 04	16:16:47.2	38.12	30.04	7	4.6
1998 04 13	15:14:30.5	39.23	41.07	9	5.0
1998 06 03	08:36:36.7	40.11	24.19	1	4.0
1998 06 03	08:47:09.0	39.92	24.26	3	4.3
1998 06 27	13:55:51.8	36.96	35.52	18	6.3
1998 06 28	03:59:24.8	37.00	35.68	6	4.9
1998 07 04	02:15:47.2	36.85	35.47	35	5.1
1998 10 18	05:22:08.4	44.04	33.61	41	4.1
1998 12 14	12:44:27.8	38.96	35.91	6	4.3
1998 12 14	13:06:08.7	38.95	35.72	5	4.6
1999 02 27	19:10:20.8	35.37	26.81	59	4.2
1999 03 03	04:28:49.0	37.32	26.82	5	4.2
1999 03 17	20:27:45.3	40.26	32.14	5	4.1
1999 04 06	00:08:22.1	39.34	38.2	5	5.1
1999 04 23	18:19:46.4	36.18	31.24	31	4.6
1999 05 22	02:14:38.1	40.49	33.74	4	4.1
1999 05 25	17:15:26.6	34.55	32.27	29	4.7
1999 06 11	05:25:17.2	39.49	36.67	9	4.8
1999 06 11	05:44:12.1	39.53	36.83	8	4.8
1999 06 16	14:50:54.6	40.94	33.87	1	4.1
1999 06 28	00:16:49.6	38.21	26.54	5	4.0
1999 08 13	15:31:40.4	34.86	32.93	25	4.7
1999 08 17	00:01:37.6	40.76	29.97	18	7.4
1999 08 17	03:14:01.3	40.64	30.65	15	5.5
1999 08 17	05:54:42.1	40.78	29.05	5	4.3
1999 08 17	09:02:12.0	40.77	31.11	16	5.0
1999 08 17	11:58:09.9	40.57	30.51	16	4.5
1999 08 17	15:06:26.6	34.7	32.87	37	5.0
1999 08 17	15:17:52.0	40.75	29.75	10	4.1
1999 08 17	17:09:15.0	40.6	30.24	11	4.0
1999 08 17	18:35:21.9	40.38	28.71	7	4.0
1999 08 17	18:52:35.4	40.66	30.81	13	4.0
1999 08 17	20:30:40.9	40.72	29.29	19	4.3
1999 08 17	21:14:07.8	40.49	31.02	6	4.5
1999 08 17	22:12:47.9	40.76	30.58	6	4.4
1999 08 18	00:45:17.1	40.81	29.09	14	4.3
1999 08 18	01:04:26.6	40.7	30.68	5	4.3
1999 08 18	09:30:57.2	40.65	29.67	5	4.0
1999 08 18	13:59:34.1	40.79	29.04	9	4.0

Table A.1 (Continued)

Date	Origin time	Lat.	Lon.	Depth	Magnitude
1999 08 18	14:27:07.9	40.74	30.67	8	4.0
1999 08 18	15:34:17.3	40.77	30.58	11	4.4
1999 08 18	15:50:12.0	40.23	31.08	31	4.0
1999 08 18	21:15:54.7	40.74	30.65	9	4.2
1999 08 18	23:17:58.0	40.67	30.65	24	4.1
1999 08 19	13:04:12.3	40.79	30.59	7	4.8
1999 08 19	14:15:58.4	40.6	29.06	12	4.5
1999 08 19	14:24:34.4	40.61	29.1	14	4.5
1999 08 19	15:17:44.9	40.59	29.08	11	5.0
1999 08 19	15:48:19.5	40.64	29.15	12	4.3
1999 08 19	18:34:56.1	40.79	30.59	1	4.3
1999 08 20	10:00:19.1	40.59	30.6	7	4.4
1999 08 20	15:59:02.2	40.82	30.92	16	4.4
1999 08 20	20:12:42.5	40.59	29.05	9	4.3
1999 08 20	20:20:39.1	40.76	30.64	1	4.3
1999 08 21	10:01:25.7	40.72	29.96	8	4.1
1999 08 21	19:21:21.2	40.69	30.64	1	4.1
1999 08 21	23:34:13.1	40.68	29.21	23	4.0
1999 08 22	01:47:45.2	40.62	29.08	10	4.3
1999 08 22	08:23:01.9	40.66	29.38	9	4.0
1999 08 22	10:09:47.5	40.66	30.06	1	4.0
1999 08 22	14:30:59.4	40.74	30.68	5	5.0
1999 08 24	17:33:15.1	39.61	32.62	8	4.7
1999 08 26	17:49:34.4	40.84	30.26	3	4.1
1999 08 29	10:14:55.3	40.88	31.23	7	4.8
1999 08 29	10:23:15.9	40.82	31.22	16	4.8
1999 08 30	03:52:44.0	40.79	30.53	4	4.0
1999 08 31	08:10:51.5	40.75	29.92	17	5.2
1999 08 31	08:33:23.6	40.78	29.96	10	4.6
1999 08 31	22:28:21.1	40.63	29.09	19	4.1
1999 09 02	14:25:15.4	40.73	30.82	5	4.0
1999 09 04	10:30:46.4	40.74	30.03	17	4.2
1999 09 04	18:27:43.6	40.76	30.32	12	4.0
1999 09 05	19:52:38.1	40.69	30.54	7	4.2
1999 09 06	06:33:26.1	40.73	29.79	12	4.0
1999 09 06	19:44:29.4	40.85	31.07	3	4.0
1999 09 09	00:42:50.2	40.71	30.77	14	4.1
1999 09 09	01:32:08.0	40.71	29.14	11	4.6
1999 09 09	08:12:02.7	40.36	26.08	33	4.5
1999 09 09	08:15:35.4	40.39	25.66	18	4.5
1999 09 09	20:21:48.8	40.75	29.95	14	4.1
1999 09 13	11:55:28.7	40.77	30.1	19	5.8
1999 09 17	19:49:06.2	40.72	30.1	15	4.5
1999 09 18	00:48:24.4	40.62	29.12	9	4.3
1999 09 19	20:26:35.2	40.64	30.52	11	4.2

Table A.1 (Continued)

Date	Origin time	Lat.	Lon.	Depth	Magnitude
1999 09 20	21:28:00.0	40.69	27.58	16	5.0
1999 09 26	06:38:38.7	39.02	27.92	9	4.1
1999 09 29	00:13:05.7	40.7	29.34	12	4.8
1999 11 07	16:54:42.0	40.71	30.7	10	5.0
1999 11 07	17:06:05.5	40.76	30.7	10	4.3
1999 11 11	14:41:25.6	40.74	30.27	22	5.7
1999 11 11	14:55:25.4	40.88	30.3	11	4.4
1999 11 12	16:57:20.8	40.74	31.21	25	7.2
1999 11 12	17:16:51.9	40.76	31.02	10	5.2
1999 11 12	17:17:57.2	40.78	31.12	10	5.2
1999 11 12	17:22:55.7	40.79	31.12	10	5.2
1999 11 12	17:26:25.4	40.7	31.51	10	5.1
1999 11 12	17:29:48.5	40.74	31.47	10	5.1
1999 11 12	17:46:57.2	40.73	30.95	10	4.8
1999 11 12	17:57:03.2	40.88	31.72	10	4.8
1999 11 12	18:07:52.0	40.76	31.3	10	4.8
1999 11 12	18:14:31.2	40.74	31.34	10	4.8
1999 11 12	18:42:38.1	41.1	31.42	1	4.7
1999 11 12	19:05:49.8	40.58	31.61	10	4.2
1999 11 12	19:06:49.9	40.78	31.18	10	4.2
1999 11 12	19:15:46.0	40.77	31.44	10	4.5
1999 11 12	20:04:55.0	40.76	31.22	10	4.5
1999 11 12	20:44:35.6	40.8	31.27	10	4.5
1999 11 12	20:53:54.8	40.72	31.6	10	4.5
1999 11 12	21:24:53.9	40.65	31.06	8	4.0
1999 11 12	21:38:32.7	40.81	31.1	10	4.4
1999 11 12	21:42:25.5	40.83	31.28	10	4.4
1999 11 12	22:20:54.5	40.76	31.34	10	4.8
1999 11 12	22:38:02.9	40.76	31.33	13	4.1
1999 11 12	22:49:29.8	40.68	30.87	10	4.2
1999 11 12	23:11:00.8	40.5	31.45	10	4.0
1999 11 13	00:14:51.6	40.82	31.5	10	4.3
1999 11 13	00:54:55.3	40.77	31.05	10	4.7
1999 11 13	01:03:02.7	40.81	31.47	7	4.7
1999 11 13	01:57:21.9	40.76	31.49	4	4.0
1999 11 13	02:53:07.7	40.83	30.22	5	4.7
1999 11 13	02:58:53.7	40.84	31.08	7	4.7
1999 11 13	03:28:20.2	40.77	31.31	2	4.0
1999 11 13	03:57:32.8	40.73	31.5	10	4.2
1999 11 13	04:10:20.8	40.63	31.51	10	4.2
1999 11 13	08:33:41.2	40.77	31.5	1	4.1
1999 11 13	08:36:17.8	40.75	31.23	8	4.1
1999 11 13	09:59:20.7	40.9	31.09	2	4.2
1999 11 13	10:10:34.4	40.82	31.57	8	4.3
1999 11 15	16:26:54.7	40.82	31.19	5	4.1

Table A.1 (Continued)

Date	Origin time	Lat.	Lon.	Depth	Magnitude
1999 11 15	22:44:43.2	40.91	30.33	7	4.0
1999 11 16	07:49:38.6	40.7	31.63	4	4.0
1999 11 16	17:51:17.0	40.79	31.6	1	4.9
1999 11 17	08:15:26.2	40.8	31.46	9	5.0
1999 11 19	14:01:13.1	40.85	31.04	11	4.3
1999 11 19	19:59:07.9	40.78	30.97	9	5.0
1999 11 20	08:44:13.2	40.78	31.47	8	4.2
1999 11 21	13:46:14.6	40.63	26.11	20	4.0
1999 11 21	22:27:32.3	40.77	31.5	9	4.2
2000 04 02	18:57:38.3	40.8	30.24	7	4.5
2000 04 21	12:23:08.0	37.92	29.29	11	5.2
2000 04 23	13:53:32.5	38.08	27.77	5	4.1
2000 06 06	02:41:50.4	40.68	32.98	9	5.9
2000 06 06	05:59:39.8	40.6	32.91	8	4.5
2000 06 13	01:43:16.8	35.22	27.05	18	5.0
2000 06 15	16:10:19.2	35.16	26.93	9	4.6
2000 07 05	23:20:36.1	40.31	26.03	5	4.0
2000 07 07	00:15:30.8	40.85	29.22	9	4.2
2000 07 25	19:34:13.5	37.94	23.21	8	4.7
2000 09 02	02:54:05.1	40.14	31.39	24	4.0
2000 09 08	05:46:47.1	39.38	27.63	9	4.6
2000 09 27	12:19:37.5	40.46	33.04	11	4.0
2000 10 04	02:33:56.9	37.94	29.03	6	4.7
2000 10 05	08:34:46.2	40.53	32.96	6	4.3
2000 10 05	08:38:08.8	40.5	33.05	5	4.3
2001 02 01	09:58:47.1	40.06	27.74	7	4.0
2001 02 02	09:51:38.9	37.75	30.18	6	4.2
2001 03 04	23:31:01.6	43.17	35.57	56	4.1
2001 03 10	11:20:56.7	34.65	25.99	37	4.5
2001 03 14	20:34:20.2	40.85	27.64	8	4.0
2001 03 30	15:30:49.2	38.74	30.85	0	4.1
2001 04 07	04:09:35.0	40.06	35.72	6	4.1
2001 05 01	06:00:54.7	35.66	27.08	60	4.8
2001 05 29	04:42:57.0	35.58	28.1	5	4.8
2001 06 10	13:11:02.1	38.57	25.69	7	5.7
2001 06 22	11:54:50.6	39.38	27.9	7	5.0
2001 06 23	06:52:37.8	35.43	27.99	8	5.1
2001 06 25	13:28:48.9	37.12	36.26	28	5.5
2001 08 12	18:31:28.3	40.31	33.74	14	4.3
2001 09 13	15:42:44.7	34.83	25.33	44	5.0
2001 09 17	18:41:25.1	36.07	31.10	11	4.1
2001 09 25	11:53:29.4	35.99	32.33	0	5.1
2001 09 26	04:19:47.5	34.48	26.96	0	4.4
2001 10 18	15:50:29.5	36.78	35.37	19	4.9
2001 10 30	21:00:02.0	35.60	29.63	0	5.6

Table A.1 (Continued)

Date	Origin time	Lat.	Lon.	Depth	Magnitude
2001 10 31	12:33:53.1	37.17	36.27	12	5.2
2001 12 21	14:25:16.1	35.65	26.75	5	4.4

Table A.2 Events recorded at both stations ISP and MALT.

Date	Origin time	Lat.	Lon.	Depth	Magnitude
2000 05 30	08:17:43.5	40.64	34.64	10	4.0
2000 06 06	02:41:49.8	40.69	32.99	10	6.1
2000 06 06	05:59:39.3	40.57	32.91	10	4.3
2000 06 08	21:27:58.6	40.72	32.94	36	4.5
2000 06 09	03:14:19.5	40.69	32.92	10	4.6
2000 06 29	14:15:26.5	38.43	26.09	37	4.1
2000 07 05	23:20:37.9	40.35	26	10	4.2
2000 07 07	00:15:31.0	40.84	29.22	8	4.2
2000 07 24	00:04:03.3	36.6	31.5	107	4.1
2000 08 10	03:47:11.8	37.26	28.96	29	4.0
2000 08 17	11:49:50.4	40.72	33.89	33	4.8
2000 08 19	21:26:15.6	39.7	41.13	33	4.1
2000 08 22	11:40:12.8	40.17	32.02	10	4.4
2000 08 23	13:41:28.1	40.68	30.72	15	5.8
2000 08 26	17:15:11.7	39.42	26.21	33	4.0
2000 08 28	22:27:47.6	40.82	33.13	10	4.1
2000 09 02	02:53:49.6	40.56	33.1	10	4.1
2000 09 07	07:32:32.5	38.41	44.99	33	4.1
2000 09 08	05:46:47.0	39.36	27.7	10	4.7
2000 09 08	15:01:05.7	36.57	25.5	37	4.1
2000 09 09	08:18:48.7	39.35	27.67	10	4.0
2000 09 16	04:41:42.8	36.72	27.5	33	4.5
2000 09 21	14:10:23.7	39.28	27.97	9	4.0
2000 09 24	07:12:16.6	39.54	43.72	40	4.4
2000 09 27	12:19:38.5	40.62	33.02	14	4.0
2000 10 04	02:33:57.0	37.92	29.05	8	4.7
2000 10 04	07:58:52.7	37.95	28.91	5	4.3
2000 10 05	08:34:46.2	40.6	33.14	10	4.1
2000 10 05	08:38:08.9	40.54	33.05	10	4.1
2000 10 05	21:32:04.9	38.23	25.23	10	4.3
2000 10 06	06:20:25.2	36.93	45.2	77	4.5
2000 10 18	22:55:37.1	36.22	28.69	10	4.4
2000 11 07	21:13:57.4	39.43	26.3	5	4.0
2000 11 13	03:12:37.1	40.76	30.81	10	4.3
2000 11 15	15:05:38.1	38.4	42.92	65	5.6
2000 11 15	16:06:14.7	38.53	42.9	60	4.4
2000 11 15	19:30:44.5	37.92	42.83	21	4.2
2000 11 16	21:13:46.7	38.26	43.01	20	4.4
2000 11 17	00:28:00.1	38.24	42.94	33	4.6
2000 11 26	17:08:33.2	37.92	29.05	10	4.0
2000 11 26	17:20:35.4	37.94	29.03	10	4.0
2000 12 05	08:24:14.6	39.12	27.93	8	4.1
2001 01 04	01:20:38.6	37.66	26.86	11	4.1
2001 01 16	03:33:02.4	40.92	29.1	10	4.2
2001 01 17	12:09:53.9	37.06	36.13	10	4.9

Table A.2 (Continued)

Date	Origin time	Lat.	Lon.	Depth	Magnitude
2001 01 19	04:38:39.9	39.18	27.94	33	4.1
2001 01 23	09:27:56.2	40.24	46.57	33	4.2
2001 01 24	05:19:43.6	39.57	26.15	10	4.0
2001 02 01	02:42:56.9	38.75	44.65	33	4.3
2001 02 01	09:58:50.0	40.1	27.75	25	4.0
2001 02 02	09:51:41.6	37.7	30.24	33	4.4
2001 02 10	20:42:22.9	38.92	43.56	10	4.4
2001 02 18	00:07:15.4	38.19	39.27	8	4.3
2001 02 18	00:24:52.3	37.98	26.66	6	4.0
2001 02 27	04:10:47.7	39.00	26.68	11	4.1
2001 02 27	06:14:54.6	39.04	26.73	10	4.1
2001 03 01	13:31:17.6	37.84	26.81	10	4.9
2001 03 11	19:21:45.5	38.59	33.8	12	4.0
2001 03 14	20:34:19.2	40.8	27.68	10	4.1
2001 03 22	06:21:20.9	38.72	30.93	33	4.8
2001 03 22	14:02:25.3	40.66	33.09	33	4.5
2001 03 30	15:30:49.8	38.69	30.93	10	4.4
2001 04 01	01:18:47.9	40.92	31.08	12	4.0
2001 04 06	03:26:32.4	36.17	26.91	151	4.4
2001 04 07	04:09:35.0	40.05	35.74	8	4.4
2001 04 09	20:05:37.6	36.43	28.58	79	4.0
2001 05 03	06:10:22.4	40.58	36.66	10	4.2
2001 05 20	03:09:42.8	38.51	25.72	30	4.4
2001 05 20	04:30:14.9	38.49	25.58	29	4.2
2001 05 24	03:18:09.7	39.3	27.92	15	4.5
2001 05 24	06:25:58.9	39.44	27.79	33	4.4
2001 05 29	13:14:30.3	39.8	41.65	33	4.8
2001 05 29	14:15:54.9	39.85	41.96	33	4.7
2001 05 31	19:39:49.7	39.46	26.34	9	4.1
2001 06 10	13:11:04.2	38.58	25.61	33	5.4
2001 06 10	14:13:30.2	38.5	25.69	33	4.2
2001 06 12	01:14:18.5	37.59	26.84	11	4.1
2001 06 13	07:05:54.5	38.51	25.59	33	4.2
2001 06 17	07:20:08.2	36.68	25.7	51	4.0
2001 06 17	11:22:15.9	39.25	45.85	33	4.2
2001 06 22	11:54:50.9	39.31	27.91	10	5.0
2001 06 22	19:56:22.4	39.33	27.82	10	4.1
2001 06 23	12:18:23.1	39.47	27.88	10	4.7
2001 06 24	11:49:37.3	39.41	27.9	5	4.1
2001 06 24	13:33:03.3	39.4	27.73	10	4.2
2001 06 25	13:28:46.5	37.24	36.21	5	5.5
2001 06 26	15:30:00.1	38.65	26.52	10	4.1
2001 06 26	17:19:45.1	38.65	26.64	19	4.3
2001 06 26	17:27:53.6	38.66	26.53	10	4.1
2001 06 26	19:28:40.3	39.72	41.84	10	4.3

Table A.2 (Continued)

Date	Origin time	Lat.	Lon.	Depth	Magnitude
2001 06 30	18:02:26.4	37.28	26.83	27	4.0
2001 07 08	02:15:48.3	38.91	26.94	10	4.0
2001 07 10	21:42:08.8	39.83	41.62	33	5.4
2001 07 18	00:58:20.7	38.73	25.97	15	4.0
2001 08 12	00:42:10.9	37.22	44.03	55	4.3
2001 08 12	18:31:28.2	40.22	33.81	10	4.4
2001 08 13	11:11:00.9	39.33	27.85	10	4.2
2001 08 20	18:50:40.2	40.17	42.12	10	4.5
2001 08 26	00:41:13.1	40.95	31.57	7	5.4
2001 09 02	19:27:40.0	38.99	31.55	33	4.1
2001 09 02	21:42:29.3	38.6	39.84	33	4.3
2001 09 12	14:52:06.9	37.95	42.55	33	4.1
2001 09 17	18:41:24.8	36.01	31.03	10	4.1
2001 09 25	11:53:33.0	36.03	32.32	33	4.4
2001 09 26	01:29:33.8	40.23	25.27	10	4.1
2001 09 26	06:21:46.6	40.34	25.88	19	4.0
2001 10 08	11:38:13.2	36.74	28.18	88	4.2
2001 10 18	15:50:30.8	36.9	35.21	33	4.7
2001 10 31	12:33:52.8	37.25	36.14	10	5.2
2001 11 05	01:43:33.4	36.48	31.25	119	4.1
2001 11 12	13:59:16.1	36.88	34.8	33	4.2
2001 11 17	07:56:11.2	36.47	25.94	176	4.2
2001 11 27	08:53:27.4	37.86	39.63	10	4.1
2001 11 29	19:36:45.3	39.72	41.49	33	4.3
2001 12 02	04:11:48.2	38.44	43.25	33	4.7
2001 12 02	17:05:24.7	37.49	44.19	33	4.3
2001 12 04	09:40:31.7	38.42	43.22	33	4.4
2001 12 04	22:35:32.8	37.11	27.77	5	4.0
2001 12 15	04:31:50.4	38.68	42.35	33	4.3
2001 12 29	23:12:30.7	36.53	28.15	103	4.2
2001 12 31	13:32:32.1	36.31	28.09	75	4.0
2002 01 21	14:34:23.8	38.68	27.82	10	4.7
2002 02 03	07:11:28.8	38.49	31.31	10	6.5
2002 02 03	09:26:43.6	38.63	30.81	10	6.0
2002 02 03	11:39:54.9	38.53	30.96	10	5.3
2002 02 03	11:54:34.6	38.56	31.03	10	5.1
2002 02 04	13:06:30.0	40.01	35.7	10	4.1
2002 03 30	22:01:21.7	40.42	25.78	29	3.4
2002 03 30	22:15:01.0	40.42	25.8	29	3.2
2002 05 08	02:00:20.2	36.91	26.65	30	3.7
2002 05 08	02:29:42.1	36.91	26.63	31	4.0
2002 05 13	11:42:49.9	38.6	31.26	10	4.4
2002 05 19	10:45:57.5	38.38	26.39	28	4.2
2002 05 19	11:07:37.2	38.39	26.59	36	3.8
2002 05 19	12:26:56.6	38.35	26.3	21	3.5

Table A.2 (Continued)

Date	Origin time	Lat.	Lon.	Depth	Magnitude
2002 05 19	12:49:01.2	38.36	26.33	21	3.5

Table A.3 The event list of 39 earthquakes in ISP-ISKB dataset used for the calibration.

Date	Origin Time	Mw(waveform)	Mw(coda) for ISKB	Mw(coda) for ISP
2000 04 02	18:57:38.3	4.3	4.34	4.32
2000 04 21	12:23:08.0	5.5	5.10	5.07
2000 06 06	02:41:50.4	6.0	6.00	6.08
2000 06 13	01:43:16.8	5.4	5.46	5.24
2001 05 01	06:00:54.7	5.2	5.01	5.32
2001 06 23	06:52:37.8	5.7	5.54	5.55
2001 06 25	13:28:48.9	5.5	5.54	5.40
1998 03 09	11:21:16.2	5.2	5.13	5.08
1998 04 04	16:16:47.2	5.3	5.16	5.00
1998 04 13	15:14:30.5	5.3	5.29	5.61
1998 06 27	13:55:51.8	6.3	6.27	6.38
1998 07 04	02:15:47.2	5.4	5.33	5.52
1999 04 06	00:08:22.1	5.4	5.45	5.50
1999 05 25	17:15:26.6	5.6	5.54	5.59
1999 08 17	00:01:37.6	7.6	-	7.40
1999 08 17	03:14:01.3	5.3	5.43	5.14
1999 08 17	05:54:42.1	4.7	4.98	4.89
1999 08 17	09:02:12.0	4.7	4.66	4.72
1999 08 17	20:30:40.9	4.1	3.95	3.91
1999 08 18	01:04:26.6	4.0	3.97	3.93
1999 08 19	13:04:12.3	4.5	4.42	4.42
1999 08 19	14:15:58.4	4.5	4.52	4.48
1999 08 19	15:17:44.9	5.0	5.04	5.17
1999 08 20	15:59:02.2	4.1	4.05	4.06
1999 08 31	08:10:51.5	5.0	5.10	5.16
1999 08 31	08:33:23.6	4.4	4.61	4.37
1999 08 31	22:28:21.1	4.3	4.41	4.34
1999 09 04	10:30:46.4	4.0	3.92	3.85
1999 09 09	01:32:08.0	4.0	4.21	4.03
1999 09 13	11:55:28.7	5.8	6.01	5.83
1999 09 20	21:28:00.0	4.7	4.85	4.83
1999 09 29	00:13:05.7	5.0	5.07	5.20
1999 11 07	16:54:42.0	4.5	4.68	4.86
1999 11 11	14:41:25.6	5.5	5.38	5.66
1999 11 12	16:57:20.8	7.2	7.03	7.14
1999 11 13	00:54:55.3	4.8	4.93	5.04
1999 11 16	17:51:17.0	4.8	5.00	5.07
1999 11 17	08:15:26.2	4.9	4.95	4.96
1999 11 19	19:59:07.9	4.8	4.80	4.79

Table A.4 The event list of 49 earthquakes in ISP-MALT dataset used for the calibration.

Date	Origin Time	Mw(waveform)	Mw(coda) for ISKB	Mw(coda) for ISP
2000 06 06	02:41:49.8	5.9	5.72	6.00
2000 06 06	05:59:39.3	4.4	4.39	4.43
2000 06 08	21:27:58.6	4.7	4.44	4.88
2000 06 09	03:14:19.5	4.8	4.65	4.78
2000 07 05	23:20:37.9	4.2	4.18	4.08
2000 07 07	00:15:30.9	4.3	4.27	4.28
2000 08 10	03:47:11.8	3.9	3.85	3.88
2000 08 17	11:49:50.3	4.2	4.19	4.15
2000 08 22	11:40:12.8	4.6	4.67	4.87
2000 08 23	13:41:28.1	5.2	5.13	5.33
2000 08 28	22:27:47.5	4.3	4.15	4.49
2000 09 08	05:46:47.0	4.5	4.58	4.51
2000 09 24	07:12:16.6	4.5	4.43	4.60
2000 10 04	02:33:57.0	4.8	4.61	4.71
2000 10 05	08:34:46.2	4.3	4.16	4.27
2000 10 18	22:55:37.1	4.4	4.16	4.50
2000 11 07	21:13:57.4	4.0	3.98	4.01
2000 11 13	03:12:37.1	3.9	3.84	3.94
2000 11 15	15:05:38.1	5.3	5.01	5.37
2000 11 26	17:08:33.2	4.0	4.00	4.01
2001 01 17	12:09:53.9	4.5	4.59	4.76
2001 03 01	13:31:17.6	4.2	4.25	4.18
2001 03 11	19:21:45.5	3.9	4.08	3.96
2001 03 22	06:21:20.9	4.3	4.22	4.22
2001 03 22	14:02:25.3	4.5	4.41	4.68
2001 03 30	15:30:49.8	4.3	4.13	4.27
2001 04 07	04:09:35.0	4.2	4.19	4.19
2001 05 24	03:18:09.7	4.1	4.31	4.26
2001 05 29	13:14:30.3	4.7	4.60	4.54
2001 06 10	13:11:04.2	5.5	5.28	5.56
2001 06 22	11:54:50.9	5.0	4.93	5.21
2001 06 23	12:18:23.1	4.6	4.65	4.82
2001 06 25	13:28:46.5	5.3	5.00	5.40
2001 08 12	00:42:10.9	4.4	4.39	4.36
2001 08 12	18:31:28.2	4.3	4.12	4.35
2001 08 20	18:50:40.2	4.5	4.33	4.51
2001 08 26	00:41:13.1	4.9	4.65	4.83
2001 09 02	21:42:29.3	4.6	4.67	4.83
2001 09 25	11:53:33.0	4.4	4.49	4.74
2001 10 18	15:50:30.8	4.4	4.44	4.51
2001 10 31	12:33:52.8	5.0	4.88	5.15
2001 11 27	08:53:27.4	4.1	4.10	4.44
2001 11 29	19:36:45.3	4.5	4.31	4.53
2001 12 02	04:11:48.2	4.6	4.49	4.36
2002 02 03	07:11:28.8	6.3	6.26	6.28

Table A.4 (Continued)

Date	Origin Time	Mw(waveform)	Mw(coda) for ISKB	Mw(coda) for ISP
2002 02 03	09:26:43.6	5.6	5.57	5.71
2002 02 03	11:39:54.9	5.0	4.89	5.11
2002 02 03	11:54:34.6	5.0	4.87	5.05
2002 05 13	11:42:49.9	4.4	4.26	4.22

APPENDIX B:

Distance-dependent γ and b parameters

a

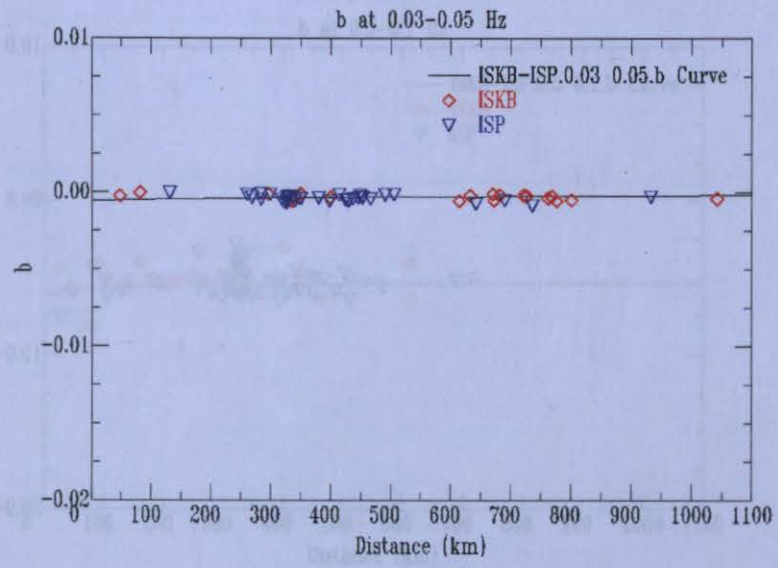

b

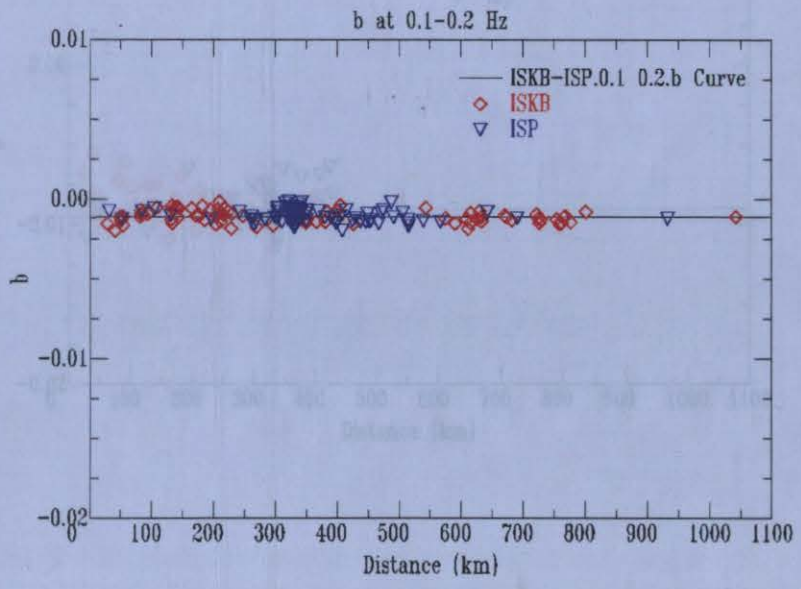

Figure B.1 The b values plotted versus distance at some frequency bands. **a)** b values obtained at 0.03-0.05 Hz for the events recorded at ISP and ISKB stations, **b)** b values obtained at 0.1-0.2 Hz for the events recorded at ISP and ISKB stations.

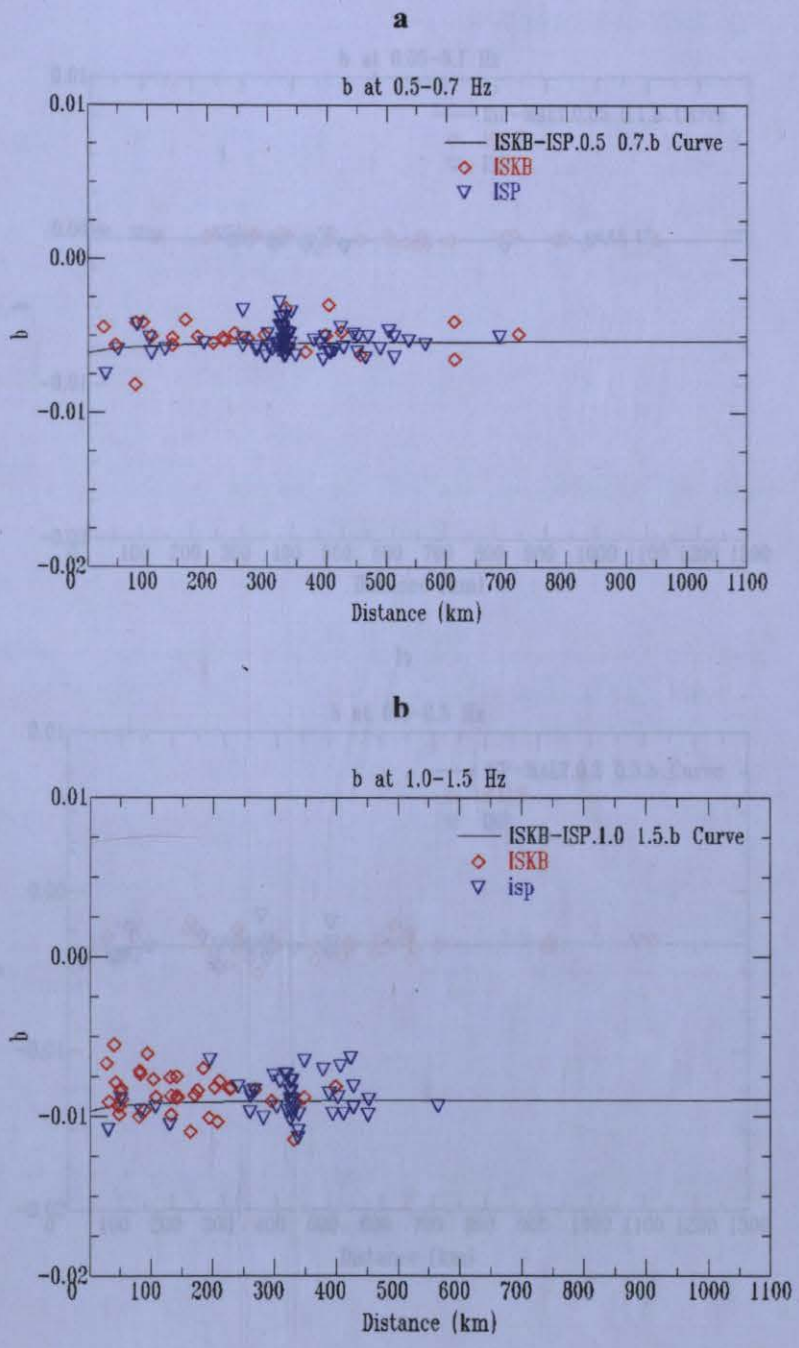

Figure B.2 The b values plotted versus distance at some frequency bands. **a)** b values obtained at 0.5-0.7 Hz for the events recorded at ISP and ISKB stations, **b)** b values obtained at 1.0-1.5 Hz for the events recorded at ISP and ISKB stations.

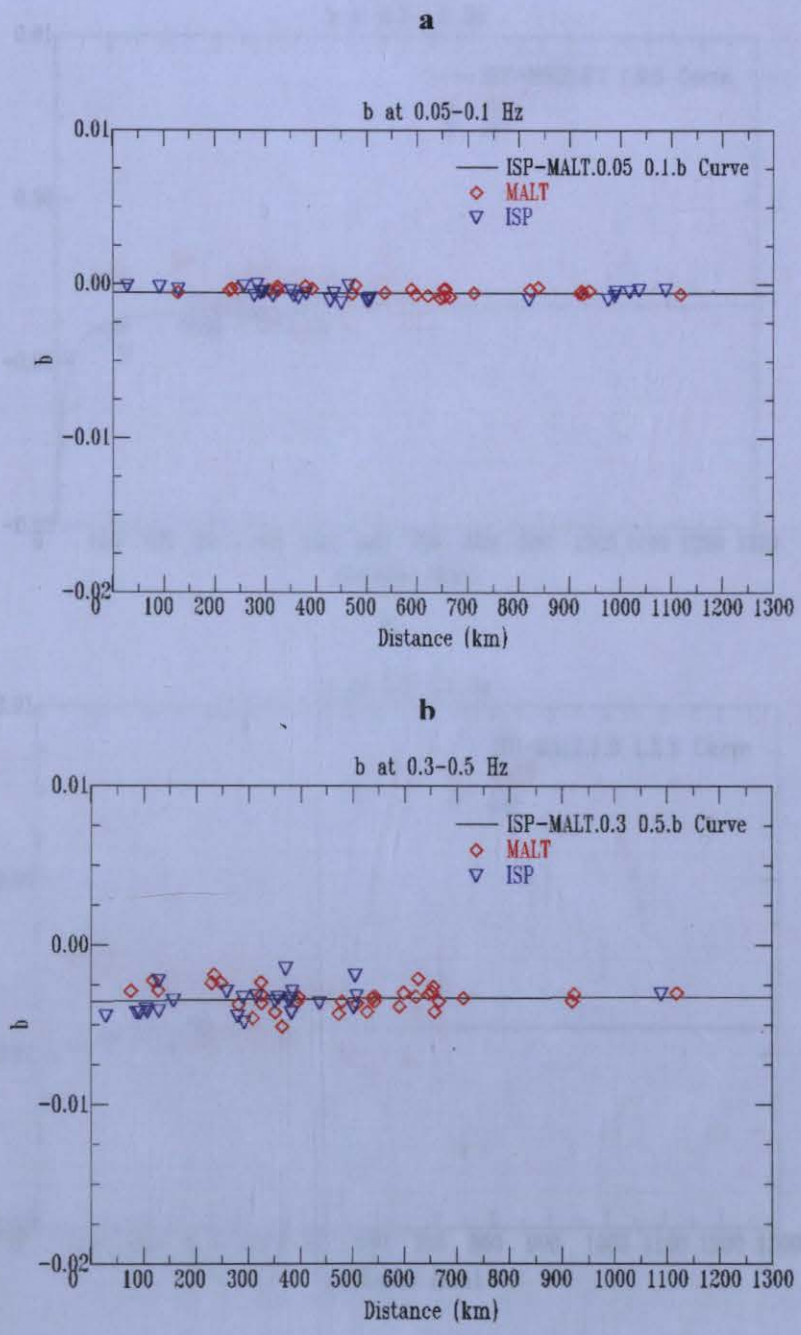

Figure B.3 The b values plotted versus distance at some frequency bands. **a)** b values obtained at 0.05-0.1 Hz for the events recorded at ISP and MALT stations, **b)** b values obtained at 0.3-0.5 Hz for the events recorded at ISP and MALT stations.

a

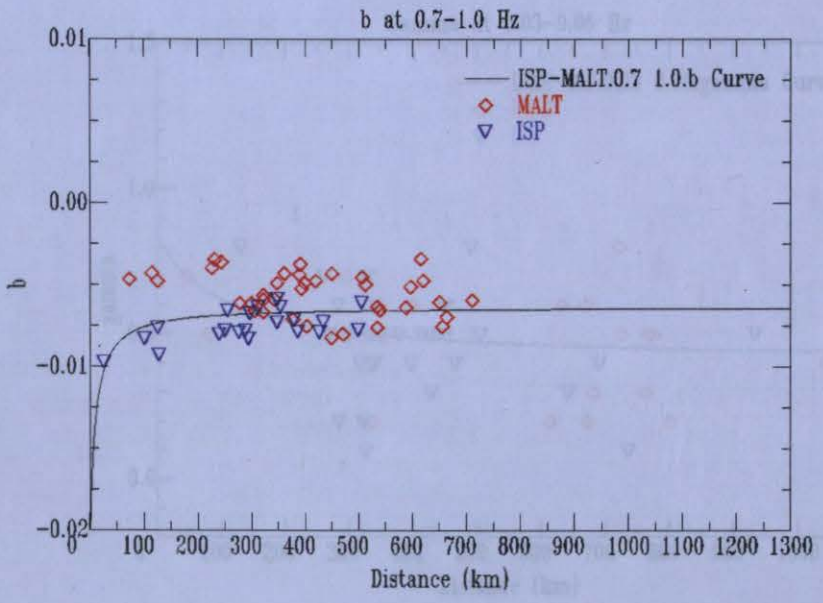

b

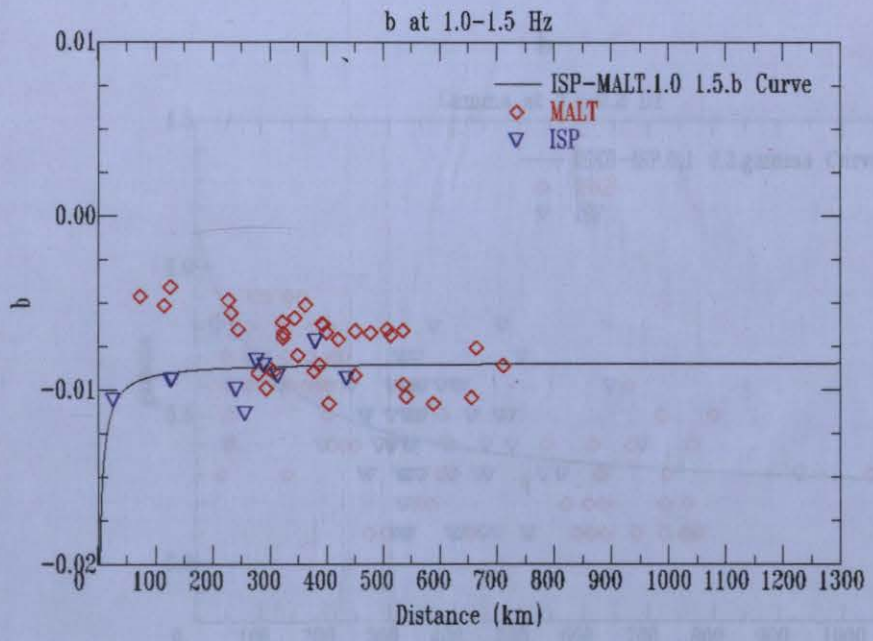

Figure B.4 The b values plotted versus distance at some frequency bands, **a)** b values obtained at 0.7-1.0 Hz for the events recorded at ISP and MALT stations, **b)** b values obtained at 1.0-1.5 Hz for the events recorded at ISP and MALT stations.

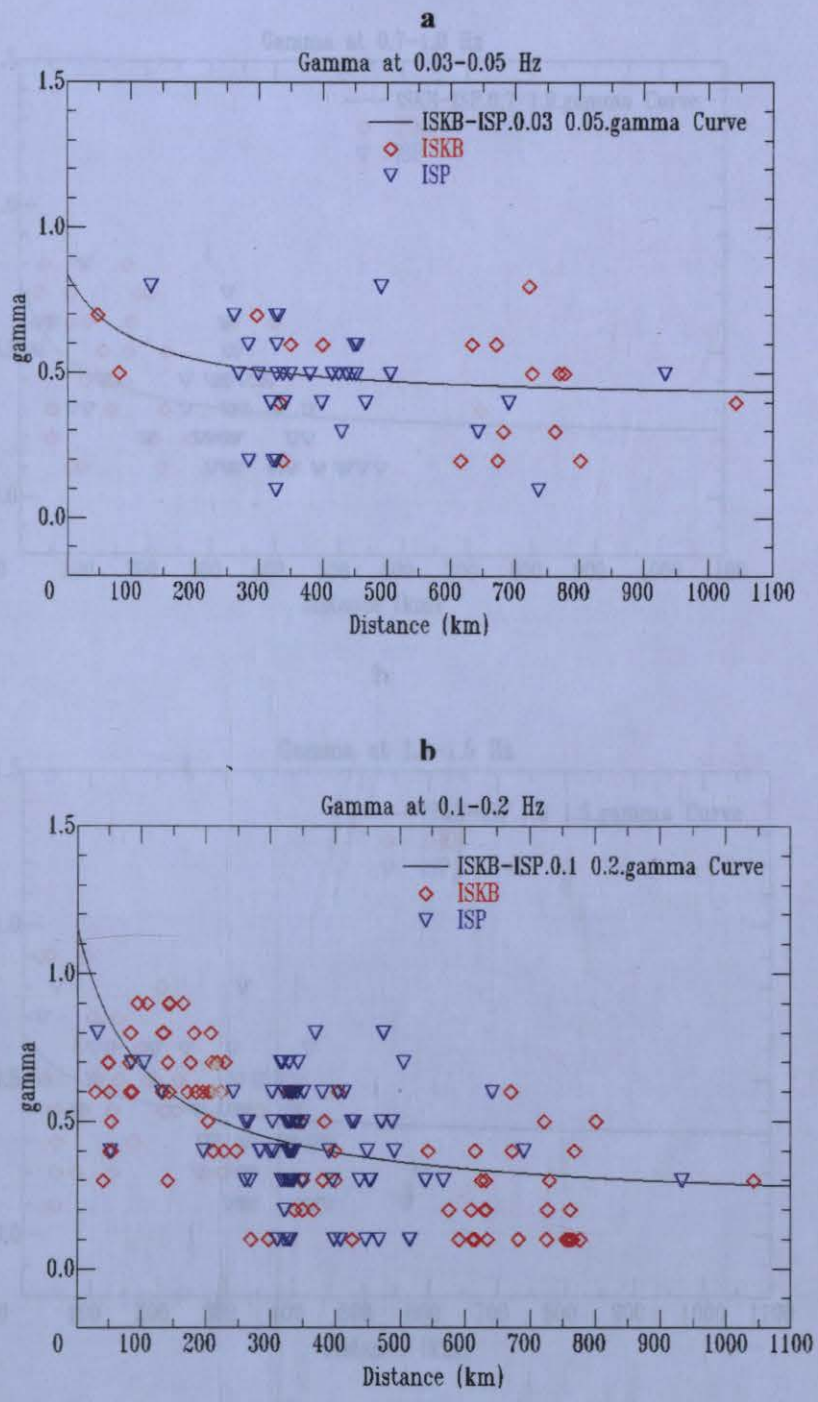

Figure B.5 The gamma, γ values plotted versus distance at some frequency bands, **a)** gamma, γ values obtained at 0.03-0.05 Hz for the events recorded at ISP and ISKB stations **b)** gamma, γ values obtained at 0.1-0.2 Hz for the events recorded at ISP and ISKB stations.

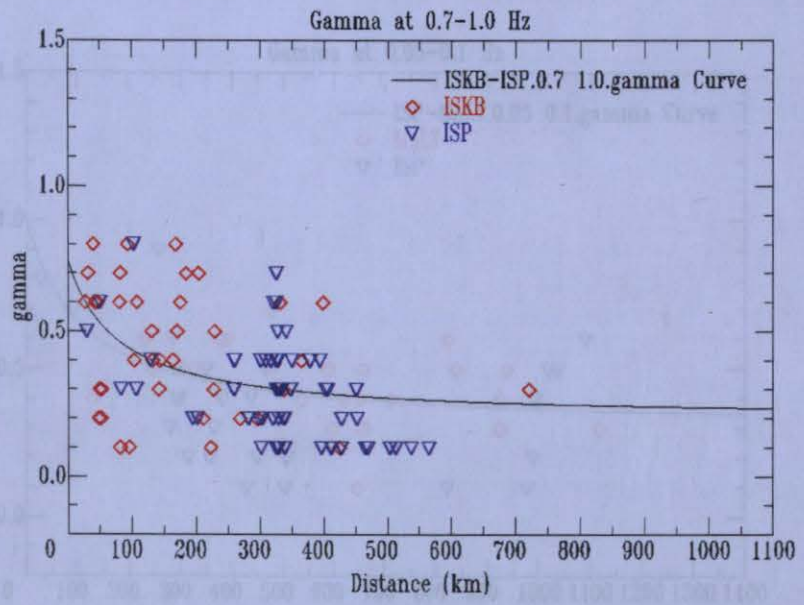

b

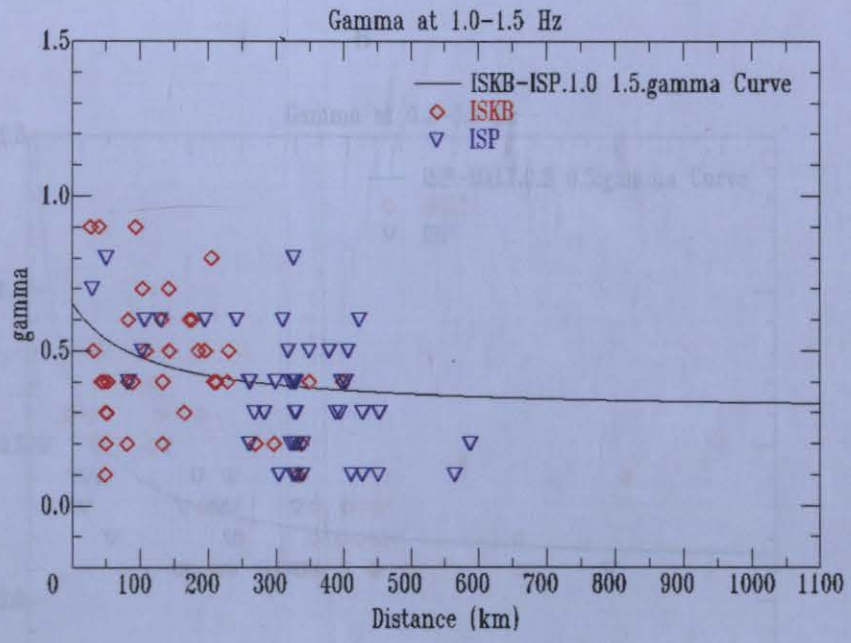

Figure B.6 The gamma, γ values plotted versus distance at some frequency bands, **a)** gamma, γ values obtained at 0.7-1.0 Hz for the events recorded at ISP and ISKB stations, **b)** gamma, γ values obtained at 1.0-1.5 Hz for the events recorded at ISP and ISKB stations.

a

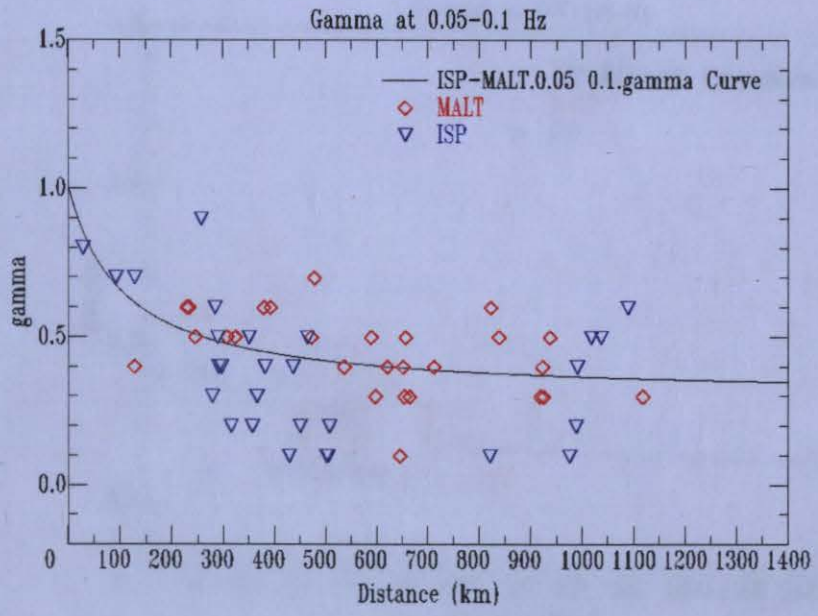

b

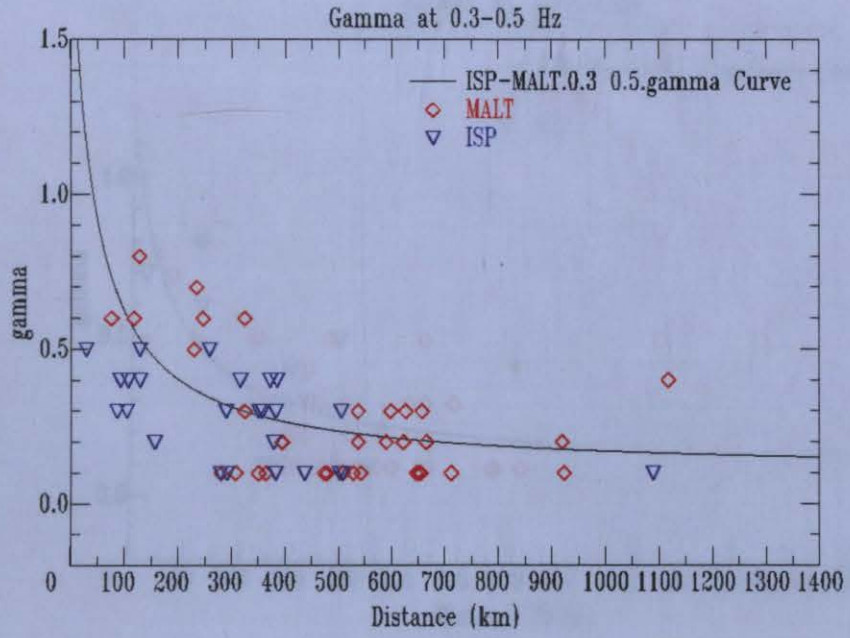

Figure B.7 The gamma, γ values plotted versus distance at some frequency bands, **a)** gamma, γ values obtained at 0.05-0.1 Hz for the events recorded at ISP and MALT stations, **b)** gamma, γ values obtained at 0.3-0.5 Hz for the events recorded at ISP and MALT stations.

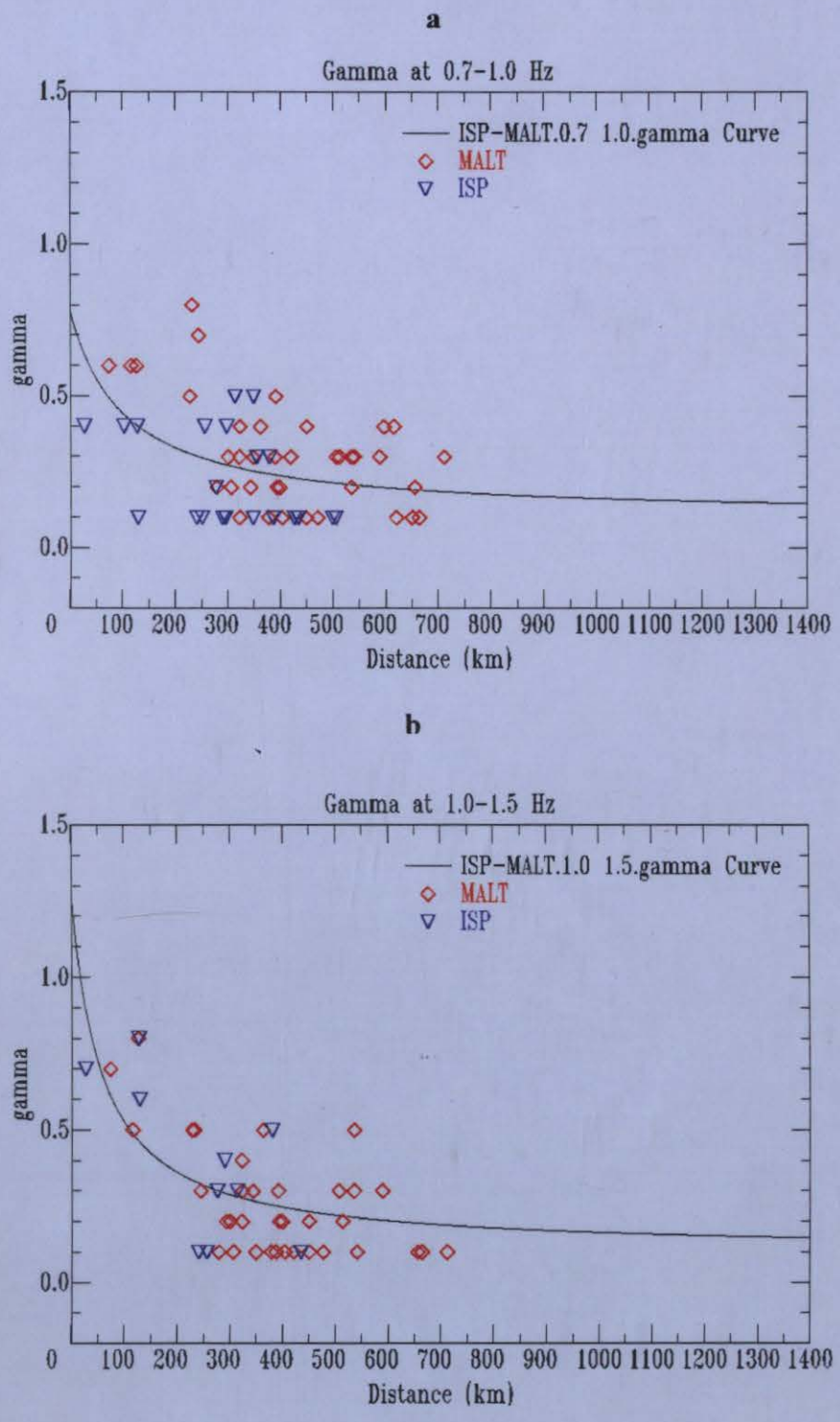

Figure B.8 The gamma, γ values plotted versus distance at some frequency bands, **a)** gamma, γ values obtained at 0.7-1.0 Hz for the events recorded at ISP and MALT stations, **b)** gamma, γ values obtained at 1.0-1.5 Hz for the events recorded at ISP and MALT stations.